Année :   **2010**

THÈSE

présentée à

**L'UFR des Sciences et Techniques
de l'Université de Franche-Comté**

pour obtenir le

GRADE DE DOCTEUR DE L'UNIVERSITÉ DE FRANCHE-COMTÉ

en Sciences pour l'ingénieur
(École Doctorale Sciences Physiques pour l'Ingénieur et Microtechniques)

Microrobotique numérique fondée sur l'utilisation de modules bistables :

conception, fabrication et commande de modules monolithiques

Digital Microrobotics Based on Bistable Modules:

Design, Fabrication and Control of Monolithic Modules

par :

Qiao CHEN

Soutenue le 18 Mars 2010 devant la commission d'examen :

Rapporteurs :
Etienne DOMBRE, Directeur de Recherche CNRS, LIRMM
Herbert SHEA, Professeur, IMT Neuchâtel, EPFL

Examinateurs :
Moustapha HAFEZ, Directeur de Recherche, CEA LIST
Franck CHOLLET, Professeur, FEMTO-ST, Université de Franche-Comté

Directeurs de thèse :
Yassine HADDAB, Maître de Conférences, ENSMM
Philippe LUTZ, Professeur, Université de Franche-Comté

Acknowledgments

To my parents
To my sister

VI

CONTENTS

VII

VIII

X

Figures

XIV

Tables

Introduction

Product miniaturization is a strong tendency for several reasons: energy saving, mass reduction, lower CO_2 release, etc. In addition to the miniaturization, the integration of complex functions and intelligence makes them more competitive. However, size reduction and increasing complexity lead to important challenges that need research and developments. The miniaturized product design turns into micromechatronics design by the integration of mechanical, optical, acoustic and electronic components. Because of the use of various technologies that are not compatible and the need of 3D structures, assembly systems are required with performances adapted to the small sizes. For the miniaturization of products, in particular in very competing sectors of high technology, it becomes increasingly necessary to develop flexible technologies allowing reliable manufacture of very small components with a high quality level at low cost. In fact, micromanipulators and microassembly systems are needed in order to manufacture these products. Considering the need of flexibility, microrobotics appears as an effective way to work in the microworld.

Microrobotics is the science and technology that involves the design, fabrication and control of microrobots. To succeed in microrobotics, an interdisciplinary approach is necessary. The concerned fields are electronics, computer science, artificial intelligence, mechatronics, nanotechnology, and bioengineering [ROB].

Typically, microrobots have dimensions ranging from a fraction of a millimeter up to several millimeters, miniaturized and sophisticated machines designed to perform a specific task or high precision repeated tasks.
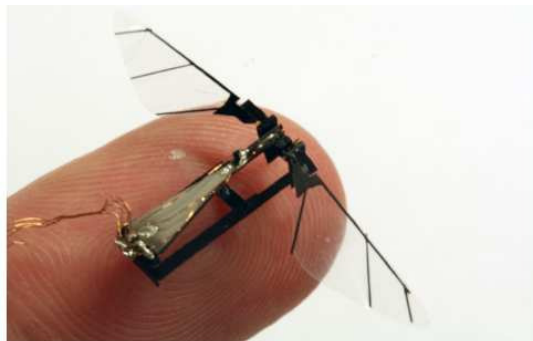
A flapping microrobot on a finger [BEN 2009].

In the above figure, a flapping microrobot is designed, bio-inspired by a flying insect. This

microrobot use two piezoelectric bimorph actuators connected. This design gives each wing two degrees of freedom (DOFs).

The domain of microrobotics leads to a great number of challenges in terms of physics, control, mechanical structures, actuations, etc., that is why it is so attractive for the researchers. The microworld gives a different world in terms of force interactions, perception, design, and realization. In fact, when the dimension goes down to submillimetric range, the manipulation of micro-objects is difficult because of the scale effects. The main difference between microscopic and macroscopic scales is due to the change of dominant forces. From the geometry dimension 1µm to 1 mm, the object contact is influenced by all of the electrostatic force, the surface tension, the capillary force and the Van Der Waals force. These mixed actions make the micromanipulation and microassembly a real challenge.

In order to achieve micromanipulation tasks, microrobots with some specific characteristics are required. Resolution and accuracy in the submillimetric range are needed in order to interact with micrometer sized objects. The size of the robot itself must be very low in order to facilitate handling of micro-objects and enable the execution of tasks in confined environments.

The traditional solutions used to build microrobots are based on active materials and closed-loop control. These active materials present some drawbacks making both their modeling and efficient control designs a hard task. Their behaviors are often complex, nonlinear and sometimes non stationary. Closed-loop control of the microrobots requires the design and the integration of very small sensors and the use of bulky and expensive instruments for signal processing and real-time operating. These solutions are confronted with many difficulties.

In order to avoid the drawbacks of traditional microrobots and open a new approach to design microrobots, the work presented in this thesis deals with the study of a new generation of microrobots using a modular concept and an open loop control strategy: digital microrobots.

Chapter 1 presents the research background and the motivation. The structure of microrobots based on microactuators and kinematic chains is studied. The various microactuation principles are investigated. Based on the microactuation principles, two kinds of control strategy are presented: one is the proportional signal control and the other is the repeated control (step by step). Perception technologies in microscale are also presented.

The chapter 2 presents the concept of digital microrobotics. We give the potential performances of a microrobot based on the association of several bistable modules. Notably, we obtain a microrobot that can reach a discrete workspace of which each reachable position is repeatable, stable with a blockage force through an open-loop control.

In chapter 3, an entire bistable module is designed. Three components are designed to obtain a bistable module with two stable and blocked positions switched by integrated actuators.

Firstly, bistable mechanisms are studied to establish a basic model. This model can ensure the bistable behavior of this mechanism. Secondly, several actuators that can be used to actuate the bistable mechanism are studied. Thirdly, a special compliant mechanism is designed to give a blockage force in stable position.

In chapter 4, according to the microfabrication limits, final dimensions of the bistable modules are defined. Several microfabrication processes have been tried. The use of a SOI wafer permits us to obtain the desired structure.

In chapter 5, static and dynamic characteristics of bistable modules have been studied. Static characteristics include the force versus displacement relation of bistable mechanisms and the voltage versus displacement of actuators. Dynamic characteristics consist in the study of the switching to those two stable positions. Based on the dynamic analysis, we propose a control strategy for switching between the stable positions with performances adapted to microrobotics tasks.

Chapter 1 Microrobotics

"Look back to the old, if you would learn the new."

– Confucius

(551 B.C. – 479 B.C.)

1.1 Introduction

Miniaturized systems integrating complex functions and intelligence are more and more present. Modern industry aims to develop manufacturing and assembly systems enabling to produce smaller and smaller goods. Moreover, even if the interfaces with the human require human scale dimensions, the active part has to be smaller and smaller. For example, the size of the switch (3 mm) under the keys of mobile phones has been divided by 3 in less than five years and in some cases, this switch is transformed into a small joystick to perform more complex functions.

To succeed in this miniaturisation, more and more products design becomes micromechatronics design in the sense that the functions are realized by the integration of mechanical, optical, acoustic and electronic components.

In order to adapt the miniaturization of the products to their fickleness and fast obsolescence, in particular in very competing sectors of high technology, it becomes increasingly necessary to develop flexible technologies allowing reliable manufacture of very small components and products with a high quality level and at low cost. For mini and micromechatronic products manufacturing, micromanipulators and micro-assembly systems are required. Considering the need of flexibility, microrobotics appears then as an effective way to work in the microworld. Fig. 1.1 shows the assembled microobjects with 250 µm dimension with microrobot system.

Microrobots are robots designed to perform tasks in the microworld, i.e. the world of the objects of which dimensions are micrometric; their workspace can be some micrometers to some millimeters.
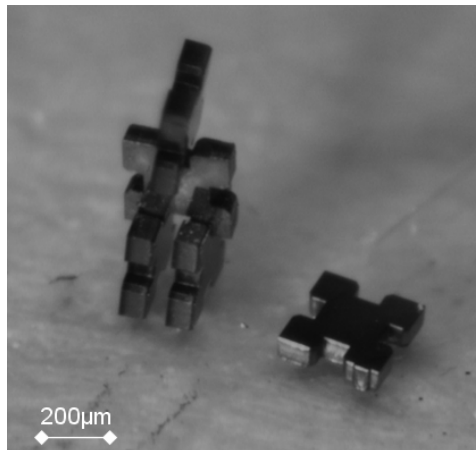
Fig. 1.1. Assembled microobjects [TAM 09].

According to the mode of work, two kinds of microrobots can be considered.

This first kind of microrobots has micrometer dimension, usually are made as mobile robots which can work in confined environment. Shown in Fig. 1.2, a mobile microrobot has 200 μ μm in length [DON 06]. It is actuated by electrostatic force. Two kinds of motions (rotation and translation) can be controlled.

This kind of microrobots presents advantages such as adapted dimension, good agility and untethered operation. However, it has drawbacks, such as missing integrated sensors, only plane DOFs and limited force.
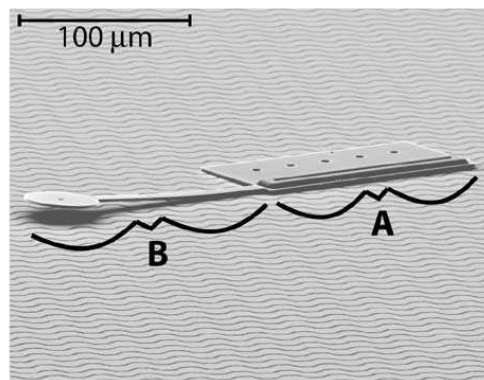
Fig. 1.2. A mobile microrobot. A: scratch drive actuator, B: cantilevered steering arm (B) [DON 06].

The second kind of microbots consists in robots which dimensions are not microscopic but are small enough to allow submicrometric resolution to manipulate micro-objects. This kind of microrobot are kitted out with micrometric size end-effector that permits to manipulate micro-objects.

Fig. 1.3 shows a microrobot from Kleindiek Nanotechnik kitted out with a 10 µm size gripper [KLE]. For physical reasons, end-effectors of the microrobots have to be at micrometric size.

Since they are directly in contact with the micro-objects, they are included in the microworld. Unlike the last kind, it needs to work in a specific plane area. This kind of microrobot can work in the 3D area.
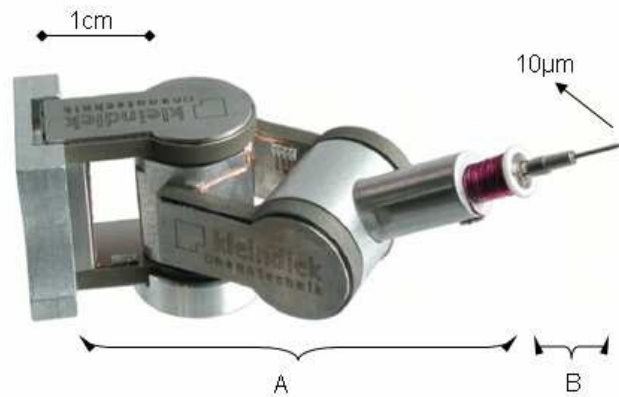
Fig. 1.3. A centimeter robot mounted end-effector. A: Robot mechanism, B: end-effectors [KLE].

When components have submillimeter dimensions, their manipulation is technically embarrassed because of scale-effects which increase when the dimensions decrease. Indeed, the range of the micromanipulation is currently defined as the manipulation of objects whose volume is between 10 and 10^4 μm^3 or who's the greatest dimension varies from some tens to some hundreds of μm. We are near the low limit of the classic mechanics. The laws of the Newtonian physics are most of the time valid and the quantic effects can be neglected. However, the main difference between microscopic and macroscopic scales is due to the change of dominant forces. Let us consider L as a length that is characteristic of a problem, the value of L^3 being inferior to the one of L^2 in the [0, 1] interval, the volume forces become negligible compared to the surface forces. Therefore, the forces relying on contact surface (electrostatic force, surface tension, van der waals force) become important in the microworld (see Fig. 1.4).

Moreover, precise determinations of the interaction force need deep studies crossing the model at the micro/nano-scale and the deformation of the surface. As in Fig.1.4, the forces are getting on for sphere/plan. Because of the mixture action of these forces, it leads to micromanipulation a big difficulty.

The scale effect arises many challenges, it requires new robotic functions, actuations, perceptions, handling and controls. These functions can not be directly transferred from the macroscale robotics and new principles of design have to be studied. The integration of these functions in a complete micromanipulation system and micro-assembly is also an ambition on which several proposals have been done but getting a station or a set of stations which are precise, repeatable, safe, efficient and flexible remain a challenge.

7
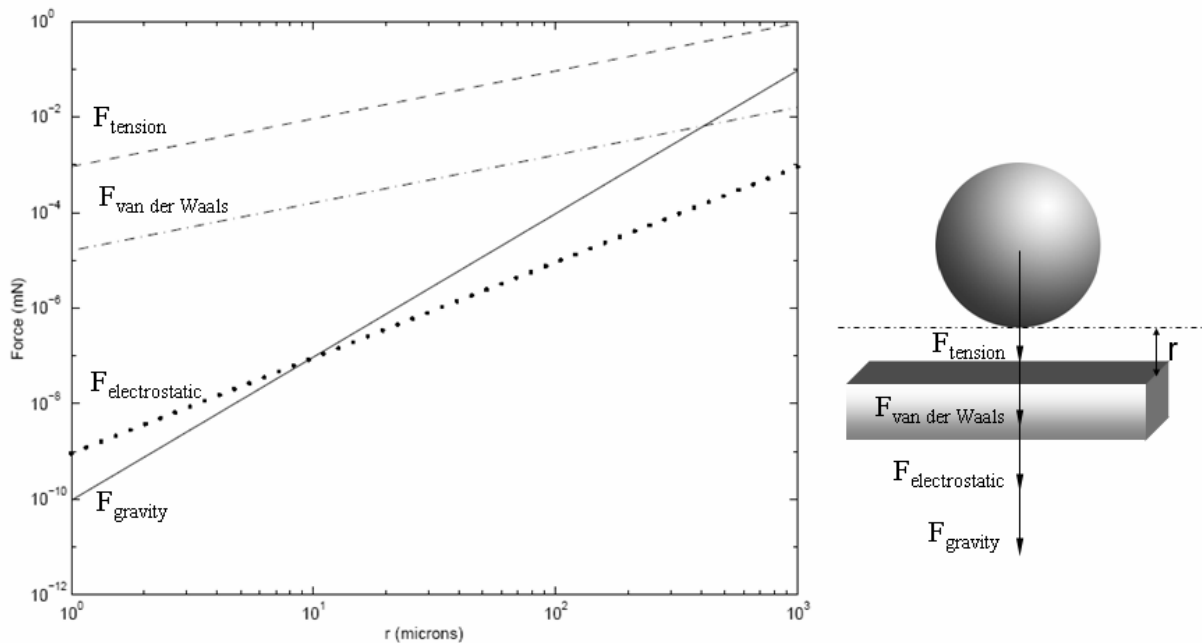
Fig. 1.4. The different forces in the microworld for a sphere/ plane interaction.

In this chapter, we first give some application fields. After that, we focus on the main components of microrobots: the structure, the actuators, the sensors and the control.

1.2 Application fields of microrobots

1.2.1 Microrobots in microfactories

The integration of microrobots inside microfactories which work as production systems is a challenge. This integration can be considered at different levels from the teleoperated station until the totally automated microproduction systems. The microfactory concept is the answer to the need of microrobotics systems integrated in automated stations.

An example of microfactory was developed by Mechanical Engineering laboratory (MEL). It is shown in Fig. 1.19. The entire system contains a micro-lathe, a micro-milling machine, a micro-press machine, a micro-transfer arm and a micro-manipulator. All the components are integrated into a portable box with 625 x 490 x 380 mm^3 in sizes. This microfactory is controlled by two multi-DOFs joysticks and vision assistance.
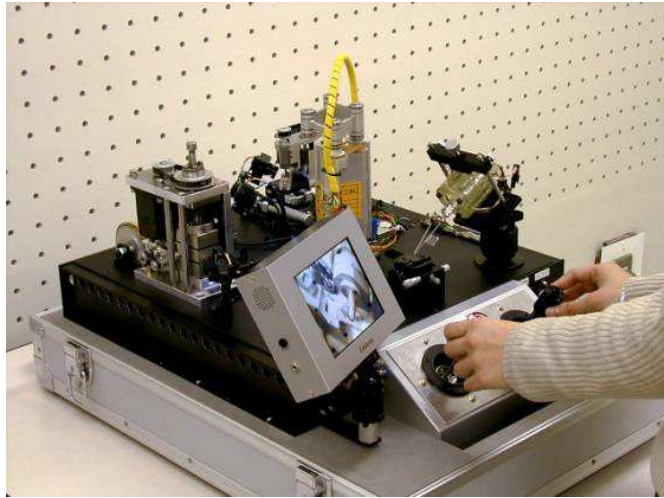
Fig. 1.5. A microfactory by Mechanical Engineering Laboratory (MEL), Japan [MEL].

Femto-st has developed several stations dedicated to micromanipulation and microassembly. One of stations is composed of 5 high accuracy axis (3 linear axis and 2 rotational axis) carrying a microgripper. This microgripper was designed in Femto-st (old Laboratoire D'automatique Besançon) and patented in 2002. This robotic device is associated to a vision device, which is a motorized binocular microscope. An environmental control is ensured by dust filtration (class 100). Robot is controlled by two computers, one for operator inputs (joystick, keyboard) and the other for real-time video stream. Video is used by both operator and computer for manual control and computer vision control.

As well as technical demonstrator and experimental platform, this microassembly robotic system is used to experiment research work on microassembly.
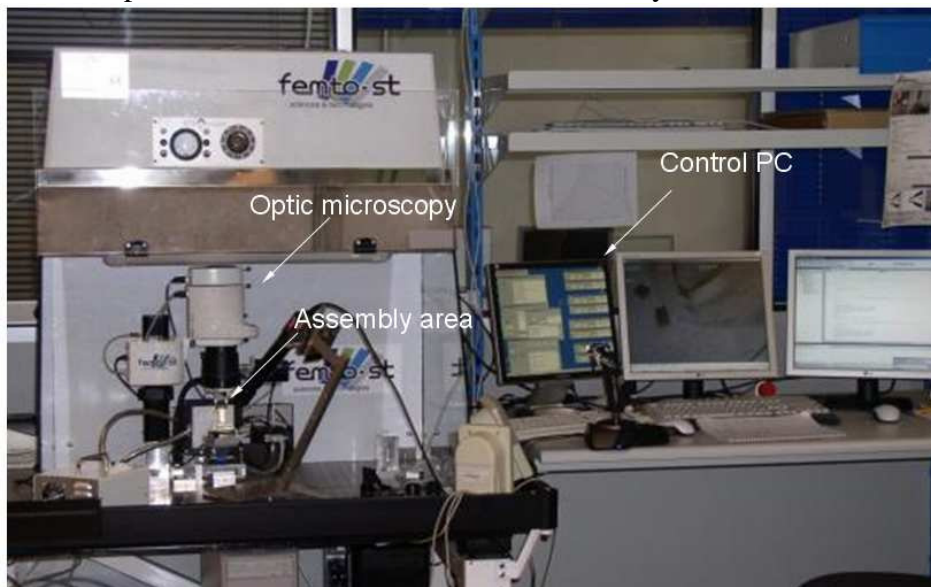
Fig. 1.6. Microassembly station at Femto-st/As2m.

Fig. 1.6 shows the large view of the micromanipulation/microassembly SAMMI platform. The robot is fixed on a vibration filtering table and protected by a laminar flow cabinet. Computers and joystick are visible on the right.
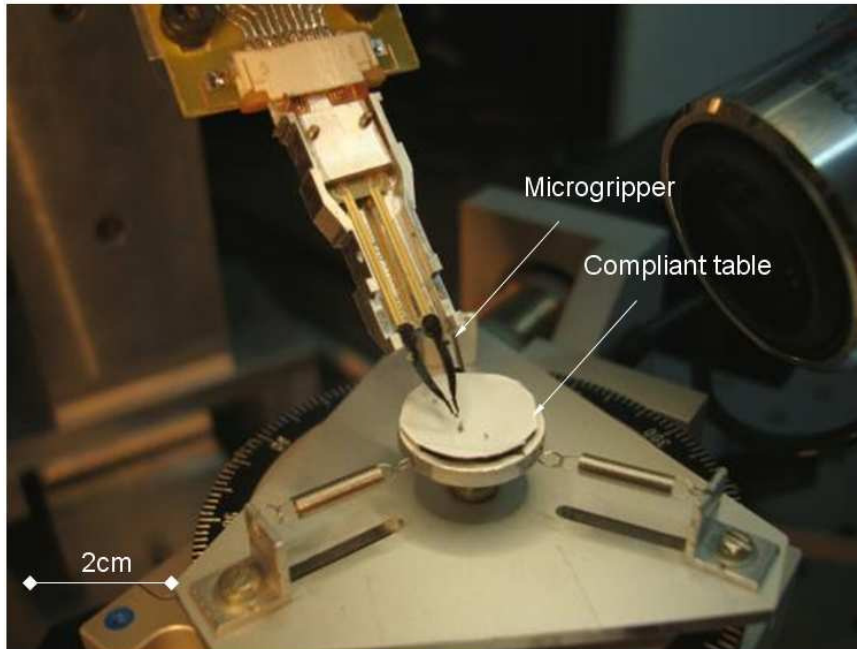
Fig. 1.7. Large view of assembly area.

A component placed on a compliant table with 400 µm in length is handled by microgripper visible on the center of Fig. 1.7. Two pieces with 100 µm are assembled in this station (see Fig. 1.8).
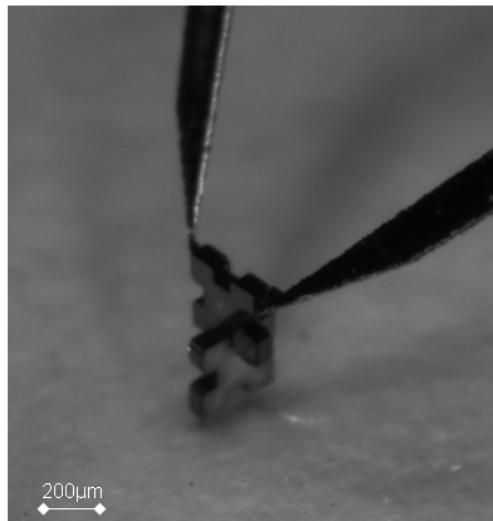
Fig. 1.8. Two assembled components by microgripper [TAM 09a].

10

This kind of system based on microrobots aims to perform automatic control of micromanipulation and microassembly tasks. These tasks allow us to fabricate complex devices and products for industrial or consumption applications.

1.2.2 Microrobots in biology and medical applications

Another field of application for microrobotics is in the biology. In the biology field, cells have typical micrometer dimensions. Researchers in this field wish to manipulate biologic cells, including positioning, sorting, selecting and separating biological cells. These manipulations permit to study various behaviors of different cells. Furthermore, in the genetic engineering, they also require manipulations to decode the gene, or even improve the human gene.

Fig. 1.9. Microinjection of the cell [TMW].

These manipulations need high accuracy and precise tools enable to perform complex tasks on fragile objects, in changing environments (see Fig. 1.9).

In the medical field, Microrobots may be used to inspect, treat or eliminate medical problems. The use of microrobots can inspect inside of human body, and reduce the pain using traditional inspecting approach. Moreover, some problems may arise due to the accumulation of unwanted organic substances, which interfere with the normal body functions, such as tumors, life threatening blood clots, accumulation of scar tissue, arterial blockage, and localized sites of infection. The microrobots can be introduced into the body through the circulatory system.

One of the effective approaches to kill the cancerous cells would be to enclose the entire tumor in a nano box and destroying everything in the box. The prospective scene in Fig. 1.10 shows a microrobot going to take out the cancerous cell in the human body.
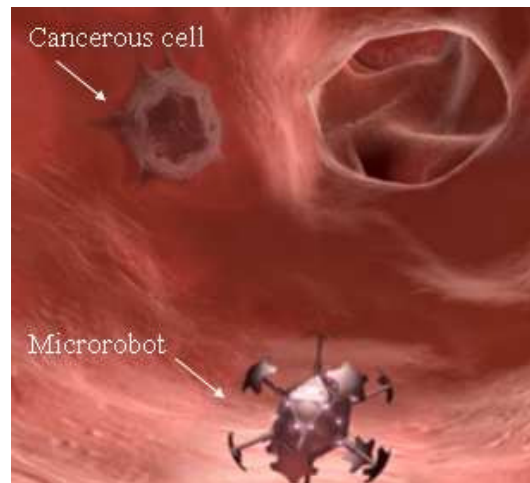
Fig. 1.10. Prospective view of microrobot in the human body [BMM].

1.3 Design of microrobots

Either for assembly or packaging of micro-objects including MEMS and MOEMS or the characterization of mechanical or biologic objects, specific microrobots have been designed. They are different from the traditional robots in the sense that their architecture, their actuation or their control are often different. We have seen that the main reason of this difference is the predominance of surface forces in the microworld. Microrobots have to feel their environment and their action on the objects they are touching. The sensing system has to be adapted to microscale, by which informations are given as the base for an automatic process.

The design of microrobots concerns the design of the carrier and the end-effector.
Concerning the design of the end-effectors which permit to handle and release the components, lot of works have been done in the world [LANG 08]. Indeed, because surface effects become predominant at microscale, the release of objects is difficult to perform and the study of necessary strategies is particularly interesting. Moreover, handling systems are often designed based on the use of smart materials that lead to control difficulties [LANG 08].

Concerning the carrier, usually, they are designed based on the miniaturization of mascroscopic concepts, and the size is centimetric or decimetric. The analyses of kinematics structure adapted to micromanipulation have been done most of the time for the handling system and not for the whole microrobotic structure.

Therefore, according to these considerations, we consider the design of microrobots through three main aspects:

- microrobot kinematics;
- adapted actuators for the microrobot kinematics;
- control and perception.

1.4 Kinematics for microrobots

The kinematic chains of traditional robots are built by three components: actuators (electromagnetic motors), links (most frequently rigid bodies), and joints (kinematic pairs) to obtain the desired degrees of freedoms (DOFs). However, microrobots can not be built on the same approach because of the physical reasons described previously. Special kinematics for microrobots has to be designed.

Kinematics chains aim to build connections from energy input (actuators) to mechanical energy output (end-effectors) to create desired motions. Different approaches are developed to design kinematic chains of the microrobots such as the bimorph mechanism [CAR 98], the parallel mechanisms, the topology syntheses of mechanism [KOTA 01], etc.

Before talking about these various mechanisms, we firstly introduce different connection joints. The transmission of the rotation and translation motions is realized by the connection joints. There are many traditional joints, such as hinges, sliders and universal joints. However, in microrobotics, there is another type of joint called compliant joint. The researches already done show that the use of compliant joints presents many advantages in the microworld.

1.4.1 Compliant joints

The traditional joints use the sliding area to create motions. Unlike this kind of joints, the compliant joint uses deformation to create motions. The compliance of the structure is defined by the structure geometry.

Two kinds of compliant joint are mentioned: the revolute joints (see Fig. 1.11a) and the translational joints (see Fig. 1.11b).

(a)

13

Concentrated compliant joint   Distribute compliant joint
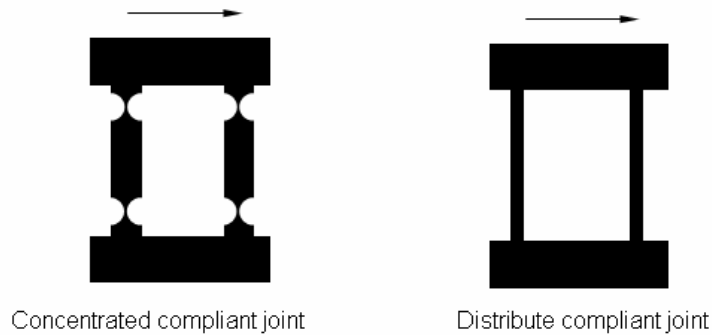
(b)

Fig. 1.11. (a) rotation of joint (b) translational joints.

The compliance of the joint depends on geometry and dimensions. For example, rotation stiffness of the compliant joint (see Fig. 1.12) can be given by:

$$k = \frac{2EI}{L^2}$$

E is Young's modulus, I is the moment of inertia.
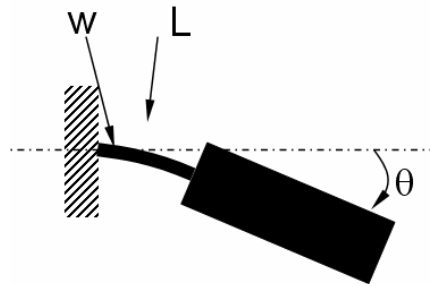
Fig. 1.12. Deformation of a compliant joint.

These compliant joints eliminate friction, backlash and wear. Further benefits include sub-micron accuracy due to their continuous monolithic construction. Such accuracy is important in many micro or nano-applications. The monolithic fabrication also enables a low-cost process. However, it presents some drawbacks such as the limited motion range, changing rotation centre, etc.

1.4.2 Bimorph mechanisms

The bimorph mechanism is a kind of mechanism widely used in microrobotics, as bimetal beam, bimorph actuator, etc. Generally, Bimorph mechanism consists of two active layers. The displacement can be created because of the asymmetric deformation via:

- Thermal activation (a temperature change causes one layer to expand more than the other).
- Electrical activation as in a piezoelectric bimorph (electric field(s) cause one layer to extend and the other layer to contract).

(a)

(b)
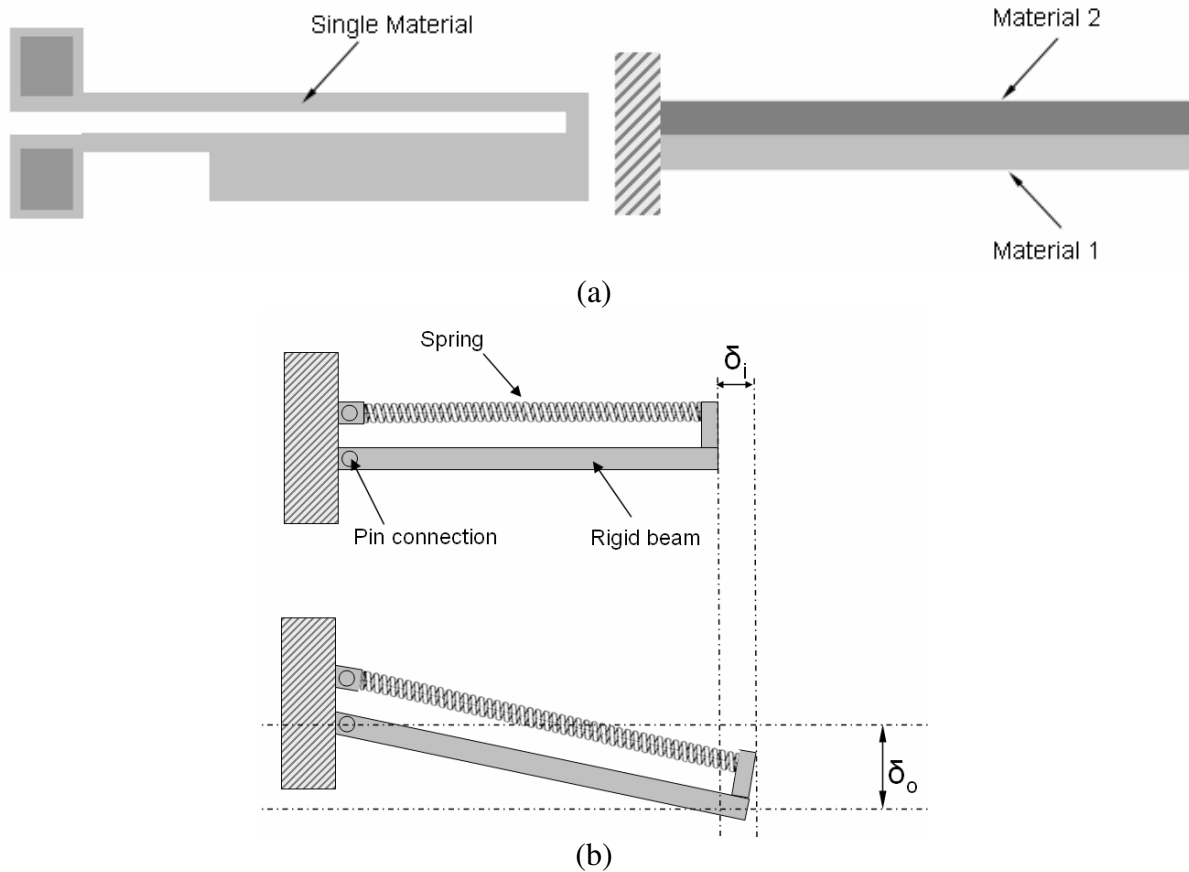
Fig. 1.13. (a) classic bimorph mechanism (b) a model of a bimorph mechanism.

As shown in Fig. 1.13b, the input displacement δ_i of spring leads to an output deflections δ_o. In fact, in the real situation, the pin connection is replaced by a compliant joint, and the elongation of spring is made by actuating active material or electrothermal expansion effect.

Another example uses this principle (see Fig. 1.14). A PZT stack is used as the input end, the output ends are two fingers [CAR 98]. The input PZT gives the external beam (as spring) elongation, which leads to the internal beam deflection at the position A. So, the position B is led to a bigger deflection.

In fact, the use of the piezoelectric material, electro polymer bimorph, etc, can take the same principle to amplify the motion range. To sum up, the key of this amplification mechanism is to create the deformation difference between two materials.
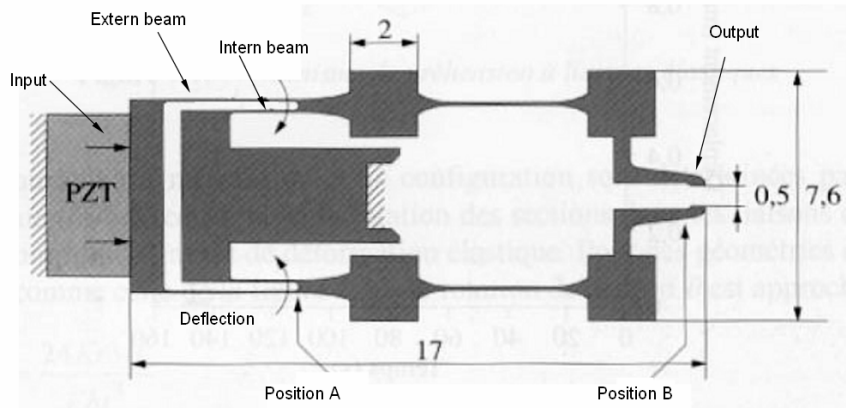
Fig. 1.14. Example of bimorph principle [CAR 98].

1.4.3 Topology synthesis of compliant mechanisms

Compliant mechanism synthesis has been performed by large number of researches. This method includes two common tasks: (a) topology generation (b) size and shape optimization [KOTA 01].

Topology generation provides qualitative results of a kinematics. This mechanism may not be the best solution in the size and shape. Therefore, once the topology is generated, the next step is to perform a size and shape optimization.

The goal of this first stage in compliant mechanism design is to generate a topology (configuration) to meet defined input-output force-displacement relationship. There are two commonly used schemes for initial discretization in the topology synthesis: the use of homogenization method and the use of an initial beam/truss element network.

As can be seen from the flowchart in Figure 3, the proposed approach includes 3 major components:

- The embedded finite element analysis that solves the structural deformation.

- The curve comparison algorithm that measures the deviation between the deformed and target curves.

16

- The overall optimization problem that searches for the optimal topology and dimensions.
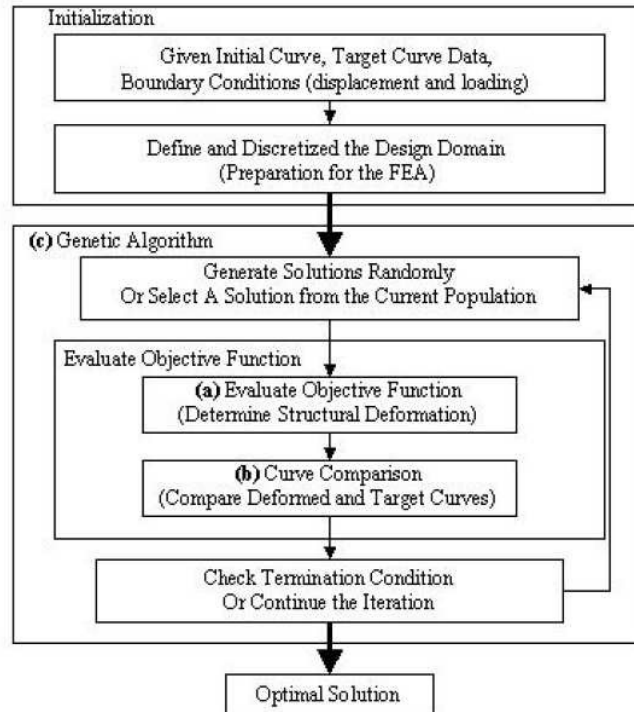
Fig. 1.15. Flowchart of compliant mechanism synthesis [KOTA 01].

Fig. 1.16 shows an example of amplification mechanism designed by compliant mechanism synthesis, which amplify the input motion 20 times.
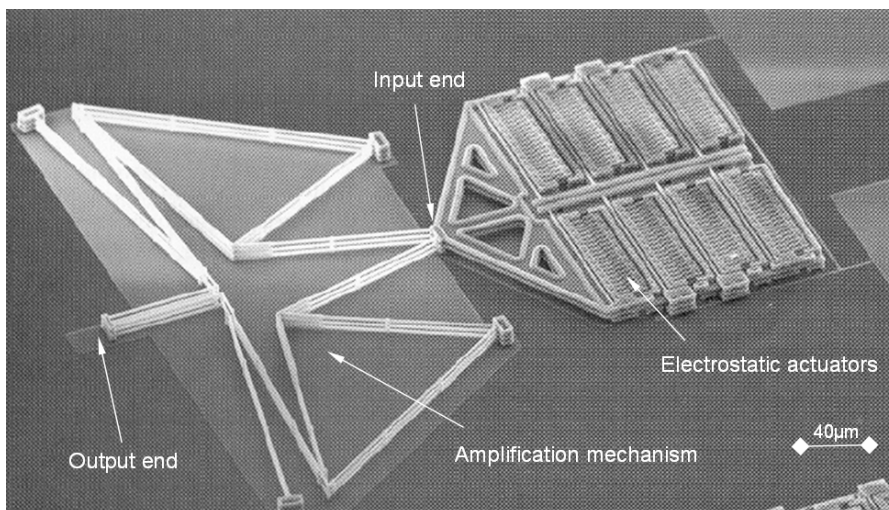
Fig. 1.16. Example of topology synthesis mechanism [KOTA 01].

17

This method is complex and requires special computer program to perform the design. But, it gives optimized solution to satisfy the requirement between input and output. The main developed program resolves the single input-output problem. Recently, some researches are done in developing algorithm to resolve multi-input and multi-output problem [GROS 08].

1.4.4 Parallel microrobots

Parallel robots have played an important role over the last 20 years wherever they were used in the macro or micro world. A parallel robot is a closed-loop mechanism in which the mobile platform is connected to the base by at least 2 serial kinematics chains.
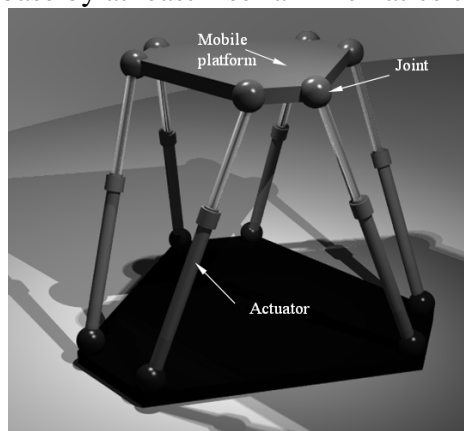
(a)

(b)   (c)
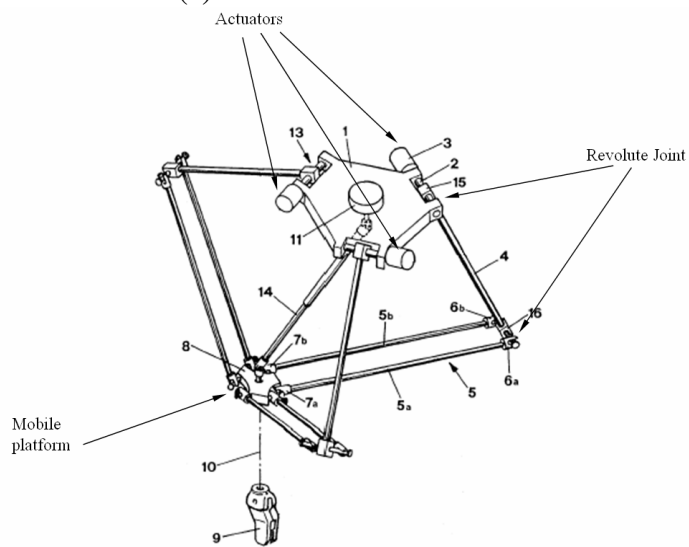
Fig. 1.17. (a) Steward platform (b) Delta robot (c) Schematic of the Delta robot (from US patent No. 4,976,582).

Typical parallel robots are Stewart platforms or Delta robots (see Fig. 1.17). The joints have rotation DOF as the passive connection which can support the platform and increase the stiffness of the whole structure.

This traditional robot requires accurate assembly of sensors, actuators and connection joints. Due to previously presented scale effects, traditional assembly can not be realized in the microworld. However, researches found that the use of monolithic structures fabricated by microfabrication technology present many advantages. Thanks to these techniques, the parallel microrobot with integrated actuators and the various parts can be fabricated. It is a potential candidate for microrobotics applications.

D. Mukhopadhyay [MUK 08] proposed a parallel mechanism (see Fig. 1.18). It is a planar $xy\theta$ positioner with linear electrostatic actuators.

(a)

(b)
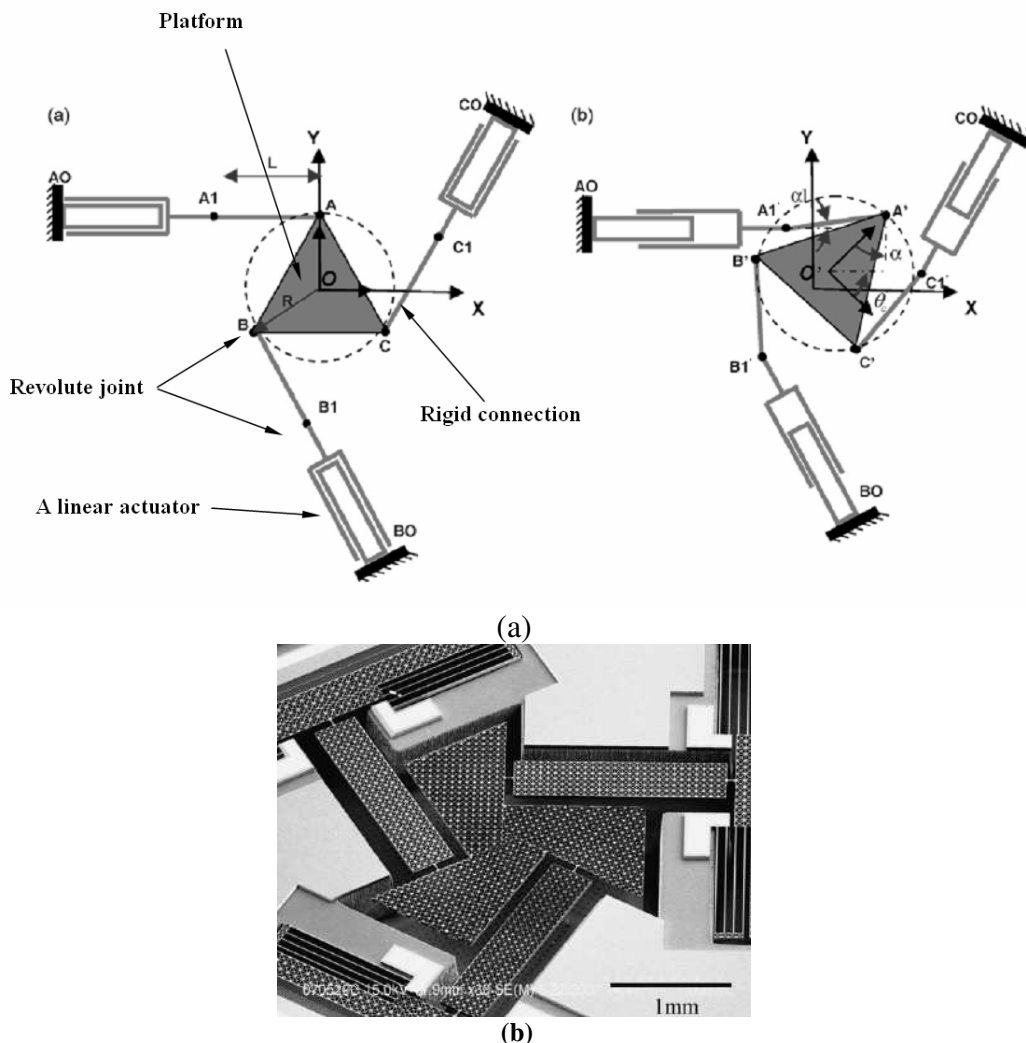
Fig. 1.18. (a) Schematic of a xyθ positioner (b) Fabricated positioner [MUK 08].

19

This parallel mechanism consists of a platform connected to the base by three identical kinematic chains. Each chain consists of a prismatic joint connected to a fixed base on one end and to a rigid link on the other end via a compliant joint. This parallel mechanism can be open-loop controlled by identifying the Jacobian matrix. Since there is no any sensor, the repeatability and the accuracy can no be ensured.

The use of microfabrication technology permits to fabricate parallel microrobots with high resolutions, monolithic structure and micrometer dimensions. However, repeatability and accuracy can not be ensured because the sensors are not integrated.

1.5 Actuators for microrobotics

Microactuators are key components for MEMS or microrobots. Microactuators transform electrical energy, thermal energy, magnetic energy, etc. into mechanical energy.

Thanks to the efforts of researchers, various microactuation principles such as thermal expansion, magnetic actuation, electrostatic actuation, piezoelectric actuation and shape memory alloys have been developed. Many original, smart microactuators have been designed, fabricated and tested. In the next section, a brief review based on actuation principles is presented.

1.5.1 Electrothermal microactuators

Thermal expansion is the property of materials to change in volume in response to a change in temperature, where the change is approximately proportional to the material's coefficient of thermal expansion. The table gives the coefficient of linear thermal expansion of three types of materials: metal, semiconductor and insulator.

Tab. 1.1. Coefficient of linear thermal expansion of different materials.

Material		Coefficient of linear thermal expansion (1/C)
Metal		13 to 25×10^{-6}
Semiconductor		3 to 6×10^{-6}
Insulator	Silicon oxide	0.5×10^{-6}
	Glass	8×10^{-6}

As shown in the table 1.1, the linear expansion leads to very few changes in length and researchers have design various mechanisms to amplify this linear motion.
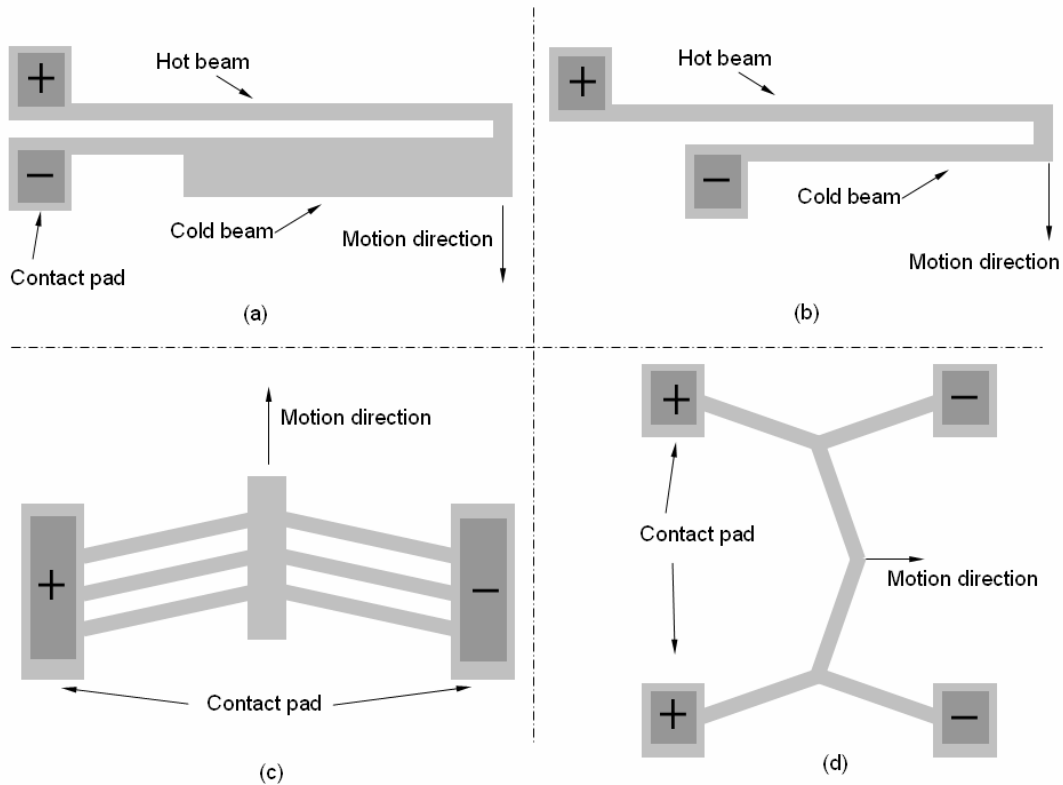
Fig. 1.19. Example of amplification of thermal actuators (a, b) U-shape, (c, d) V-shape, cascaded V-shape.

Fig. 1.19 shows the U and V shape thermal microactuators and their mutant shapes. The U-shape microactuator consists of two beams: a thin beam and a thick beam. Because of the asymmetric expansion in these two beams, transverse motion is obtained. The V-shape thermal microactuator consists of a curved beam. The symmetric expansion creates a flexion in the middle of the beam.

Since the asymmetric expansion results from Joule effect, this approach permits to build an actuator with a single layer (unique material). The temperature change can be achieved internally by electrical resistive heating (Joule heating) or externally by a heat source capable of transferring the heat to the actuator.

Fig. 1.20 presents a bi-metallic thermal actuator. In this configuration, both materials are heated to the same temperature, but deflection results from different coefficient of thermal expansion.
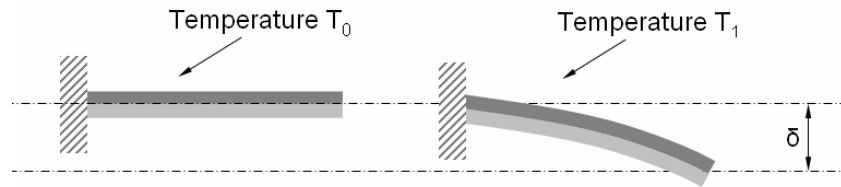
Fig. 1.20. Bi-material thermal microactuator.

The advantages of thermal microactuators are the fast heating (electro-thermal effect) and compatibility with microfabrication technology. The drawback is the reverse transformation. The cooling will reduce the response time of the actuator.

1.5.2 Electromagnetic microactuators

Ferromagnetic material (such as Ni, Fe, Co, NiFe, NdFeB) presents attractive effects when subjected to a magnetic field [GIB 04]. Ferromagnetism is the basic mechanism which is widely used for most phenomena of magnetism.

The ferromagnetic material can be soft magnetic material or hard material, while soft materials such as permalloy (FeNi) are relatively easy to prepare in film form by electrodeposition and sputtering.
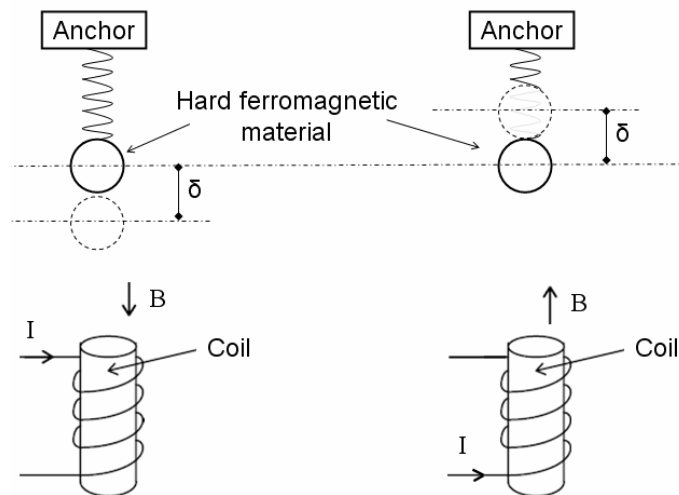
Fig. 1.21. Electromagnetic force.

Although soft magnetic materials can be obtained easier than hard magnetic materials, hard magnetic or permanent magnetic materials would be more appropriate in some cases. For

example, hard magnetic materials with a high remanent magnetization can be conveniently used in bi-directional (push-pull) microactuators [CHO 00].

In order to make an electromagnetic microactuator, a ferromagnetic material and a coil are required (see Fig. 1.21). However, the fabrication of a microcoil is a hard task. This is why traditional electromagnetic motor are not widely used in the microworld.

L.K. Lagorce [LAG 99] designed an electromagnetic microactuator based on polymer magnets. The basic structure of the fabricated cantilever beam microactuator is illustrated in Fig. 1.22. A polymer magnet magnetized in thickness direction is screen-printed onto the free end of a copper cantilever beam. On the other side of the substrate, a planar square coil produces the magnetic field gradient necessary for the actuation of the magnet. Because Polymer magnet is a permanent magnet, the change of the electric current direction can result in a change of the deflection of the magnet.
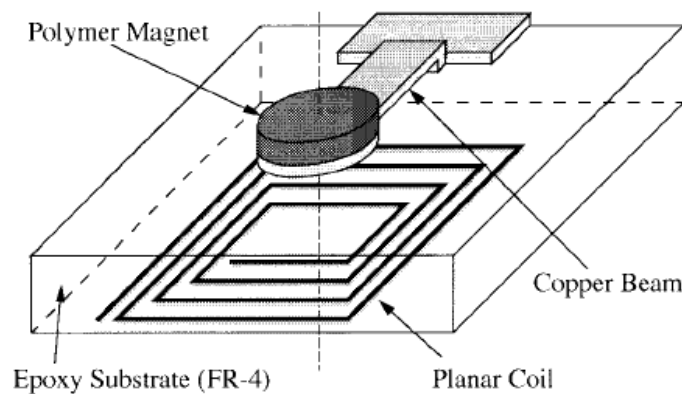
Fig. 1.22. Electromagnetic microactuators based on polymer magnets [LAG 99].

Magnetostrictive materials are a type of material which deforms due to the applied magnetic field; it has been firstly discovered by James Joule. Typical magnetostrictive material is known as Terfenol-D, including rare earth elements with iron which has the available strains of more than 1000 parts per million at room temperature with a relatively small applied fields [TDD] [ROT 92]. Fig. 1.23 shows the strain versus magnetic field (H) that presents saturation at high field.

The use of electromagnetic materials presents fast response time, great force, wireless actuation, bi-direction actuation (for hard magnetic materials), etc. However, the fabrication of coil limits their applications in the microworld [CHO 00] [OKA 09].
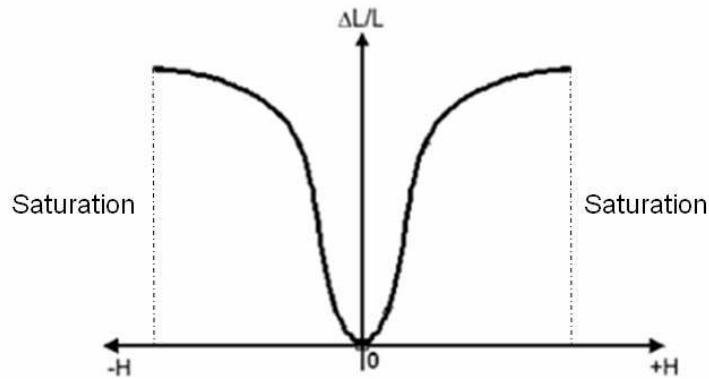
Fig. 1.23. Magnetic field Vs strain for a Terfenol-D material.

1.5.3 Electrostatic microactuators

Electrostatic charge can exert a force between the charged objects according to the Coulomb law [CL]. Although only a small force can be obtained, this could be useful in the microworld.

The simplest type of electrostatic actuators consists of a movable plate which is pulled toward a parallel electrode under the application of a voltage difference. This type of actuator is illustrated in Fig. 1.24.
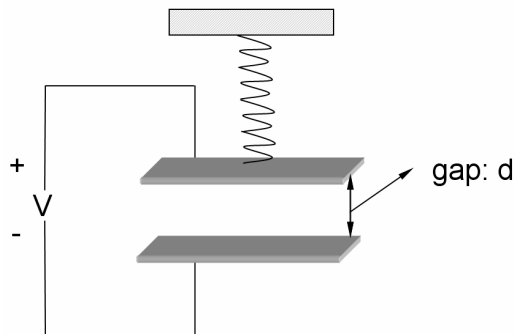
Fig. 1.24. Parallel plate electrostatic actuator.

The movable electrode is suspended by a mechanical spring, which is usually a simple microfabricated cantilever. When a voltage is applied across the electrodes, opposite charges on each plate attract each other. However, unless they touch, the electrodes only draw sufficient current to charge the actuator's effective capacitance, resulting in low power requirements.

The attractive force is given by:

$$F_e = \frac{\varepsilon S V^2}{2d^2}$$

S: area

24

d: gap
ε : Permittivity

The spring force increases linearly with the gap between these two plates, but the electrostatic force increases faster while there is a small gap. So there is a maximal applied voltage, when we go though this voltage, these two plates will be contacted, this is called pull-in effect.

The spring force is given by:
$$F_s = k(d_0 - d)$$
k: the spring constant
d_0: initial gap

$$\begin{cases} F_g = F_s \\ \dfrac{\partial F_g}{\partial d} = \dfrac{\partial F_s}{\partial d} \end{cases}$$

Using these equilibrium conditions, the maximum applied voltage can be found:

$$V_m = \sqrt{\frac{8kd_0^{\ 3}}{27\varepsilon S}}$$

The gap is:
$$d = \frac{d_0}{3}$$

This gap is the maximum motion distance. If the motion is beyond this distance, these parallel-plate actuators suffer from instability for voltages beyond a threshold known as the "pull-in" voltage. For voltages beyond the pull-in voltage, the electrostatic force grows more quickly than the mechanical spring force, causing the two plates to contact each other.

Hence, these actuators can not be stable operated for deflections larger than this unstable position. However, many types of mechanical springs, including fixed-fixed beams, exhibit nonlinear deflection characteristics, leading to a larger usable deflection range. To avoid the pull-in effect, Comb drive electrostatic microactuators are a good solution. As parallel-plate actuators, comb drives consist of one fixed and one movable electrode. The electrodes are shaped as interdigitated combs as shown in Fig. 1.25.

This configuration leads to a constant force over the whole range of deflection of the movable comb. As long as each comb finger is perfectly centered between two opposed comb fingers, the transverse force acting on that finger will be null.

The electrostatic actuator offers a very high efficiency actuation because of low current consumption, and the response time is very fast. They could be designed and fabricated easily

by micromachining technology. But, when the electric field must act over larger distances, a higher voltage will be required to maintain a given force.
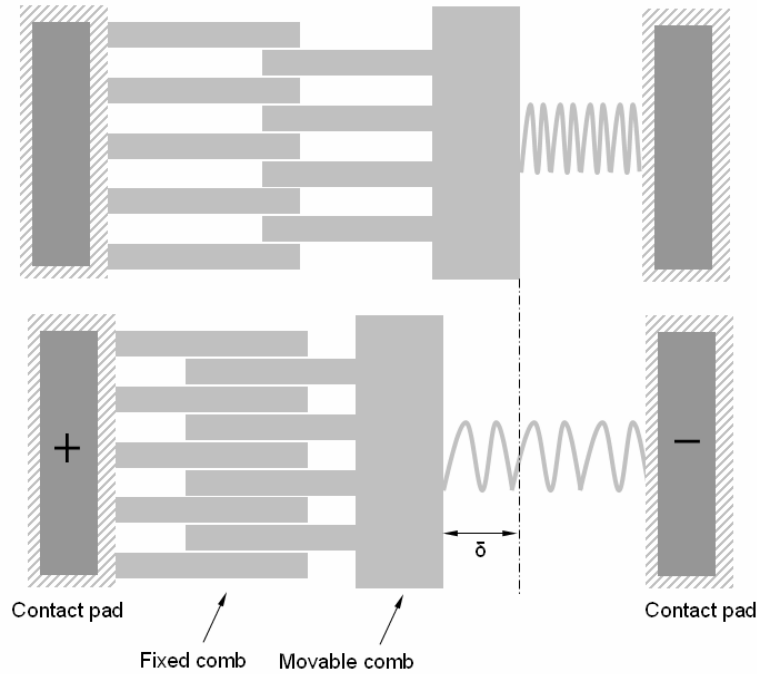
Fig. 1.25. Principle of the comb drives electrostatic microactuator.

1.5.4 Piezoelectric microactuators

Piezoelectric actuators are the most widely used actuators as active material because of their high operating frequency range and power density.

Piezoelectric materials change their shapes under an electric field. This change can be described by defined directions. Since the polarization of piezoelectric materials leads to an anisotropy deformation, the direction of the piezoelectric material is defined as in Fig. 1.26.
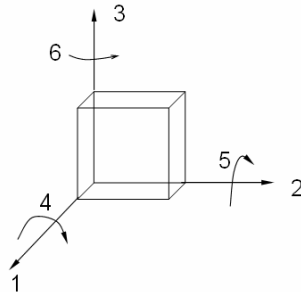
Fig. 1.26. Numbering of the direction for the piezoelectric parameters.

Typical piezoelectric materials include quartz (SiO_2), lead zirconate titanate (PZT), lithium niobate, and polymers (polyvinyledene fluoride (PVDF)). Fig. 1.27 shows the deformation of a piezoelectric material under different electric fields. The coefficients d_{15}, d_{33}, d_{31} represent the deformation ratio versus voltage in the different directions.
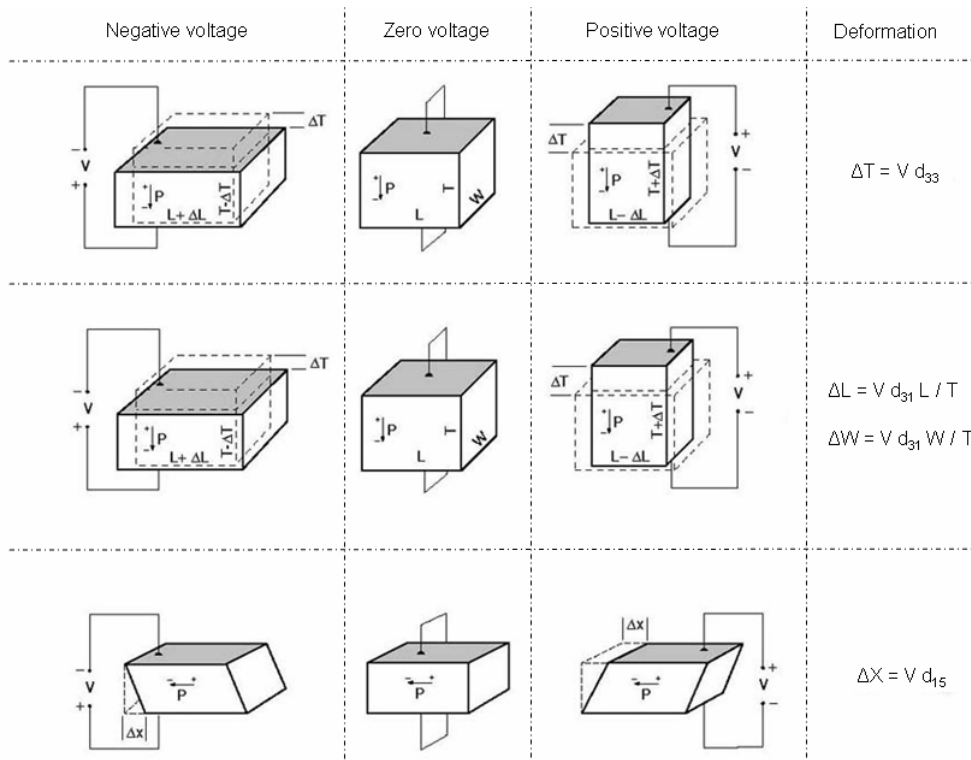
Fig. 1.27. The piezoelectric material under voltage.

Tab. 1.2. The range of the coupling coefficients.

Materials	Coupling coefficients		
	d_{31} (10^{-12} C/N)	d_{33} (10^{-12} C/N)	d_{15} (10^{-12} C/N)
PZT	From -100 to-300	From 300 to 600	From 500 to 800
Quartz	-2.3	-0.67	4.6

According to this table, the motion range of piezoelectric material is very small. The actuator is usually realized by building a piezoelectric stack or a piezoelectric unimorph or bimorph to amplify the motion range. Many devices, such as microgrippers, micropositionners and oscillators have been realized using this principle.

Unimorph piezoelectric structure is made by bonding a piezoelectric material with another material (usually metal). Unimorph structure results in out of plane displacement under voltage [see Fig. 1.28 a]. Two piezoelectric unimorph beams build a microgripper to manipulate microobjects.

(a)
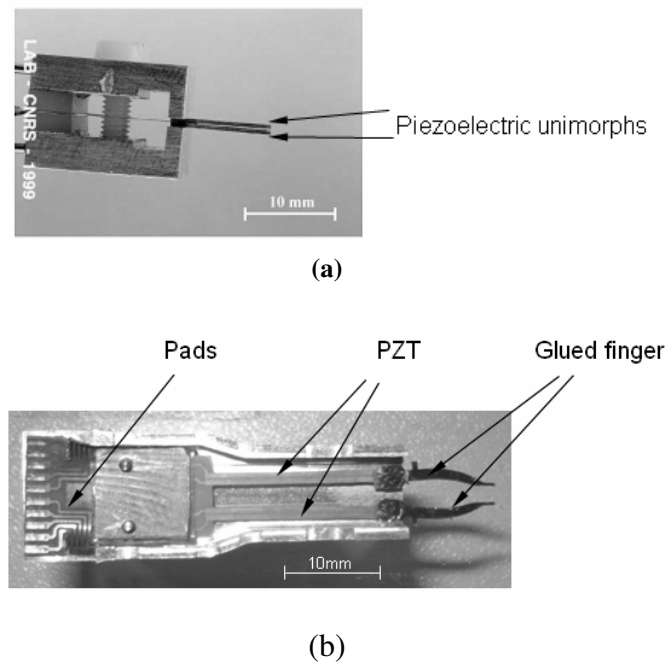
(b)
Fig. 1.28 (a) Microgripper including two unimorphs (Y. Haddab of Femto-st institute) [Yas 04](b) Two DOF microgripper (J. Agnes of Femto-st, institute) [AGN 03].

Although most of piezoelectric microactuators are based on traditional machining, piezoelectric thick film integrated silicon substrate has received considerable attentions in recent years for potential applications in MicroElectroMechanical Systems (MEMS) devices [MURA 05] [AKA 04] [WANG 07]. These piezoelectric thick film are made by dispersing submicro-sized (100-300nm) PZT powder (APC 850) into PZT sol-gel precursor solution (Zr/Ti = 53/47). PZT films were patterned by photolithography with S1818 photoresist and wet etched in HF/HCl [HAI 09].

1.5.5 Shape memory alloys microactuators

Shape memory alloys (SMA) are materials that present the property to recover its initial shape after a deformation due to heating induced phase changing. The phase from martensite to austenite is induced by a thermal energy.

The principle of SMA is shown in Fig. 1.29. SMA material endures firstly an elastic deformation at temperature T. When it is heated to temperature T+ΔT, it turns back to original shape, and it keeps this form at temperature T. When SMA material is deformed plastically, the induced plastic deformation can not be reversed completely.

28

The transition from the martensite phase to the austenite phase is dependent on the temperature and stress. While martensite can be formed from austenite by rapidly cooling carbon-steel, this process is not reversible, so steel does not have shape memory properties.
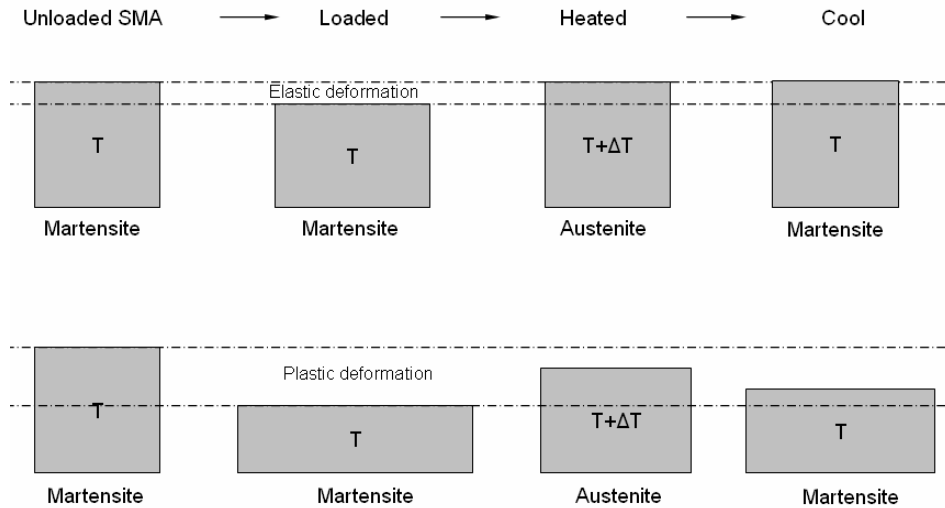
Fig. 1.29. Principle of SMA.

Shape-memory alloys (SMAs) have a lot of desirable properties: high power to weight (or force to volume) ratio, thus the ability to recover large transformation stress and strain upon heating and cooling, pseudoelasticity (or superelasticity), high damping capacity, good chemical resistance and biocompatibility [OTS 99] [HUM 99].

Besides the traditional applications, thin film SMA has been recognized as a promising and high performance material in MEMS applications, since it can be patterned with standard lithography techniques and fabricated in batch process [KAL 97] [MAK 00a] [MAK 00b]. The main advantages of TiNi thin film include high power density, large displacement and actuation force, low operation voltage, etc [FU 04].

Ferromagnetic shape memory alloys

Ferromagnetic shape-memory alloys (FSMA or MSH) are materials that exhibit large changes in shape and size due to an applied magnetic field. The key factor behind this phenomenon is martensite transformation of the crystal lattice below a certain temperature. In fact, a FSMA is first a SMA but it presents more interesting property that different variants of martensite can be changed under magnetic fields.

In FSM materials, when a sample is exposed to an external magnetic field in the martensitic phase, the magnetic field tends to realign the magnetic moments along the field. The resulting deformation can be as large as 10 % [GAU 08a], [GAU 08b].

29
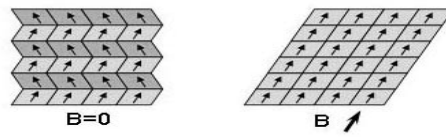
Fig. 1.30. Principle of FSMAs.

Therefore, the material is an attractive candidate for a new class of magnetic actuators or microactuators. Since then, various ferromagnetic shape memory alloys are investigated.

1.5.6 Electroactive Polymers microactuators

Electroactive polymers (EAPs) are polymers whose shape is modified under voltage (see Fig. 1.31). They present a large amount of deformation and sustaining large forces possibilities. Due to the similarities with biological tissues in terms of achievable stress and force, they are often called artificial muscles, and have the potential for application in the field of robotics, where large linear movements are often needed.
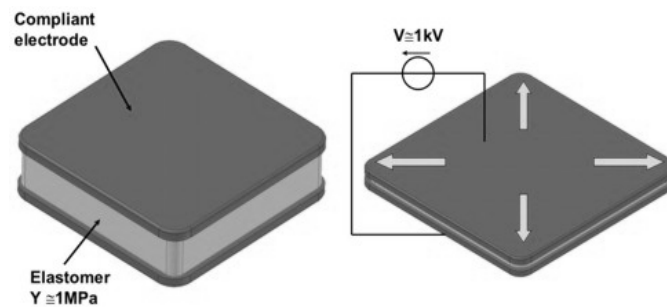
Fig. 1.31 Principle of electroacticve polymers [LMTS].

EAP can have several configurations, but are generally divided in two main classes: Dielectric EAPs and Ionic EAPs.

Dielectric EAPs: the actuation results from electrostatic forces between two electrodes which squeeze the polymer. This kind of EAP is actuated by large voltages (usually several thousand of volts), but very low electrical power consumption. Dielectric EAPs require no power to keep the actuator at a given position.

Ionic EAPs: the actuation results from the displacement of ions inside the polymer. Only a few volts are needed for actuation, but the ionic flow implies a higher electrical power needed for actuation, and energy is needed to keep the actuator at a given position. Examples of ionic EAPS are conductive polymers, ionic polymer-metal composites (IPMCs) [FUK 05] [SHA 98].

1.5.7 Summary on the actuators based on smart materials

Each of the previous microactuators offers advantages and drawbacks. There is no microactuator with perfect performance. Usually we should find the tradeoff between the power/mass ratio, machining, integration, etc. to choose a microactuator for a specific application.

We can classify these microactuations by three classes from the point of view of energy transformation. The first class is the transformation from magnetic to mechanic energy. The second one is the transformation from thermal to mechanic energy. The third one is the transformation from electric to mechanic energy.

Table 1.3 summarizes the main characteristics between different principles of microactuators. The characteristics of the microactuation include work per unit volume, work per unit volume, typical response time, microfabrication process, connection approach.

Tab. 1.3. Comparison between different microactuation principle.

Energy transformation	Actuator Method and Device	Work per Unit Vol (J/cm³)	Bi-direction actuation	Typical Response	MicroFabrication	Connection
Magnetomechanic	Magnetic	0.9	Yes	1ms-10ms	yes	No connection needed
	Magnetic shape memory alloys		No		yes	
	Magnetrotrictive		Yes		yes	
Thermomechanic	Thermal expansion	0.02	No	100-800ms	yes	By convection or wire
	Shape memory alloys	6	No		yes	
Electromechanic	Piezoelectric	0.02	Yes	1ms-100ms	yes	wire
	Electrostatic	0.4	No		yes	
	Electroactive polymers		No		yes	

1.5.8 Control of the microrobot

1.5.8.1 Control of the microactuator

Microactuators are designed based on these microactuation principles. They produce mechanical deformations by response of the energy input. The mechanical deformation presents intrinsic drawbacks. The typical intrinsic characteristics are [RAK 06a] [RAK 06b] [RAK 09a] [RAK 09b]:
- Hysteresis
- Creep

- Plasticity
- Relaxation
- Fatigue

Fig. 1.32 shows the creep and hysteresis phenomena of piezoelectric bimorph beam.

(a)   **(b)**
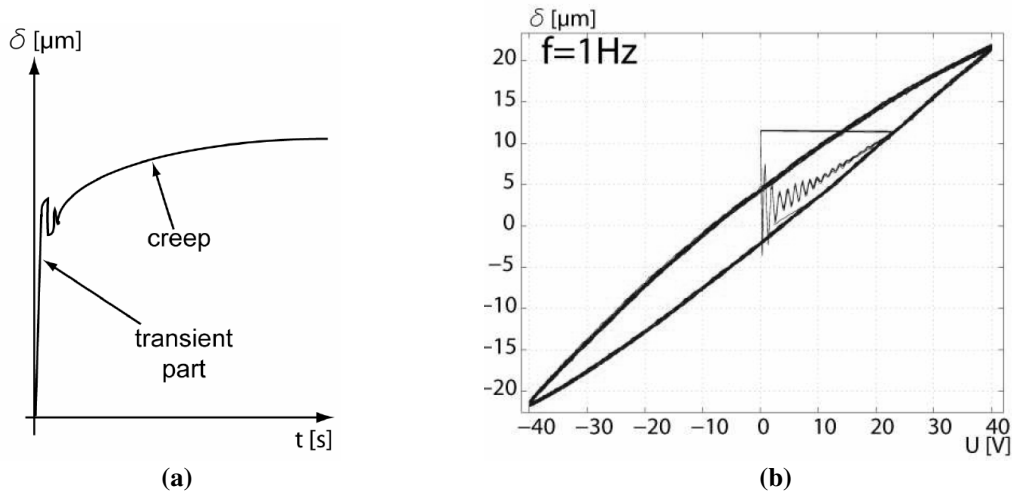
Fig. 1.32. (a) A creep phenomena of piezoelectric bimorph beam [RAK 09a]. (b) Hysteresis of a piezoelectric bimorph beam [RAK 09a].

These characteristics lead to unwanted behaviors when they are used in microactuator. It will reduce repeatability and accuracy. A precise mathematical model could be built to make a precise open-loop control. Otherwise, Closed-loop control techniques can be a solution to reach substantial performance (accuracy, repeatability, disturbances and vibration rejection.) [RAK 09a] [RAK 09b]. However, the integration of smaller sensor into a small actuator is also a hard problem.

Furthermore, the change of work conditions will result into the loss of high precision. There are a lot of factors which influence the control of microactuator such as the temperature, noises, and humidity [RAK 09a] [RAK 09b]. These uncertain factors increase hugely the difficulty to perform a precise control.

1.5.8.2 Microrobots controlled by proportional signals

As presented previously, the active material presents small deformations, For example, a piezoelectric ceramic of 1 mm in length produces a displacement of 1 µm under electric field [CHA 09]. The use of amplification mechanism can increase this displacement.

The final displacement of a single DOFs microrobot is controlled by amplitude of input signal, we call it proportional control. This kind of control can be used to control the bimorph mechanism, compliant mechanism, mechanism based on topology synthesis, and parallel mechanism, etc.

Fig. 1.33 presents an amplification mechanism which is designed by topology synthesis. This mechanism is built with an electrostatic actuators and an amplification mechanism. A voltage is applied to the electrostatic actuators, and the output tip moves. Their final position is maintained by the input voltage. It is possible to reach a high precision using calibration techniques. This single DOF mechanism can reach the desired position by a simple proportional signal.
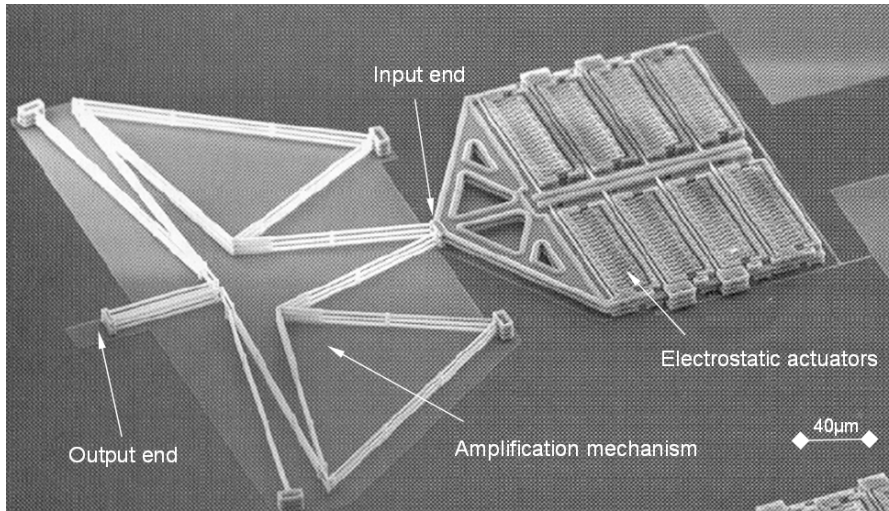
Fig. 1.33. Single input-output mechanism [KOTA 01].

A parallel mechanism is designed by Q. Yao (see Fig. 1.34 and Fig. 1.35) [YAO 08]. It is a 3 DOFs parallel mechanism actuated by linear piezoelectric actuators. Three identical piezoelectric actuators are placed at a vertical angle (Z). This configuration permits to create a displacement in plane (X and Y) and out-of-plane (Z).
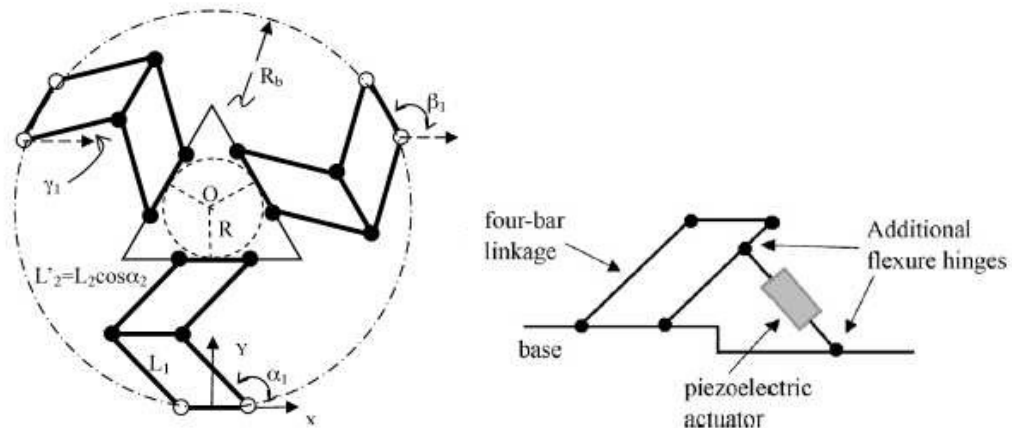
Fig. 1.34. A parallel mechanism with piezoelectric actuators.
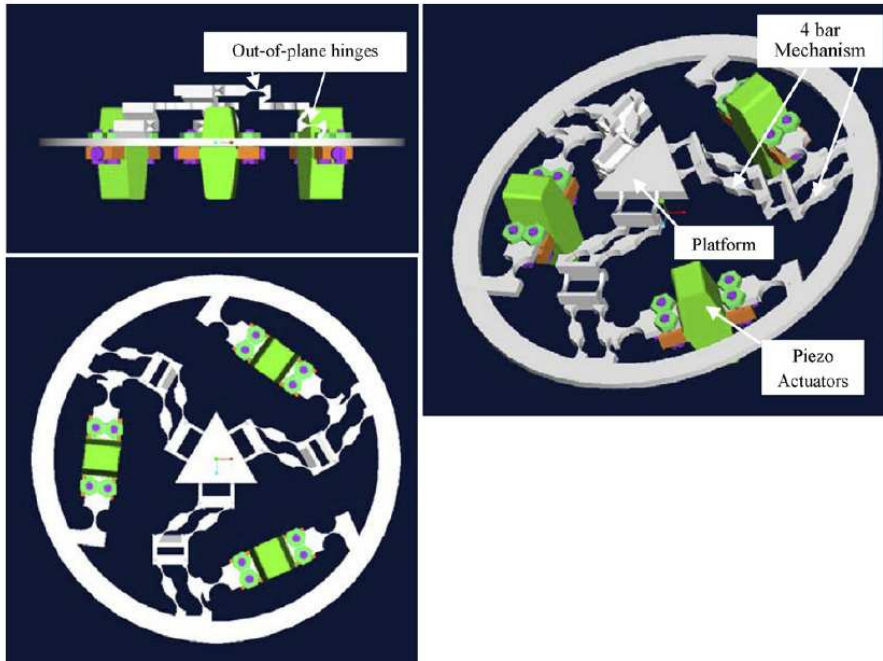
Fig. 1.35. The overall image of this mechanism [YAO 08].

The displacement can be defined by this formula;

$$\begin{Bmatrix} \Delta x \\ \Delta y \\ \Delta z \end{Bmatrix} = \begin{bmatrix} a_{11} & a_{12} & a_{13} & a_{14} & a_{15} \\ a_{21} & a_{22} & a_{23} & a_{24} & a_{25} \\ a_{31} & a_{32} & a_{33} & a_{34} & a_{35} \end{bmatrix} \begin{bmatrix} \alpha \\ \beta \\ \gamma \end{bmatrix}$$

a_{ij}: the Jacobian matrix (3 x N, and N is the number of bistable modules)
$_{abri}$; the relative angle.

This parallel mechanism can be controlled by proportional signal. Their final position is maintained by the input voltage on the actuators. Although this is assembled parallel mechanism with a centimeter dimensions, it presents high resolution because of high resolution of piezoelectric actuators.

However, as introduced in the last section, microactuators present many drawbacks [RAK 09a] [RAK 09b]: creep, plasticity, and hysterisis. These difficulties have to be resolved to reach desired performance. Some researches proposed some solutions of closed-loop control, such as robust control, state feedback control based on Kalman estimator [HAD 09].

1.5.8.3 Microrobots controlled by periodic signals

Unlike the last approach, which amplifies the range by the compliant mechanism, and uses the input electric power to maintain their position, this approach uses periodic signals to increase the motion range, and uses the friction to maintain their position.

Applying repeated control signals on the microactuator, a repeated and high resolution motion can be created. These approaches can create a theoretical unlimited range. Microactuators using this control approach are the stick-slip motors and ultrasonic motors. Sawtooth signals or harmonic signals are applied in order to obtain an accumulation of the displacement.

Step motor

The typical example is the step motor, such as piezoelectric motor, electrostatic motor, and inchworm. Step motors are actuated by the surface contact alternating between sticking to each other and sliding over each other, with a corresponding change in the friction force. Usually, the static friction coefficient between two surfaces is larger than the kinetic friction coefficient. If an applied force is large enough to overcome the static friction, then the reduction of the friction to the kinetic friction can cause a sudden jump. This will lead to a small forward step. If repeat signals are applied on actuators, the small step can be accumulated to obtain great motion range.

Fig. 1.36 shows the motion during a period cycle. The microactuator can be a piezoelectric bimorph beam, it deforms under the applied voltage. A step is created after a period cycle. Repeated motions can be obtained due to repeated applied signals. Because the piezoelectric material has a fast response, the speed can be controlled by the frequency or the amplitude of the signal.
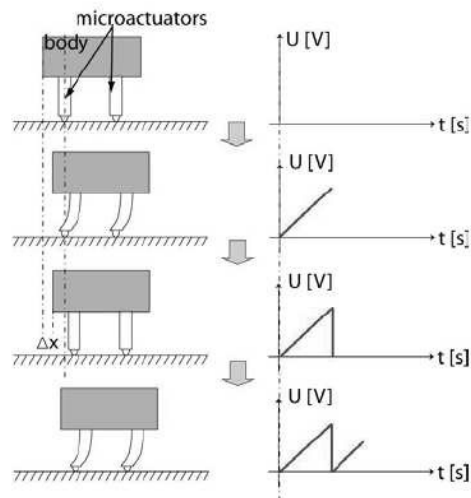
Fig. 1.36. Principle of stick-slip motion [RAK 09a].

This principle offers high resolution and theoretically unlimited range. It could be a good solution to make a microrobot.

Fig. 1.37 shows an example of the stick-slip piezoelectric motor; it has 2DOFs: translation and rotation.
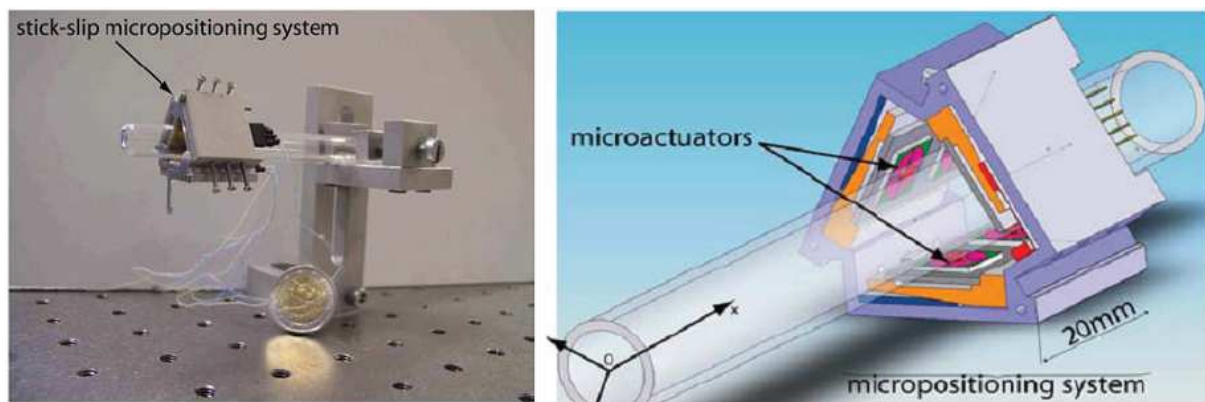
Fig. 1.37. The fabricated stick-slip motor with 2DOFs [RAK 09a].

Two pairs of electrode are designed on the actuators (see Fig. 1.38). The actuation of each pair of electrode on the piezoelectric material can create in plane displacement.
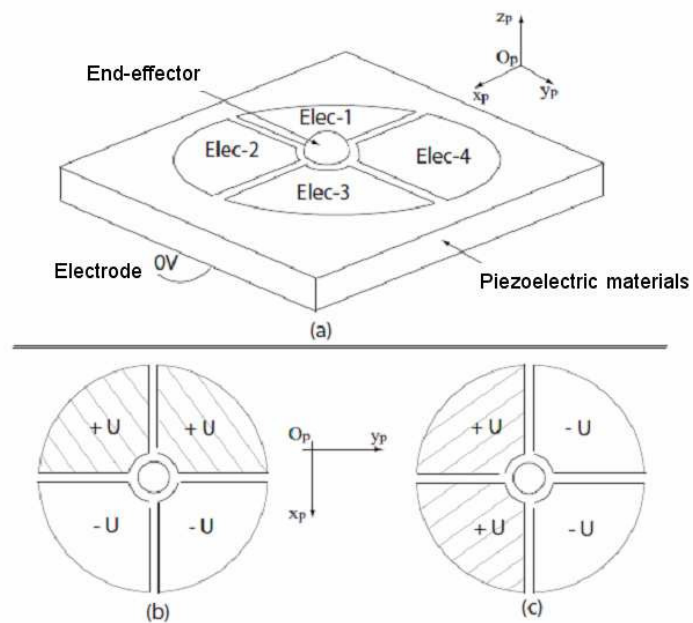
Fig. 1.38. Configuration of 2DOFs piezoelectric actuator, (a) Four used electrodes, (b) motion following O_px_p, (c) Motion following O_py_p [RAK 06a].

Shown as Fig. 1.39, the saw-tooth voltage is applies with amplitude U = +/−150V a frequency 100 Hz. A resolution of 100 nm is reached.
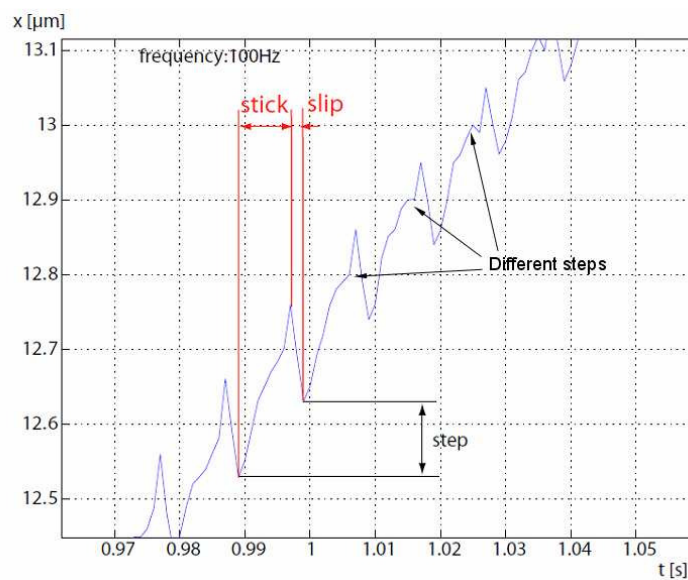
Fig. 1.39. Measurement of steps in linear motion (voltage U = 150V) [RAK 06b].

However, since each step depends on the state of the surface (roughness, flatness, etc), it is impossible to repeat exactly the same step. When it goes through a great displacement range, the error accumulation in each step leads to an unpredictable final position in the open-loop control mode.

Ultrasonic motors

An ultrasonic motor takes use of the induced ultrasonic vibration of a component, the stator, placed against another component, the rotor (rotation) or the slider (translation) to actuate this moving part.

Ultrasonic motors utilize the resonance to amplify the vibration of the stator in contact with the rotor. Ultrasonic motors also offer unlimited rotation or sliding distances.
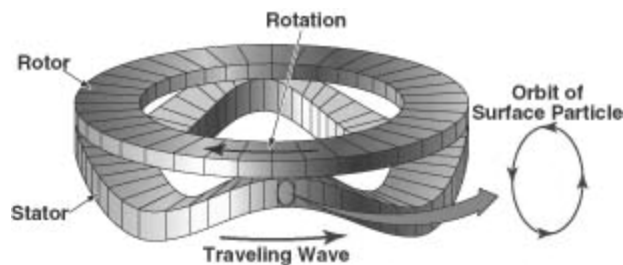
Fig. 1.40. Example of ultrasonic motor.

The surface acoustic wave induced by periodic signal pushes the rotor by friction. Two different ways are generally available to control the friction along the stator-rotor contact interface, traveling-wave vibration and standing-wave vibration.

They have important advantages such as high holding torque, high response characteristics, high torque density, silent operation, no electromagnetic noise and compact size. Consequently, Ultrasonic motors have been used for precise and accurate speed and position applications in recent years.

Summary

Proportional control and step control are widely used in microrobotics. Using these two approaches, we can reach high resolution and accuracy position by building precise mathematical models. However, in the microworld, drawbacks of microactuator make it big challenges.

1.6 Perception for microrobotics

When the dimension of manipulated objects is very small, it becomes difficult to have a perception of the scene which is sufficient for the control of microrobotic systems. Indeed, it is necessary to combine different views on the operations to obtain position information, orientation and involved force (see example Fig. 1.41). The multi-sensory perception is a fundamental function for the development of cells of automated micro assembly.
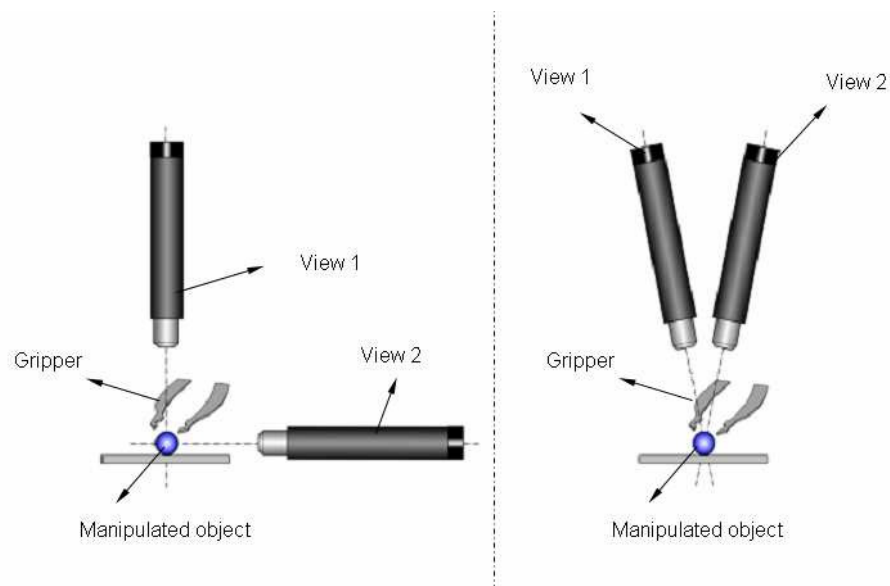
Fig. 1.41. Two views for micromanipulation.

Visual perceptions [BER 06] permit to characterize and locate parts and handled tools of manipulation, and control the quality of microassembly. Work in this area concerns the development of vision algorithms taking into account the specificities of imagery, this scale (small field of vision, poor depth of field, small working distance, high dependency lighting) [VIK 99] [RAL 00] [FAT 07] [FED 98]. The reference command based on vision has enabled the automation of micro assembly task for objects whose characteristic dimensions are greater than $100\,\mu m$ [TAM 09].

The perception of force can control the interaction between end-effector and component, and ensure the integrity of both pieces handled and the fragile tools used. It is based on two approaches working in this area:

The first concerns the characterization and development of deformation sensors integrates the tools of micromanipulation and treatment of the measured effort which is very noisy at this scale. As in Fig. 1.42, a microgripper integrates the strain gauge to estimate the force.
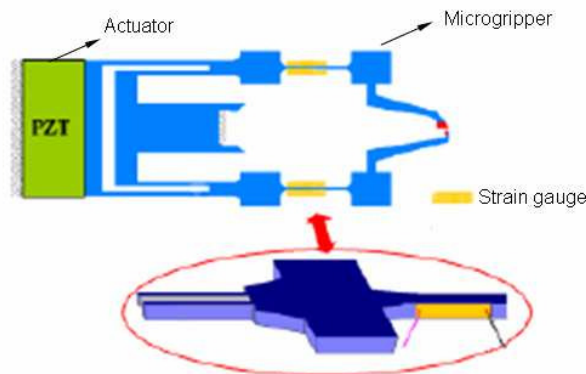
Fig. 1.42. Microgripper with integrated force sensor [MEN 01].

The second approach the estimation of force by state feedback (synthesis of observers). The work adapted in the microworld is extent of forces from the micro-Newton to few tens milli-Newton.

The measurement may be capacitive [ENI 00] [SUN 02] piezoelectric [29.30], frequency (on a vibrating beam) [BLO 89] [FAB 94] [ARA 04a] or a deformations gauge [ARA 04b] [PAK 03] [MOL 05]. We must also note the work on the use of impedancemeter for measuring position and force. Because of the use of active materials, it is complex to implement especially due to nonlinearities and high sensitivity to the environment (e.g. temperature for the piezoelectric material) [IVA 09].

1.7 Conclusion

Microrobotics is micromechatronic system that performs micromanipulation or microassembly tasks in the microworld. The traditional robots are difficult to be fabricated at the microscale due to the scale down effects. Microrobots are constituted by microactuators and kinematics chains and perception systems. These various microactuators present different advantages and drawbacks.

Electrothermal microactuations
This actuation takes use of the thermal expansion to create motion. This thermal expansion effect results in limited displacement range. That is why various different amplification mechanisms have been designed, such as U-shape or V-shape mechanisms. Since the actuation is induced by electric-thermal effect, the response could be fast. However, the cooling is the main difficulty to reduce the response time.

Electromagnetic microactuations

Ferromagnetic material is actuated by applying magnetic field. Since it dose not require the wire connection, the wireless actuation can be made. To build complete electromagnetic microactuators, the coil, ferromagnetic material should be fabricated. The fabrication techniques limit the applications of this kind of microactuators.

Electrostatic microactuations
Electrostatic microactuators are made by two approaches: the parallel plate and the comb-drive actuator. The charge difference creates motions. This kind of actuator presents pull-off effect which may limit the application in some cases.

Microactuations based on active materials
The microactuators based on active materials make use of the deformation under electric or magnetic fields. Although they present high resolution and fast response, only small deformation is induced. The adapted kinematic chains should be designed to obtain the desired motion range.

Based on these microactuation techniques, two kinds of control have been proposed: the control based on the proportional signal and the periodic signal. In the first kind, we apply the proportional signal to reach and maintain the desired position. In the second kind, we apply the periodic signal to create the repeated step with high resolution to reach the desired position.

To make a whole microrobot system, two kinds of perception are required: the position and the force. Visual perceptions permit to know the position information by developing the vision algorithm. The force information can be obtained by integrating the proprioceptive force sensors.

Chapter 2 Digital microrobotics

"If at first the idea is not absurd, then there is no hope for it."

– Albert Einstein

(1879 – 1955)

2.1 Introduction

During the last decade, significant research activities have been performed in the field of microrobotics. As seen in the previous chapter, microrobotics deals with the design, the fabrication and the control of microrobots. These microrobots are intended to perform various tasks in the so-called Microworld (i.e. the world of submillimetric objects) in particular micromanipulation of single objects (artificial or biological) for positioning, characterization or sorting as well as for industrial microassembly. Achieving efficient robotic tasks at this scale remains a great challenge and requires some specific characteristics:

- Resolution and accuracy in the submillimetric range are needed in order to interact with micrometer sized objects. That is why methods and strategies used to build conventional robots are often not applicable in the microworld.

- New mechatronic approaches, new actuators and new robot kinematics are required. Researches done in the world have shown that the use of active materials to actuate microrobots gives better performance than the use of more traditional actuators. Piezoelectric materials, shape memory alloys (SMA) and active polymers have been successfully used to actuate various types of microrobots. However, despite their intrinsic high resolution, these active materials present some drawbacks, making both their modeling and efficient controllers design a hard task. Their behavior is often complex, nonlinear and sometimes non stationary.

- Closed-loop control of the microrobots requires the design and the integration of very small sensors and the use of bulky and expensive instruments for signal processing and real-time operating. Packaging technology and integration of the sensors and actuators is also a heavy problem. This is why building multi-degrees of freedom (DOF) microrobots able to perform complex tasks is difficult.

- The size of the robot itself must be very low in order to facilitate handling of micro-objects and enable the execution of tasks in confined environments.

The work presented in this thesis deals with the study and the design of a new generation of microfabricated microrobots using a modular concept and an open loop control strategy. These new microrobots named digital microrobots are built from several bistable modules fabricated in a monolithic manner. Every module has two mechanical stable and repeatable states driven by a binary signal. The position of the whole microrobot is controlled by a digital word representing the state of the modules. This opens a new paradigm in the microrobotics field, allowing the design of various kinematics adapted to the microworld and it addresses scientific and technological breakthroughs.

This new concept shows many advantages:

- Repeatability and accuracy are obtained thanks to the mechanical bistable performance of the modules.

- Neither proprioceptive sensors nor bulky and expensive instruments are needed to control the microrobot.

- Fast and/or large displacements can be obtained using the parallel control of the state of the modules.

- Microrobots can be built in great quantities (and potentially at low cost).

- Low power consumption can be obtained as power is not needed to maintain the modules in a given state but only during the transition phases.

Moreover, this subject includes highly innovative and interdisciplinary aspects:

- High modularity: various robot kinematics can be designed and state combination can be chosen in order to perform complex micro robotics tasks.

- Microrobot manufacturing using micro fabrication technology: one of the goals of this project is to design microrobots using clean room microfabrication. These technologies allow the development of high density microrobots, containing many modules in order to increase performance and reduce costs.

The aim of this work is to obtain a significant increase of the performance of the microrobots. Moreover, the modular and bistable approach allows exploring new robot kinematics. A module for digital microrobotics will be designed, and it can offer a resolution of less than 10µm and a blocked force more than 1mN.

In the next, we will first present the fundamentals of digital microrobotics. The characteristics of digital microrobots are then compared to those of current microrobots. After that, an overview about the digital approach in the macroworld and in the microworld is given. Finally, according to the requirements of digital microrobotics, special features of bistable modules are expressed.

2.2 Fundamentals of digital microrobotics

Before describing the principles of bistable modules and digital microrobots, the notion of stability is reminded.

2.2.1 Definition of stability

Let us consider that the state of a given system does not change with time (which means that the system is in a state of equilibrium). We apply small external disturbances on the system. If the system tends to leave this state, the state is said unstable. Contrariwise, if the system remains in this state, the state is said stable. The theory of elastic stability of structure was defined firstly by Timoshenko and Young [TIM].

More precisely, in a state of equilibrium, if small external disturbances are applied and the structure reacts by simply performing oscillations around the equilibrium state, the equilibrium is called stable" (Simitses, 1976) [SIM 76]. However, if the small external disturbances cause the system to diverge from its equilibrium state, then the equilibrium position is called unstable. If, on the other hand, the system reacts to the disturbances and remains in the disturbed position, then the equilibrium position is neutral. For each of these definitions, the external disturbances may be as small as desired (Simitses, 1976) [SIM 76].
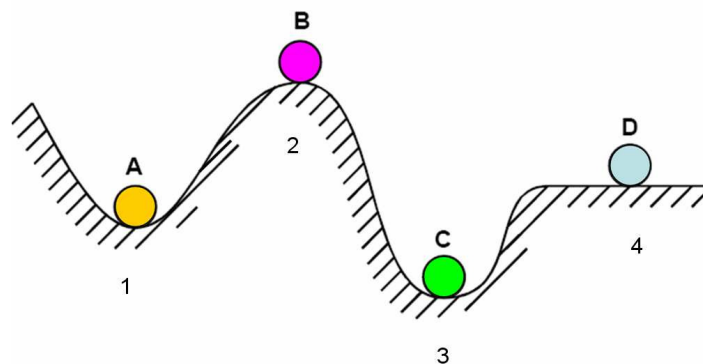
Fig. 2.1. Example of a ball in different positions.

The stability of a system may be illustrated using the system in Fig. 2.1 different positions of the ball represent the possible states of the system. Due to the gravity, the different positions show different stable behaviors.

Tab. 2.1. Ball in the different positions.

Ball	Initial position	Disturbed position	Potential energy
A	1	1	Local minimum
B	2	1 or 3	Local maximum
C	3	3	Local minimum
D	4	Unknown	Constant

In fact, the stability depends only on the possessed potential energy. Positions with local minimum energy are stable positions. A local maximum energy leads to an unstable position. The state trajectory of dynamic system tends to a position with minimum energy.

According to the definition of stability, we can define the bistable mechanism.

2.2.2 Bistable elementary modules

A digital microrobot is built based on bistable elementary modules. Fig. 2.2 shows the principle of elementary modules.
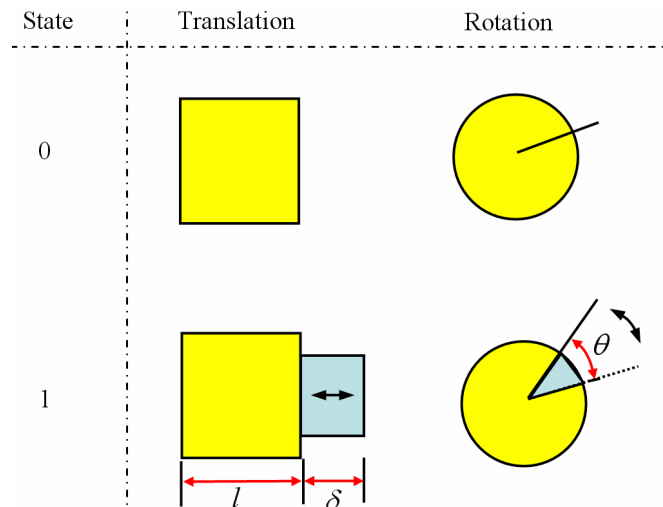
Fig. 2.2. An elementary module has two stable positions.

The bistable elementary module includes the bistable mechanism. We define state 0 and 1 as the two stable states. Between these two stable states there are motions of translation or rotation. The bistable mechanism is switched between these two stable positions by microactuators.

2.2.3 Digital microrobots based on bistable modules

A single bistable module can reach only two stable positions. In order to obtain more stable states, several bistable modules can be connected together. The number of logical states can be an exponent function of the number of bistable modules (see Fig. 2.3).

$Total \log ical\ states = 2^n$ where n is the number of bistable modules.
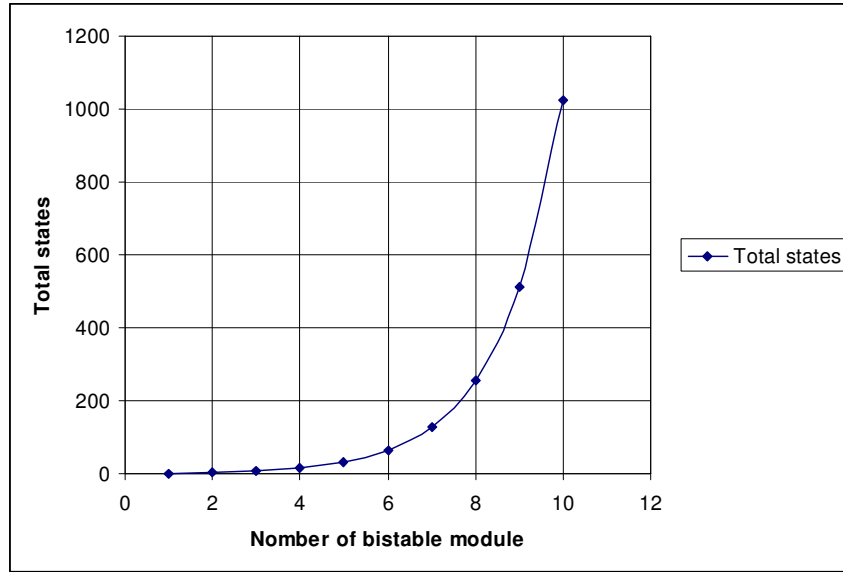
Fig. 2.3. The number of stable positions vs the number of modules.

Fig. 2.4 shows examples of serial robot axis that use several bistable modules. The displacement can be reached by switching the modules.
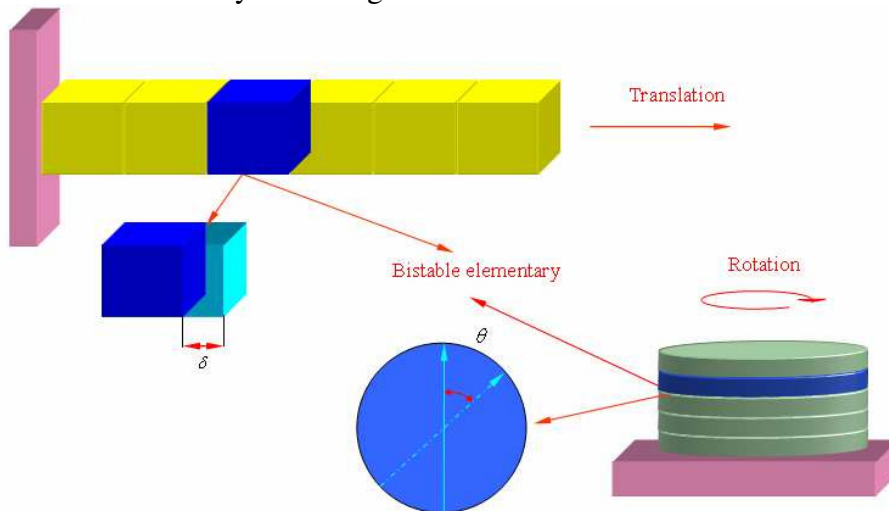
Fig. 2.4. Examples of digital microrobot axis.

47

For example, using 5 bistable modules allow reaching 32 logical states. If we choose a configuration where the module's displacements are: d, $2d$, $4d$…16d (see Fig. 2.5), where d is the minimum displacement needed. The maximum obtained displacement is:

$$D = d \times [1,2,4,8,16] \times [1,1,1,1,1]^T$$

$$= d \times \sum_{i=1}^{5} 2^{i-1} = 31d \qquad\qquad 2.1$$

According to the formula, there are 2^5 states which a with discrete distribution. d is the resolution of the discrete workspace.
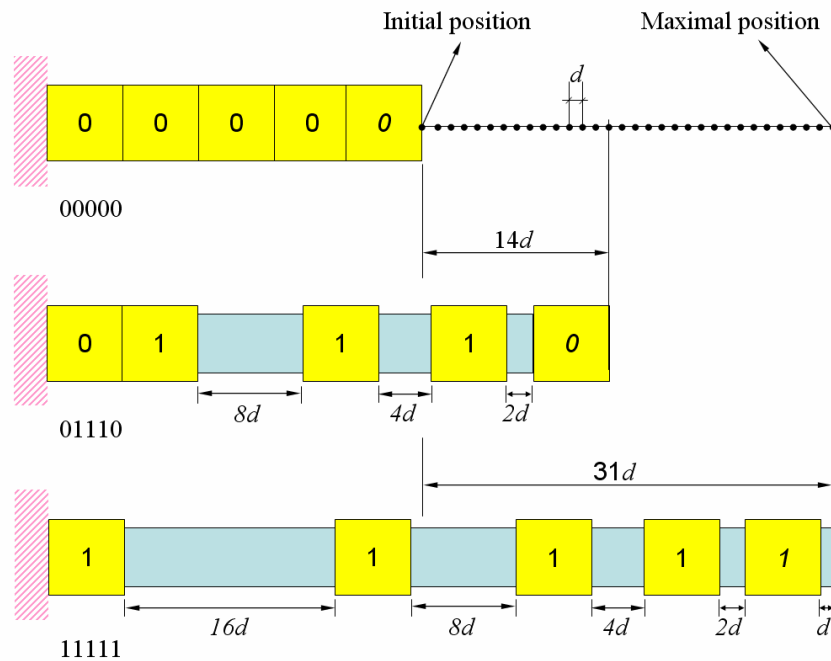
Fig. 2.5. The workspace of five cascaded bistable modules.

2.3 Comparison between digital microrobotics and current microrobotics

The microrobotics concept shows many advantages. Good repeatability and accuracy are obtained thanks to the mechanical performance of the bistable modules. Neither proprioceptive sensors nor bulky and expensive instruments are needed. Low power consumption can be obtained because external energy is not needed to maintain the modules in a given state but only during the transition phases. Moreover, the immunity to noise and environment changes is improved.

Using a parallel control of the modules, fast displacements can be obtained. Microrobots can be built in great quantities (and potentially at low cost) with microfabrication. Using bistable

structures give an approach that turns the difficulties of non-linear control into mechanical structure design. Digital microrobotics takes advantage of microfabricated mechanical bistable structures and open-loop digital control to offer a unique method to build efficient microrobots. However, some drawbacks exist: accumulation of errors, limited load, and discrete reachable area.

Tab. 2.2 gives a detailed comparison between the characteristics of current microrobots and the proposed digital microrobots. This comparison is based on informations from [ROB 99][QIU 04] [JIN 05] [DONG 02] [GUM].

Tab. 2.2. A Comparison between current microrobots and digital microrobots.

Characteristic	Current microrobots		Digital Microrobots
Actuation approach	Proportional actuation	Incremental actuation	Discrete actuation
Size	Medium	Medium	Small (microfabrication)
Cost	High	Medium	Low
Control	Closed loop Non-linear control	Closed loop control	Open loop (no sensors needed)
Energy consumption	High to medium	High to medium	Low
Sensitivity to noise	High	Low	Low
Use of sensors	Yes	Yes	No
Displacement	Continuous	Discrete	Discrete

2.4 Digital approach in the literature

2.4.1 Digital approach in the macroworld

The history of discrete actuation can date back to the adaptive structure. An adaptive structure is an engineering structure which has the ability to adapt, evolve or change its properties or behavior in response to the environment changes [WAG].

Originally, adaptive structures were developed primarily for space missions. In 1990, Wada [WAD 90] discussed an overview of adaptive structures, included several different types of adaptive structures. Based on adaptive structures, a new concept of variable geometry truss (VGT) is proposed. From 1980's the VGT became a source of interest in the field of robotics. Miura and Furuya [MIU 95] in Japan and Rhodes and Mikulas [RHO 85], in the U.S.A. explore new possibilities of adaptive structures.

A number of researchers studied VGT manipulators (see Fig. 2.6), and compared them to traditional types of robotic manipulators. Hughes et al. [HUG 91] compare a VGT manipulator to "the Canadarm" ("Canadarm" is the shuttle manipulator developed in Canada, and currently used on NASA space shuttles), in weight, degrees of freedom, maximum tip load, etc. The kinematics, dynamics, and vibrations of VGT manipulators have become important research topics. Robertshaw and Reinholtz presented an analysis of vibrations in VGTs [ROB 98].
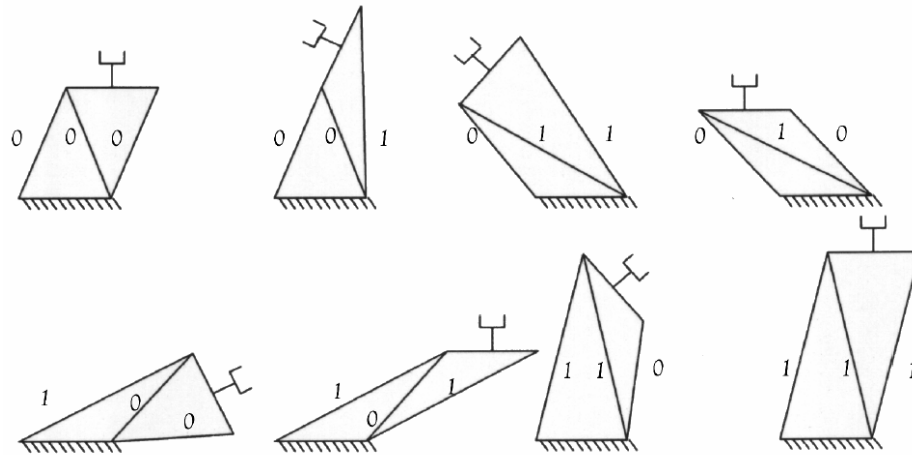
Fig. 2.6. 8-possible configuration of a 3-Bit Planar VGT [ROB 98].

G.S. Chirikjian and co-workers presented firstly the concept of the binary paradigm for robotic manipulators. A lot of work has been done about kinematics analyses, and trajectory planning for the VGT manipulator [CHI 92] [SUT 01] [CHI 94] [CHI 95b].

A planar binary VGT manipulator were designed and built [SUT 01]. It consists of three modules of 8-bit VGTs stacked on top of each other (see Fig. 2.7). This manipulator has the ability to fold back to reach its own base.
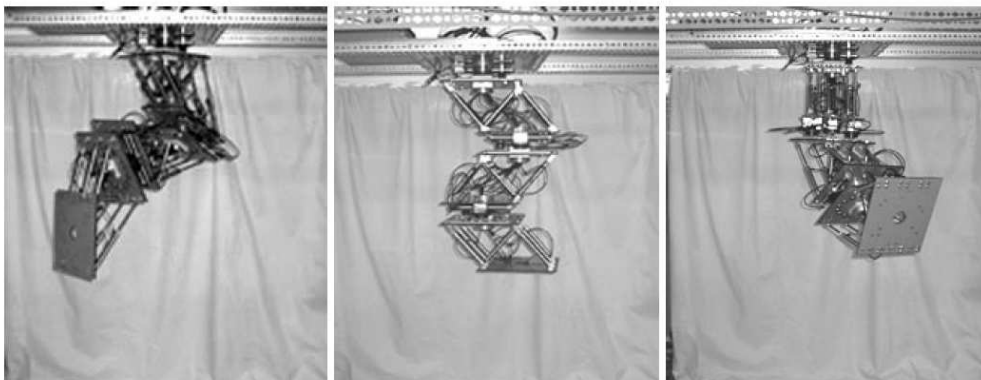
Fig. 2.7. Three modules of 8-bits manipulator.

V.A.Sujan [SUJ 04] from MIT (Massachusetts Institute of Technology) designed a device called "Binary Robotic Articulated Intelligent Device (BRAID)" (see Fig. 2.8). It consists of compliant mechanisms with large numbers of embedded actuators and is a step toward practical implementation of binary devices for space robotic systems.
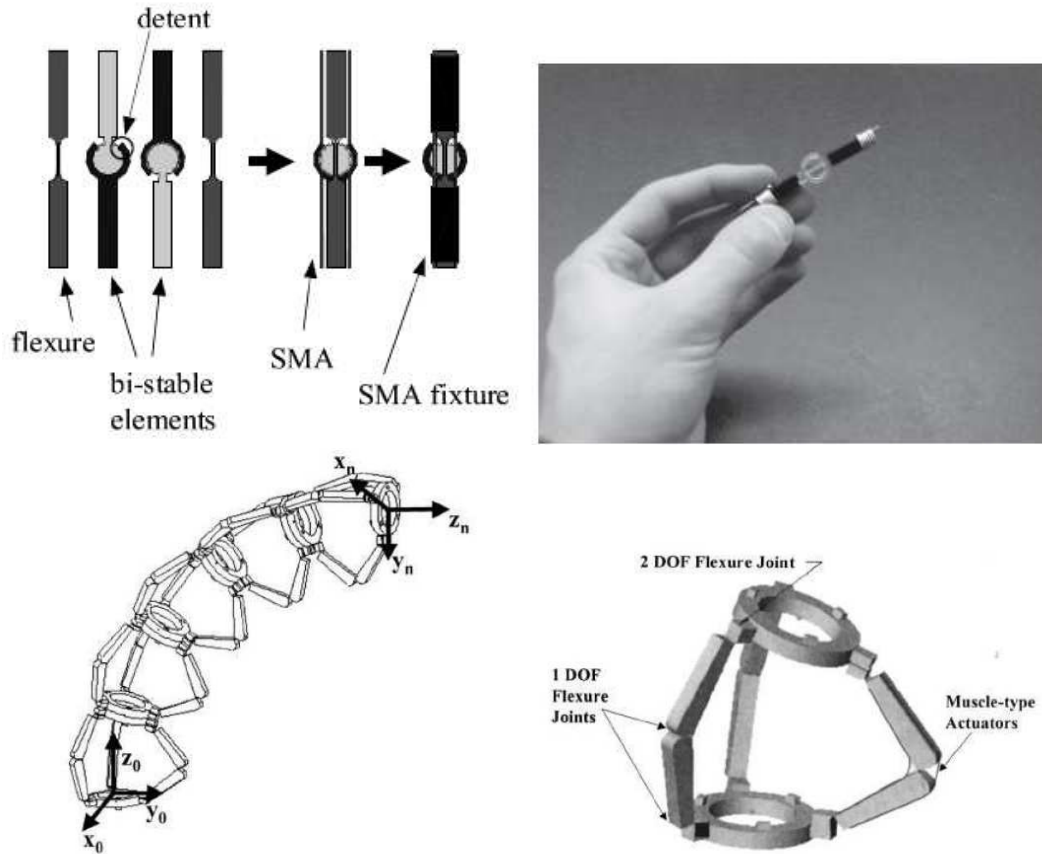
Fig. 2.8. Binary Robotic Articulated Intelligent Device (BRAID) [SUJ 04].

Actuation of each module is accomplished using a muscle-type (SMA) actuator. One position is maintained by the electric power input, and the other position can be obtained by the restoring force provided by the elastic flexure joints.

Assembling electro active polymers (EAP) and two buckled beams, a bistable element was made in MIT [WIN 06] [PLA 07]. Fig. 2.9(a) shows that the buckled beams are switched by applying voltage on actuators.

Six bistable mechanisms pile up to reach 36 different states. An open-loop control can orientate the mirror into 36 postures (see Fig. 2.9 (b)).

This discrete actuation in the macroworld presents advantages and drawbacks [CHI 94] [CHI 95b] [CHI 92] [CHI 95a] [SUJ 04] [WIN 06]:

(a)
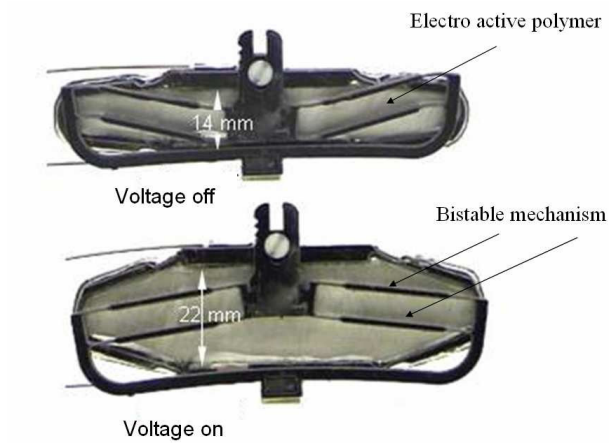
(b)

Fig. 2.9. (a) Bistable element in two positions (b) BRAID Prototype[WIN 06] [PLA 07].

Advantages:
- High repeatability.
- Low cost.
- High capacity load to manipulator weight ratio.
- No need for feedback control.
- Less complexity in computer controlled interfacing.

52

➢ Allow tasks to be performed even when some actuators fail.

Drawbacks:
➢ Discrete reachable states.
➢ Requirement of more cascaded modules to improve its performance (number of reached states).
➢ Requirement of a large amount of computations in inverse kinematics if a large number of modules is used.

2.4.2 Discrete actuation in the microworld

In the microworld, no microrobotics application using digital actuated structures can be found. However, there are some close designs in the microworld.

R.Y. Robert [ROB 99] designed a new mechanical binary-to-analog converter which was fabricated by the surface micromachine technology in 2000. Fig. 2.10 (a) shows one bit of this converter. The left input beam is controlled by the thermal actuators array. The output displacement can be reached by the output lever beam. Four converters (see Fig. 2.10 (b)) are cascaded for accumulating the output displacement by connecting the next bit's analog input to the previous bit's analog output. Despite the use of the gap stop, their accuracy will lost in the translation into next bit.
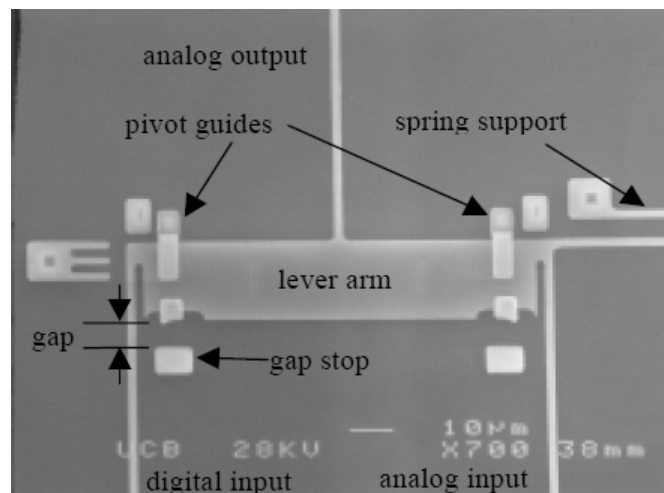
(a)
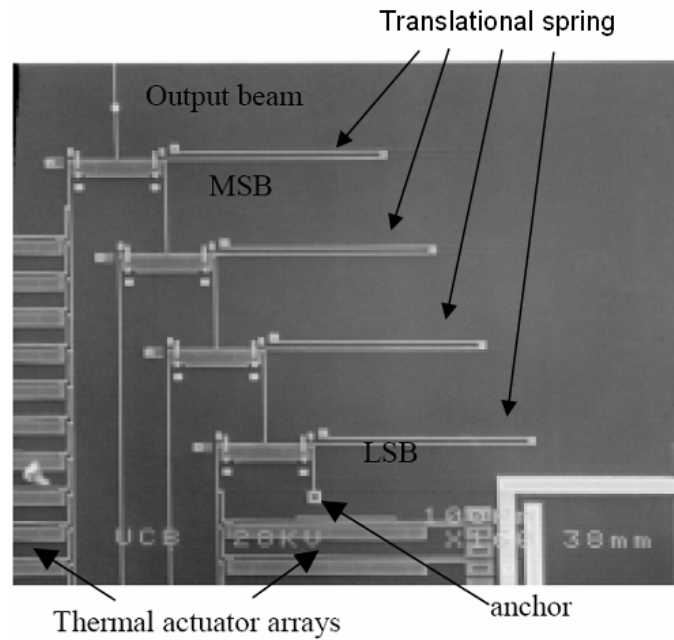
(b)
Fig. 2.10. (a) One bit of converter (b) four bits of converter [ROB 99].

2.4.3 Bistable mechanisms in the microworld

A bistable mechanism is a type of mechanism with two stable positions which can be switched between them. These stable positions can be maintained by their own behaviors, and no power is required to maintain their positions. As the example in Fig. 2.11 (a), a bistable mechanism has two stable positions (1 and 3) and an unstable position 2. This light switch is a typical bistable mechanism (see Fig. 2.11 (b)). The spring is connected with the switch button, which can be stopped in two positions.
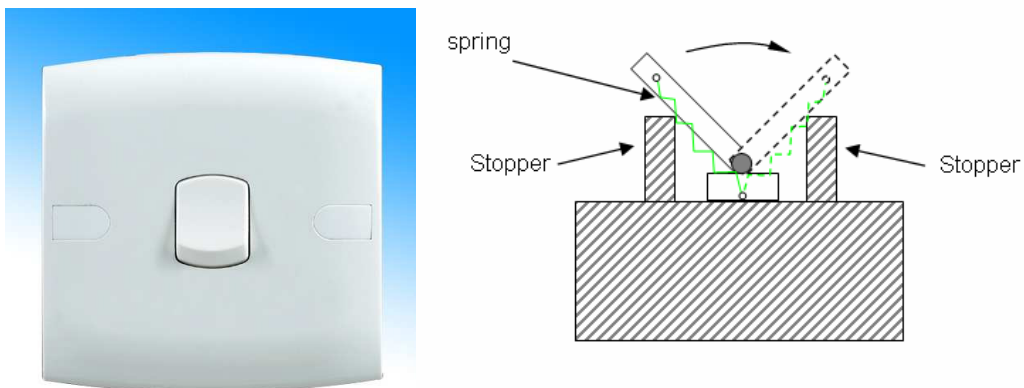
Fig. 2.11. (a) A light switch (b) typical schematic of the light switch.

This bistable mechanism are used in the microworld. Many applications have been made, such as microrelays [QIU 05], microswitches [HWA 03] [FRE 04] [KWON 05] [KRY 08], and microvalves.

In the Compliant Mechanism Laboratory at Brigham Young University (BYU), many studies about bistable mechanisms have been made, and various bistable mechanisms have been fabricated.

Fig. 2.12 shows a bistable mechanism fabricated by surface micromachining technology (the pins and compliant beams are fabricated using this technology).
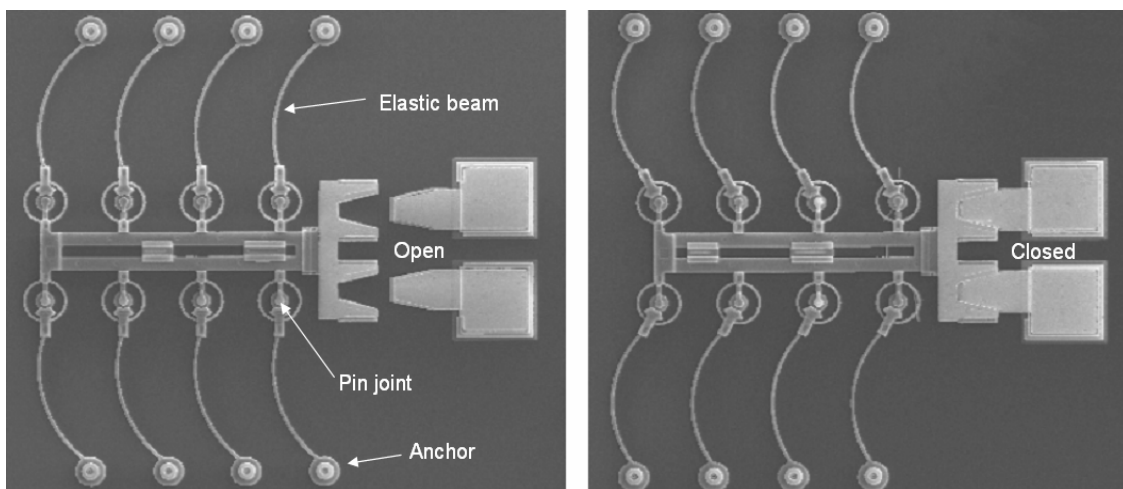
Fig. 2.12. Bistable mechanism in open and closed positions [BAK 00].

Another bistable is presented in Fig. 2.13. It is a V-shape bistable beam, fabricated by surface micromachine technology. A thermal microactuator is used to switch between the two stable states.
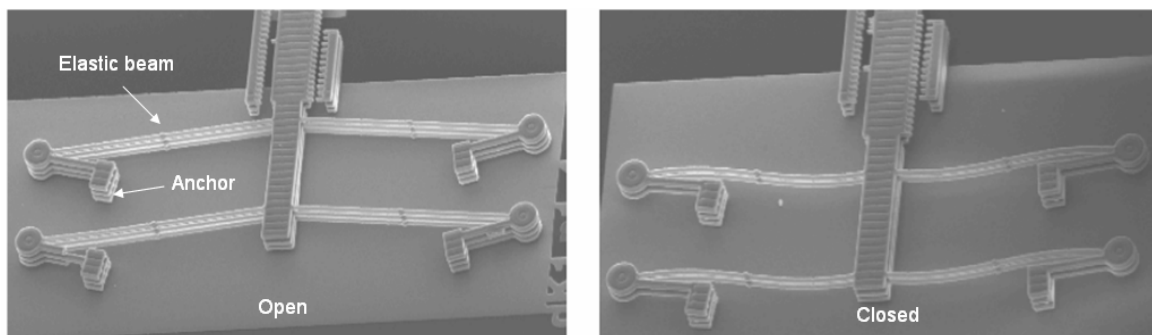
Fig. 2.13. Bistable mechanism in up and down positions [WIL 04].

M.R. Luharuka [LUH 07] presents a rotation bistable mechanism. Fig. 2.14 shows two stable states. This bistable mechanism is fabricated in a soft magnetic material called Permalloy (80% Ni, 20% Fe).
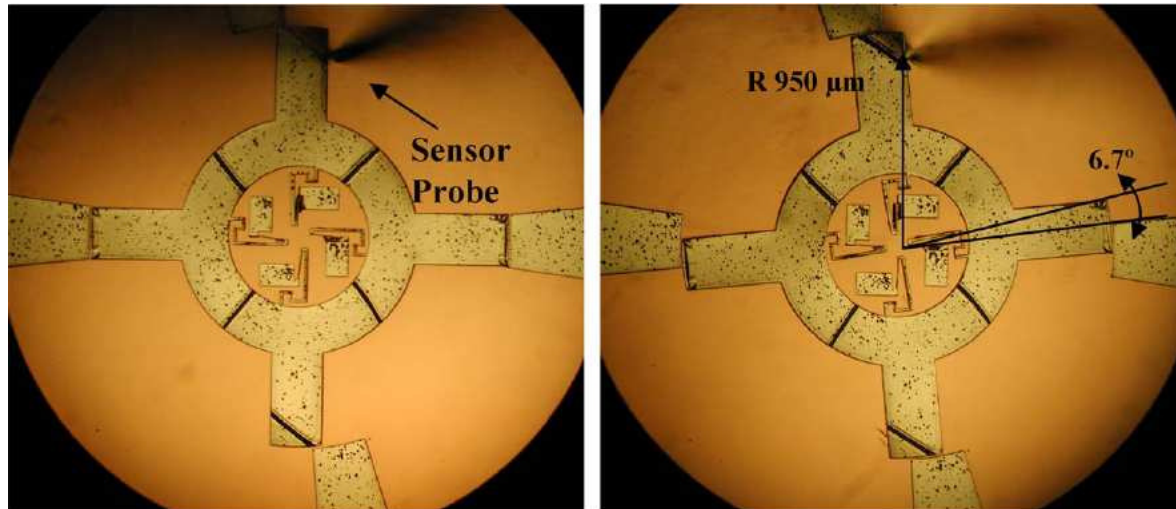
Fig. 2.14. A rotation bistable mechanism [LUH 07].

In 2004, J. Qiu [QIU 04] presented a curved-beam bistable mechanism for performing a relay (see Fig. 2.15), in which the actuator and the bistable structure were made in a wafer using the bulk micromachine technology. The thermal actuator is activated by joule effect, and produces enough force to switch on or off the curved-beam.
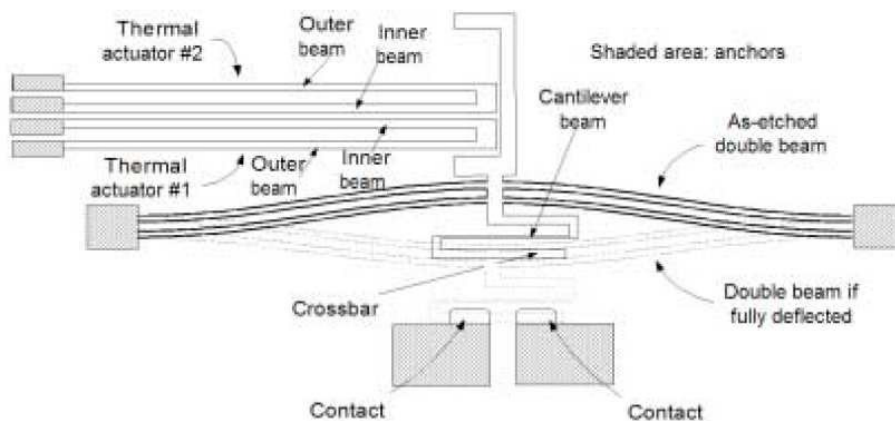
Fig. 2.15. A relay based on curved-beams and activated by a thermal actuator [QIU 04].

B. Charlot [CHA 08] presented a bistable beam using pre-stress. The pre-stress is obtained in a thin SiO2 layer, and the pre-stressed beam is fabricated by sophisticated machine (Electro beam lithography) (see Fig. 2.16). This bistable beam is switched by electrostatic force.

(a)   (b)
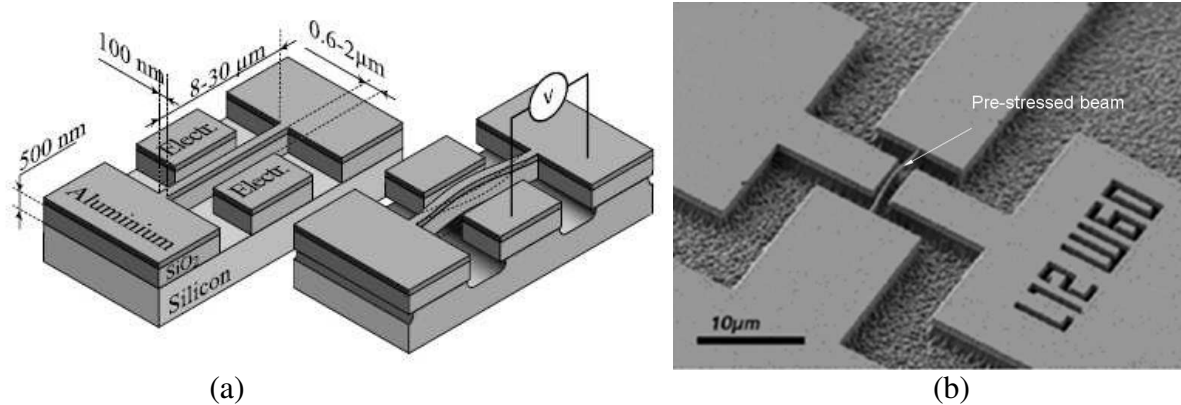
Fig. 2.16. (a) Schematic of a bistable pre-stressed beam (b) photo of the design (using a SEM: Scanning Electron Microscope) [CHA 08].

Tab. 2.3 compares the different bistable micromechanisms (BMMs).

Tab. 2.3. Comparison of different fabricated BMMs.

Actuation principle	Bistable Mechanism	Application	Micromaching (material)	Distance between two stable states (µm)
Electrothermal [QIU 05]	Curved beams	Relay	Bulk micromachining (Si)	120
Electrostatic [HWA 03] [FRE 04] [KWON 05] [KRY 08]	Curved or pre stressed beam	Latch, relay	SOI technology(Si)	5,15-120
Electromagnetic [CAO 07][KO 06]	Curved beams	Switch	MetalMUMPs Process (Ni)	100

2.5 Requirements for microrobotics

As we saw in the previous section, several bistable mechanisms have been developed in the microworld. However, building bistable modules for microrobotics requires specific features not available in the existing designs. The open loop control approach requires that the two stable positions are well defined. This can be obtained only if the two stable positions are blocked. Generally, only one position is blocked because of the constraints of the monolithic microfabrication process. While the existing modules are adequate for electrical switches and relays, new structures with two blocking systems must be developed for microrobotics applications. Moreover, a microrobot will be built using several bistable modules in series or parallel configurations. In a microrobot, a bistable module must carry the manipulated micro-object and partially the robot structure. This is why the weight of the robot structure must be taken into account.

2.6 Conclusion

In this chapter we have presented the fundamentals of a new generation of microrobots: digital microrobots. This new concept is based on the use of bistable modules. Digital microrobotics takes advantage of microfabricated mechanical bistable structures and open-loop digital control to offer a unique method to build efficient microrobots. However, realization of digital microrobots requires the raise of several scientific and technological bolts. Robust and repeatable bistable mechanical structures must be designed considering high technological constraints. Microfabrication of microrobots needs the integration of several micro actuators in a narrow area. The actuation technologies should be developed to adapt to the bistable structures. The modular approach allows building various robots architectures.

Through this project, we wish to open new possibilities in the microrobotics field to execute more and more complex tasks and thus to rapidly adapt to the building requirement of the current and future microproducts.

Chapter 3 Bistable module design

"As far as the laws of mathematics refer to reality, they are not certain, and as far as they are certain, they do not refer to reality."

- Albert Einstein

(1879 – 1955)

3.1 Introduction

In the previous chapter, a new generation of microrobots called digital microrobots has been introduced. This new kind of microrobot is based on the use of bistable modules. Taking the advantage of obtaining stable positions of bistable modules, only an open loop control is needed to generate the motions from one position to another. However, for each bistable module, we need to obtain two stable, repeatable and blocked positions that are not offered by the proposed microfabricated structures in the literature.

In this chapter, we explain the design of the bistable module. Three parts have to be designed to enable the bistability with blocked positions: the bistable structure, the stop blocks that permits to obtain the blocked positions, and the actuation that permits to go from a stable position to the other.

3.2 Design of bistable mechanisms

3.2.1 Examples of bistable mechanism

In the work of B.D. Jensen (1998) [JEN 98], a classification of bistable structures is presented and gives a good overview of mechanism configurations. Five classes have been proposed: the snap through buckled beam, the cam mechanism, the double-slider mechanisms with a pin joining the sliders, the double-slider mechanisms with a link joining the sliders and the slider-crank or slider-rocker mechanisms. Fig. 3.1 gives a representation of all these classes.
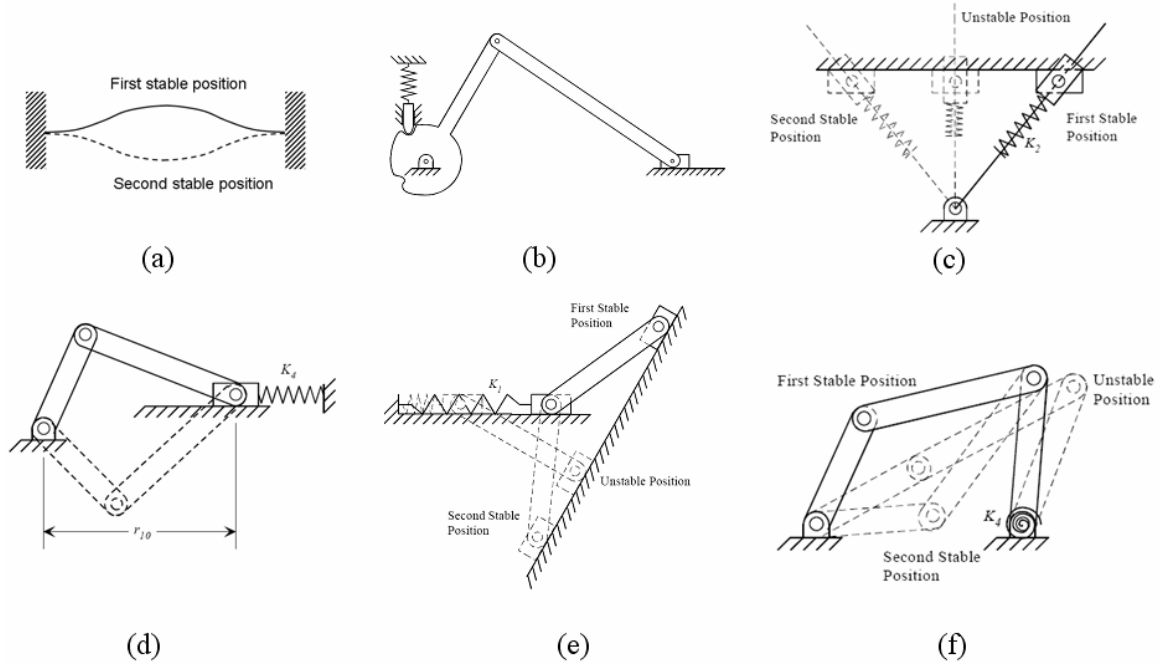
Fig. 3.1. (a) Snap-through buckled beams (b) Bistable cam mechanisms (c) Double-slider mechanisms with a pin joining the sliders (d) Double-slider mechanisms with a link joining the sliders (e) Slider-crank or slider-rocker mechanisms (f) Four-link mechanisms [JEN 98].

Concerning the compliant buckled beam in Fig. 3.1 (a), the compliant beam bends to accumulate and release energy. A vertical force enables to switch between these two stable positions. About the bistable cam mechanism presented in Fig. 3.1 (b), if a spring-loaded follower goes through two local minima of potential energy as it travels around the cam, then a bistable mechanism is generated. Multiple stable positions may even be created using this method. In Fig. 3.1 (c), the presented double-sliders mechanism with a pin joining the sliders consists in two sliders joined by a pin joint and a spring placed to accumulate and release energy. Two stable positions can be obtained in the slide surface. Just below, we detail this mechanism. The double-slider mechanisms with a link joining the sliders presented in Fig. 3.1 (d) is a bistable mechanism if a spring is placed between either of the sliders and the ground link. In Fig. 3.1 (e), the slider-crank or slider-rocker mechanism is also a mechanism having two stable positions. To finish, the four-link mechanism in Fig. 3.1 (f) is made by rigid bars and a rotation spring.

We propose to go back to the double sliders mechanism to explain the principle of the two stable positions. An elastic structure or mechanism usually goes back to its original position after unloading the applied force, but some structures go to another stable position. Such a structure is

called a bistable structure. On the Fig. 3.1 (c), the initial position is called first stable position, and the other is called second stable position. The middle position is an unstable position and external force is necessary to switch from one stable position to the other one, passing through the unstable position. The bistable mechanism shows similar characteristics between actuation force and displacement and between elastic deformation energy and displacement. As shown in Fig.3.2, there are two phases to switch from one state to the other. From the first stable position (S_1) to the unstable position (S_{un}) is the phase of accumulating energy. From the unstable position (S_{un}) to second bistable position (S_2) is the phase of releasing energy. The actuation force firstly increases until the maximal force, and then it decreases until the unstable position. After it goes across the unstable position, the force is changing to be negative. Finally, the second position is reached.
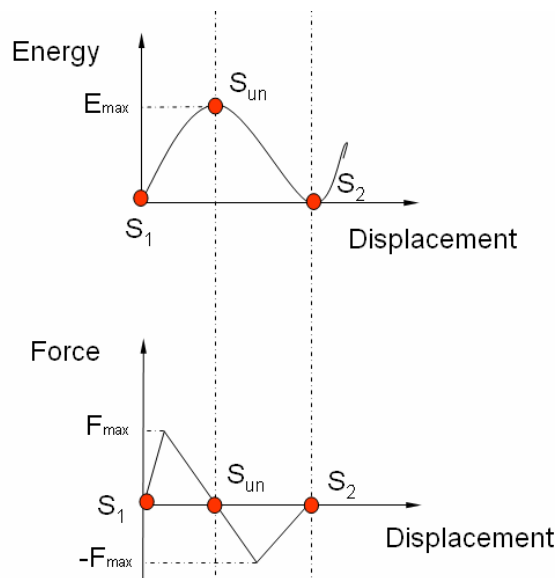
Fig. 3.1. Switching mechanical characteristics.

3.2.2 Generic representation of bistable mechanism

Although it seems that these five classes present different mechanisms, they can be derived from the same one. Through the comparison of these mechanisms, we can propose a generic representation of the bistable mechanisms as given on Fig. 3.2.
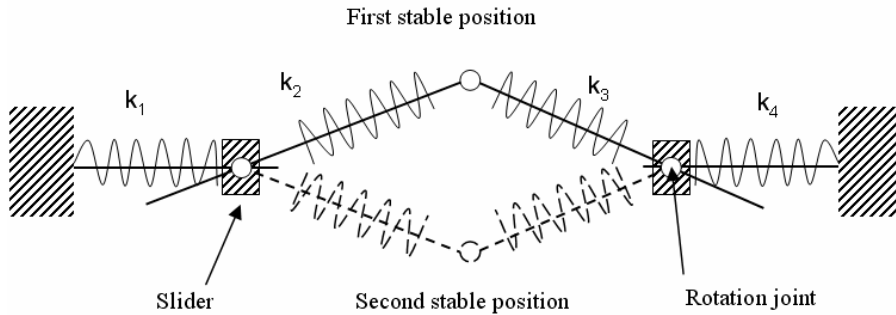
Fig. 3.2. A generic bistable mechanism.

In Fig. 3.2, k_1, k_2, k_3, and k_4 are four springs representing the elastic elements which are used to accumulate and release energy. Three rotation joints are connected by rigid links. The stiffness of these springs can be defined.

For the first class, we fix the two rotation joints, limit the slider in vertical, set the same stiffness of k_2 and k_3, and set infinity stiffness to k_1 and k_4 ($k_1=k_4=\infty$, $k_2=k_3=k$). We obtain the same mechanism as the first class shown in Fig. 3.3.
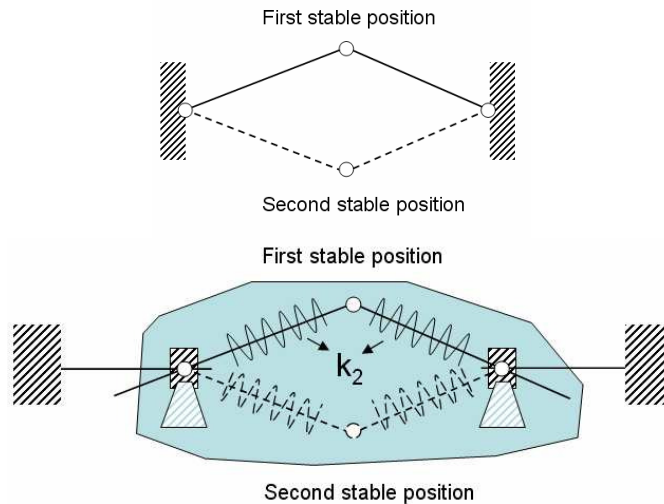
Fig. 3.3. Equivalent model of curved bistable mechanism.

For the second class: Cam mechanism. This kind of mechanism makes use of the curve surface to generate two stable positions. In fact, this can be realized by fixing the two rotations joints, and limit the slider in vertical (see Fig. 3.4).

62

First stable position

Second stable position

First stable position

k_2

Second stable position
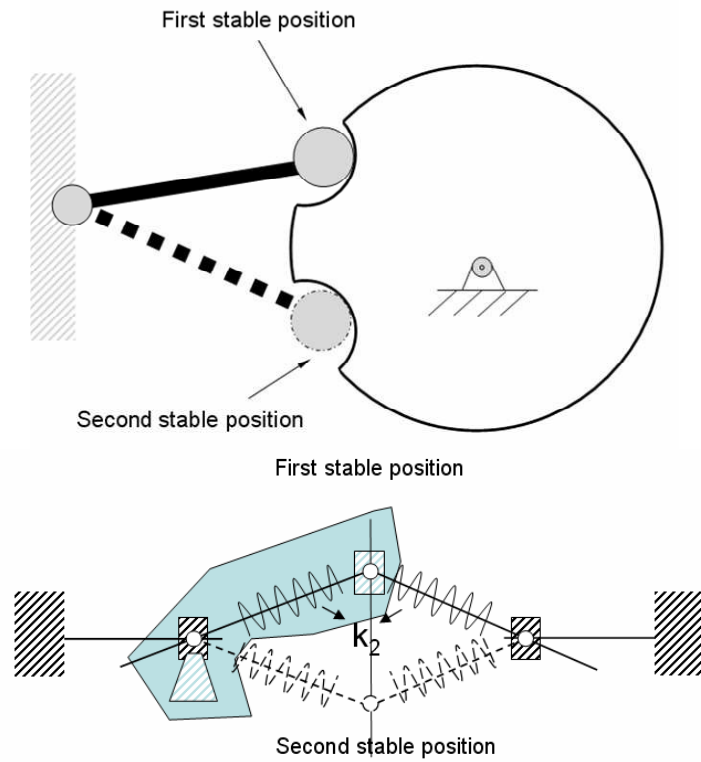
Fig. 3.4. Equivalent model of the cam mechanism.

For the third class, if we fix the two rotation joints, and limit the slider in vertical, we will obtain an equivalent bistable mechanism.

Unstable Position

Second Stable Position

First Stable Position

K_2

63
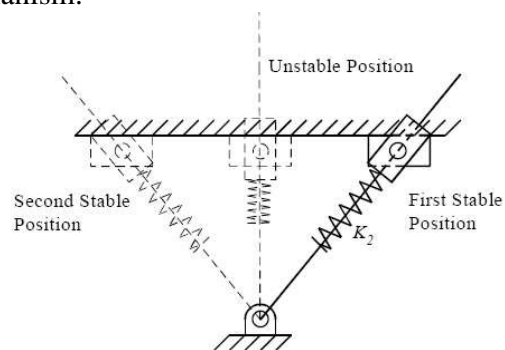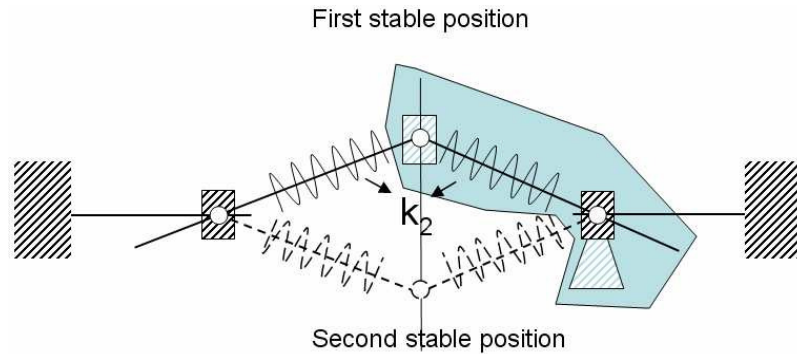
Fig. 3.5. Equivalent model of the double-slider mechanisms with a pin joining the sliders.

For the fourth class, we set k_2 and k_3 infinity stiffness, and k_1 and k_4 an equal stiffness. We can build a slider-crank or a slider-rocker mechanism (see Fig. 3.16).
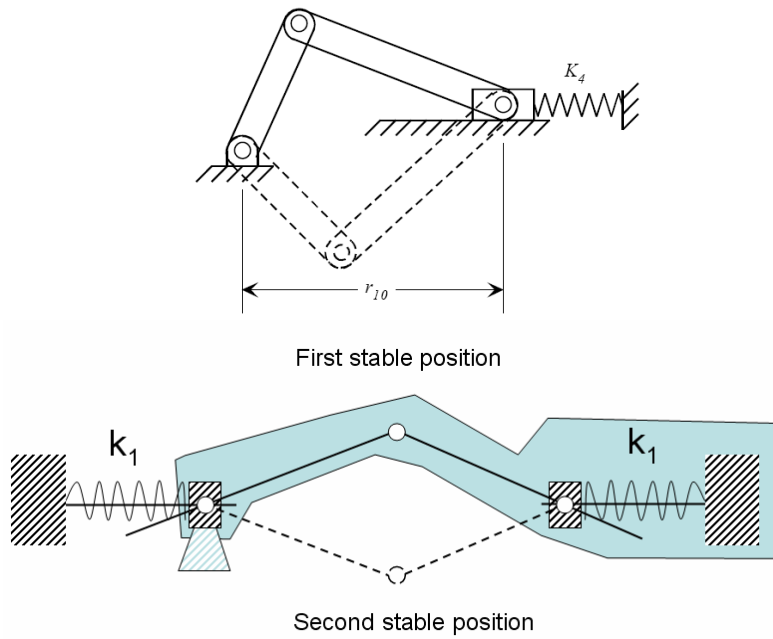
Fig. 3.6. Slider-crank or slider-rocker mechanisms.

For the fifth class, when we remove k_2, we obtain an equivalent mechanism again.

64

First Stable Position

K_1

Unstable Position

Second Stable Position

First stable position

k_1

k_1

Second stable position
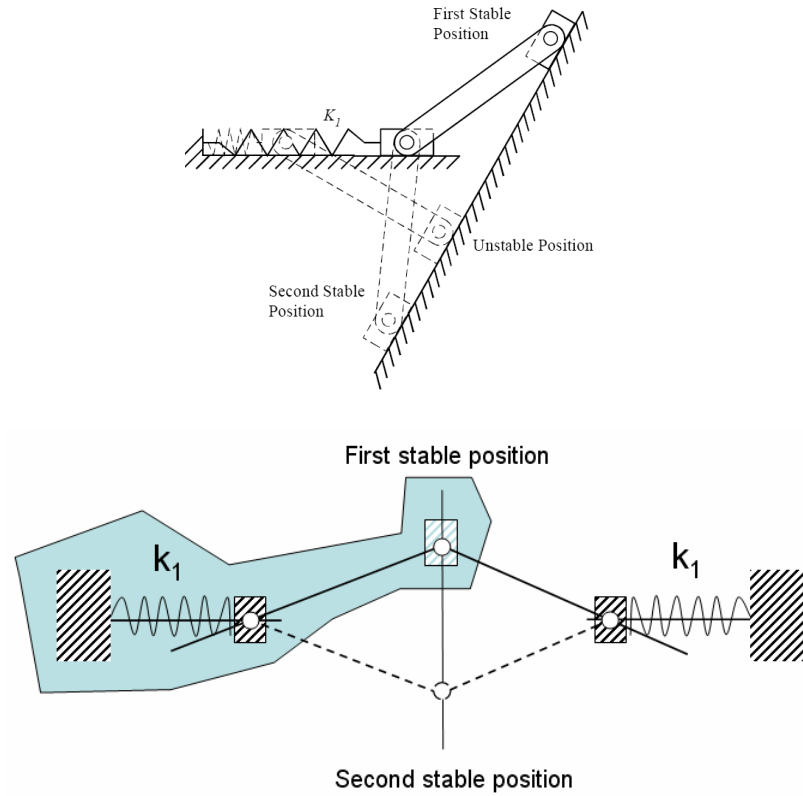
Fig. 3.7. Double-slider mechanisms with a link joining the sliders.

For the sixth class, we set k_2 and k_3 infinity stiffness, and k_1 and k_4 an equal stiffness. We can build a four bar mechanism.

First Stable Position

Unstable Position

K_4

Second Stable Position
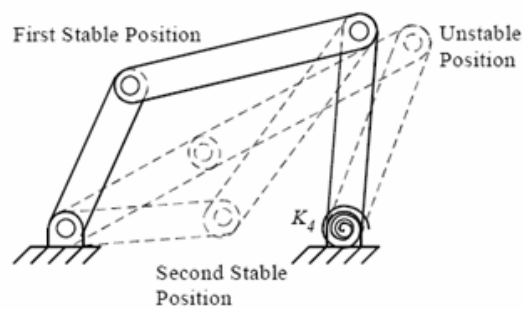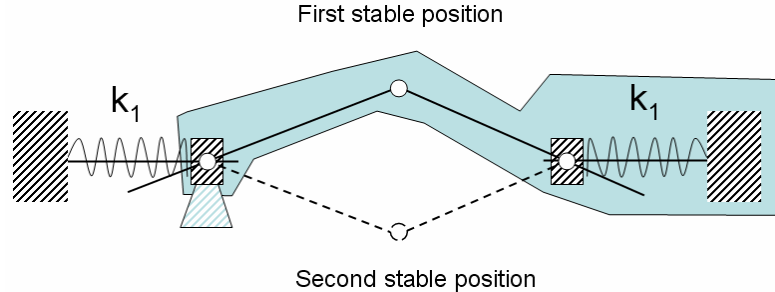
Fig. 3. 8. Four-link mechanism.

Thus, the study of a bistable mechanism can be made by studying the generic bistable mechanism. By setting the stiffness of the four springs (k_1, k_2, k_3, k_4), we can achieve the same performance as these diverse bistable mechanisms.

3.2.3 Study of bistable mechanism with ideal joints

Based on the generic bistable mechanism, we determine its characteristics to get the desired performance. To build the general model of bistable mechanism, some assumptions should be mentioned: using ideal joints (no friction, no backlash), rigid links (no deformation) and the springs (only axial displacement).

In Fig. 3.9, the four springs deform under a vertical force, the springs' stiffness are k_1, k_2, k_3, and k_4, respectively, and their lengths are listed in the table.
The total potential energy is:

$$U_{total} = \frac{1}{2}k_1\Delta_1^2 + \frac{1}{2}k_2\Delta_2^2 + \frac{1}{2}k_3\Delta_3^2 + \frac{1}{2}k_4\Delta_4^2 \tag{3.1}$$

$\Delta_{1, 2, 3, 4}$ are the length change of spring.
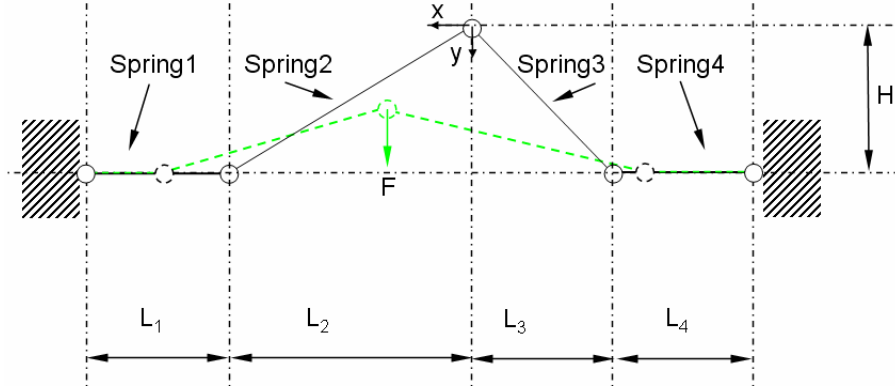
Fig. 3.9. Calculation model of basic bistable mechanism.

Tab. 3.1. The change of springs and their deformation energy.

Spring	Initial length	Changed Length	Displacement	Deformation Energy
1	L_1	L_1'	$L_1 - L_1'$	$\frac{1}{2}k_1(L_1 - L_1')^2$
2	$\sqrt{L_2^2 + H^2}$	L_2'	$\sqrt{L_2^2 + H^2} - L_2'$	$\frac{1}{2}k_2(\sqrt{L_2^2 + H^2} - L_2')^2$
3	$\sqrt{L_3^2 + H^2}$	L_3'	$\sqrt{L_3^2 + H^2} - L_3'$	$\frac{1}{2}k_3(\sqrt{L_3^2 + H^2} - L_3')^2$
4	L_4	L_4'	$L_4 - L_4'$	$\frac{1}{2}k_4(L_4 - L_4')^2$

The geometry equations:

$$(L_1' - L_1 + L_2 - x)^2 + (H - y)^2 = L_2'^2 \tag{3.2}$$

$$(L_4' - L_4 + L_3 + x)^2 + (H - y)^2 = L_3'^2 \tag{3.3}$$

$$L_1' + \sqrt{L_2'^2 - (H - y)^2} + x = L_1 + L_2 \tag{3.4}$$

$$L_4' + \sqrt{L_3'^2 - (H - y)^2} + x = L_3 + L_4 \tag{3.5}$$

These four equations give the solutions on the L_1', L_2', L_3' and L_4'. Using the total energy equation to derive about x and y, we obtain:

$$\begin{cases} \dfrac{\partial U}{\partial x} = 0 \\ \dfrac{\partial U}{\partial y} = F \end{cases} \tag{3.6}$$

This energy method permits to find out the analytical solutions of bistable mechanism with perfect springs and rotation joints. The force-displacement relation and the deformation energy-displacement relation can be obtained.

Let us consider two typical cases.
Case 1: set $k_1 = k_4 = \infty$, $L_2 = L_3 = L$, and $k_2 = k_3 = k$.
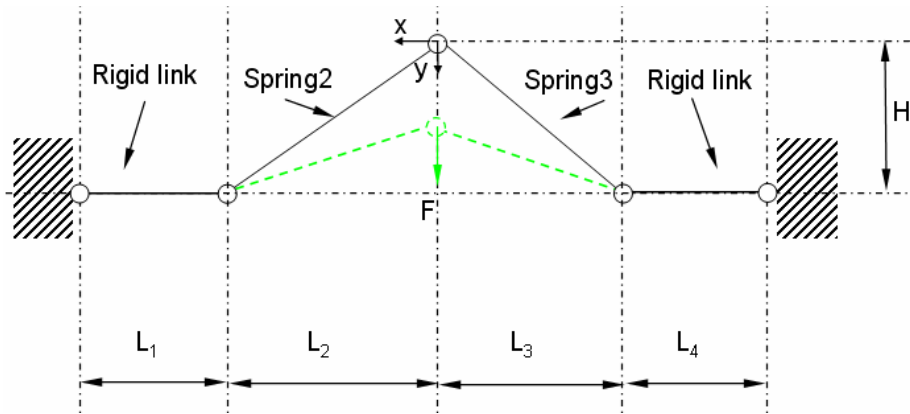
Fig. 3.10. Schematic of bistable mechanism of case 1.

The force and displacement relations can be found.

$$F_{case1} = 2 \cdot k \cdot \frac{H - y}{\sqrt{L^2 + (H - y)^2}} \cdot (\sqrt{L^2 + H^2} - \sqrt{L^2 + (H - y)^2}) \tag{3.7}$$

$$U_{case1} = \frac{1}{2} k (\sqrt{L^2 + H^2} - \sqrt{L^2 + (H - y)^2})^2 \tag{3.8}$$

To show the tendancy about force Vs displacement, we take values for example: *L=1 mm*, *H=200 μm* and *k=100 N/m.*
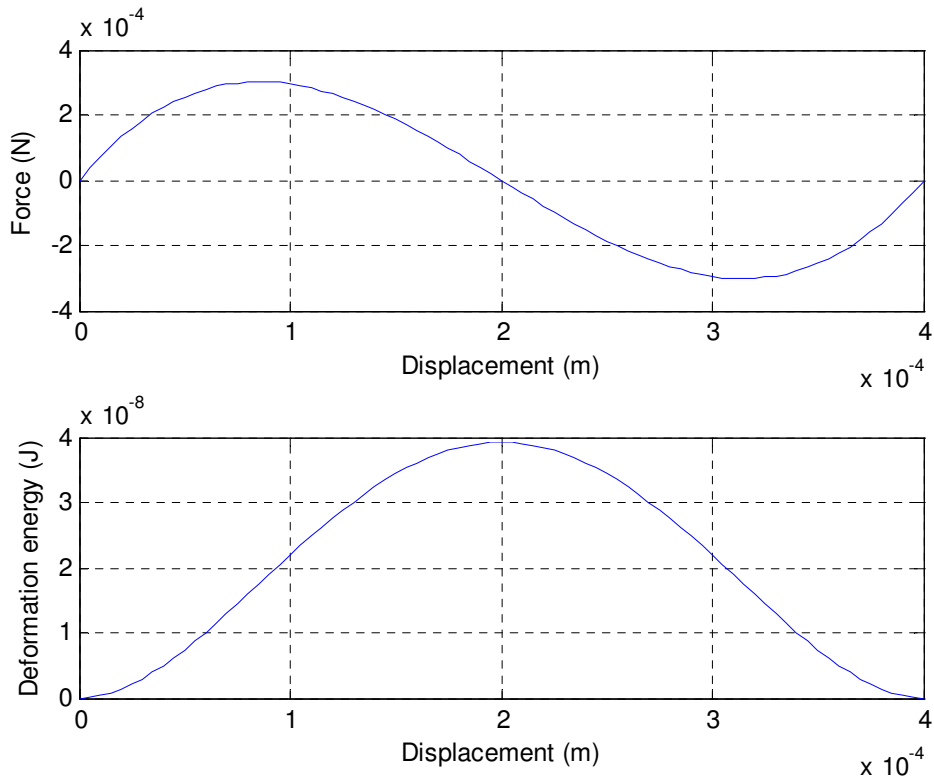
Fig. 3.11. Force –displacement and energy –displacement relations of case 1.

Case 2: set $k_2 = k_3 = \infty$, $L_2=L_3=L$, $L_1=L_4$, and $k_1=k_4=k$.

69
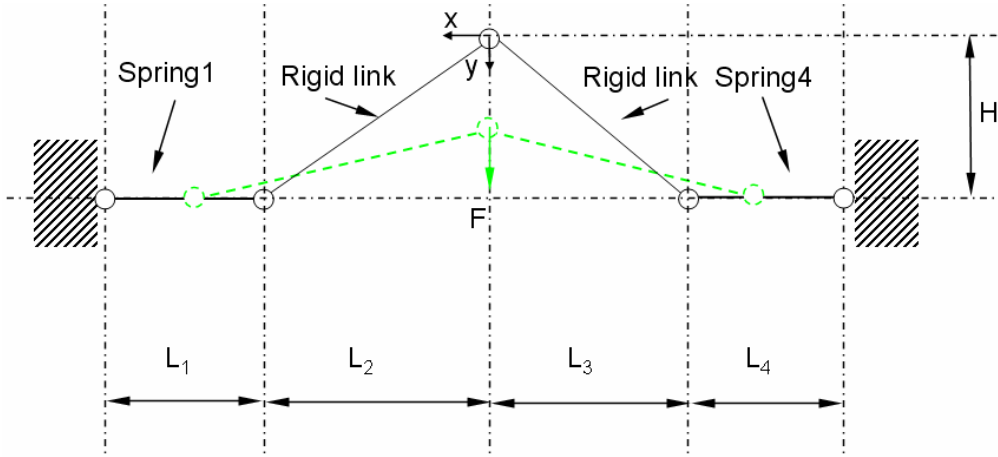
Fig. 3.12. Schematic of bistable mechanism of case 2.

The force and the displacement are given by

$$F_{case2} = 2 \cdot k \cdot (\sqrt{L^2 + H^2 - (H - y)^2} - L) \cdot \frac{H - d_1}{\sqrt{L^2 + H^2 - (H - y)^2}} \qquad (3.9)$$

$$U_{case1} = \frac{1}{2}k(\sqrt{(L^2 + H^2) - (H - y)^2} - L)^2 \qquad (3.10)$$

For example, we take the following values: L=1 mm, H=200 mm and k=100 N/m.
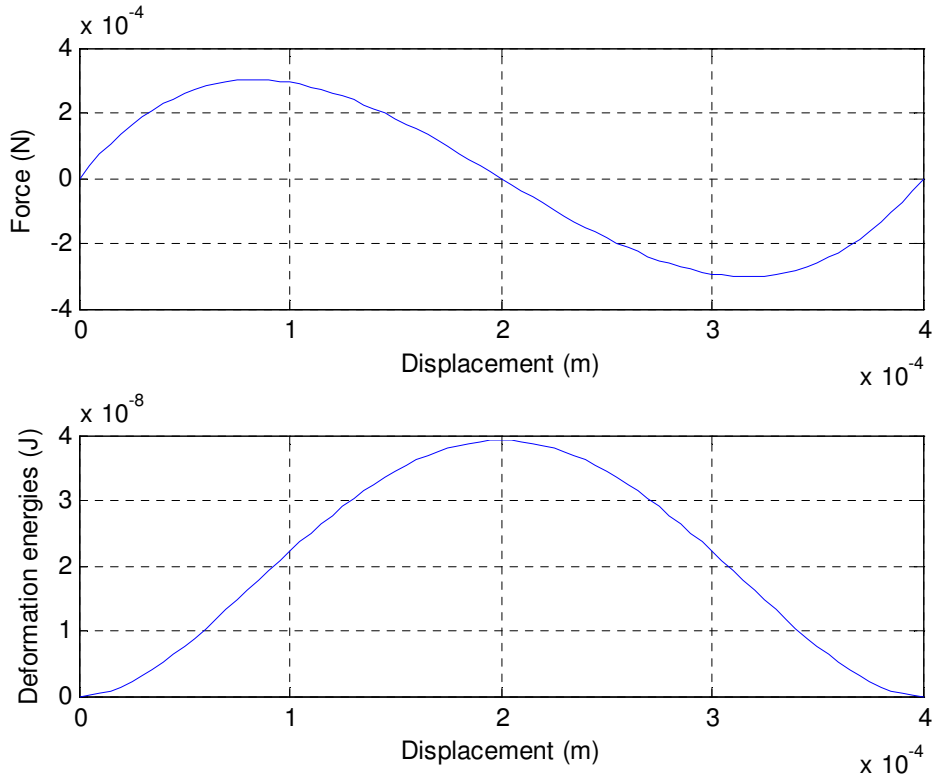
Fig. 3.13. Force –displacement and energy –displacement relations of case 2.

Thus, to build a bistable mechanism for our digital microrobot application, the symmetric setting should be respected, or it leads to horizontal displacement. The springs and the joints should be taken into account. In fact, we can fabricate the spring, but it is not worth to fabricate the perfect joint. Moreover, the friction problem and the clearance lead to inefficient joint. The compliant joints are used in stead of the conventional joints.

3.2.4 Study of bistable mechanism with compliant joints

In microrobotics, for the reasons explained in chapter 1, compliant joints are used to replace ideal joints to obtain the rotation as shown in Fig. 3.14.

71
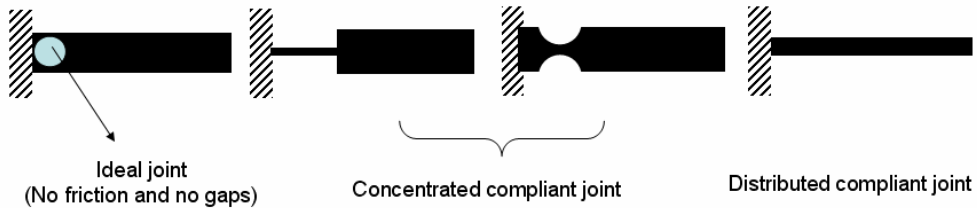
Fig. 3.14. The ideal joint and the compliant joints.

The rotation is generated by the deformation of the compliant joints. This deformation increases the deformation energy. Thus, the previous model is modified by adding the energy of the compliant joint.

The modified model is presented in the Fig. 3.15. The torsional spring and the elastic beam have a stiffness ks and kb respectively.
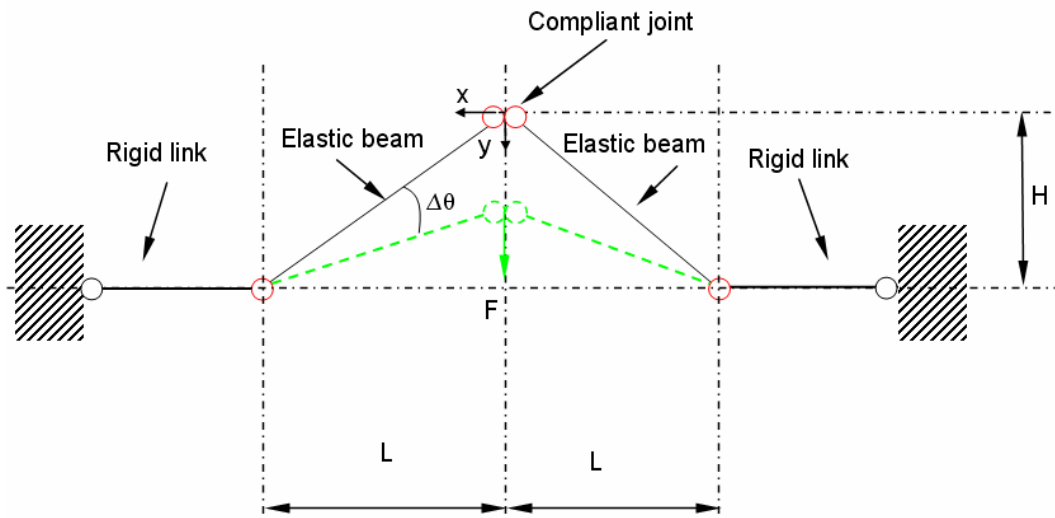
Fig. 3.15. The model of bistable mechanism with compliant joint.

For the elastic beam, the compressed length and the deformation energy are:

$$\Delta L = \sqrt{L^2 + H^2} - \sqrt{L^2 + (H-Y)^2} \tag{3.11}$$

$$E_e = \frac{1}{2} \cdot k_e \cdot \Delta L^2 \tag{3.12}$$

For the compliant joint, the compressed length and the deformation energy are:

$$\Delta\theta = \tan^{-1}(\frac{H}{L}) - \tan^{-1}(\frac{H-Y}{L}) \tag{3.13}$$

$$E_j = \frac{1}{2} \cdot k_j \cdot \Delta\theta^2 \tag{3.14}$$

The total deformation energy in the bistable mechanism can be formulated by eq. 3.12 and eq. 3.14.

$$U = 2E_e + 4E_j = 2 \cdot \frac{1}{2} \cdot k_e \cdot \Delta L^2 + 4 \cdot \frac{1}{2} \cdot k_j \cdot \Delta\theta^2 \tag{3.15}$$

The applied force can be derived.

$$F = \frac{\partial U}{\partial Y} = 2 \cdot k_e \cdot \Delta L \cdot \frac{\partial \Delta L}{\partial Y} + 4 \cdot k_j \cdot \Delta\theta \cdot \frac{\partial \Delta\theta}{\partial Y} \tag{3.16}$$

$$F = \frac{\partial U}{\partial Y} = 2 \cdot k_e \cdot (\sqrt{L^2 + H^2} - \sqrt{L^2 + (H-Y)^2}) \cdot \frac{(H-Y)}{\sqrt{L^2 + (H-Y)^2}} + 4 \cdot k_j \cdot (\tan^{-1}(\frac{H}{L}) - \tan^{-1}(\frac{H-Y}{L})) \cdot \frac{1}{(1 + (\frac{H-Y}{L})^2)L}$$

$$\tag{3.17}$$

We ignore the high order of the function, so we obtain an approximate force,

$$F \approx 2 \cdot ke \cdot \frac{(2HY - Y^2)(H-Y)}{2L^2 + (H-Y)^2} + 4 \cdot kj \cdot \frac{Y}{L^2 + (H-Y)^2} \tag{3.18}$$

For *F=0*, we have three real solutions which represent two stable positions and one unstable position. In our case, the stiffness of these two elastic elements are:

$$ks = \frac{EI}{0.1L}, \quad kb = \frac{EA}{0.8L}$$

ks is the rotation spring stiffness described by moment/angle.
kb is the compressed stiffness described by force/displacement.
For example, we use the values in the table, the curve can be plotted:

Tab. 3.2 Values of parameters.

E	b	h1	L	h2	I	A	h
169 GPa	100 µm	16 µm	4 mm	50 µm	b*h1^3/12 m^4	b*h2 m^2	60 µm
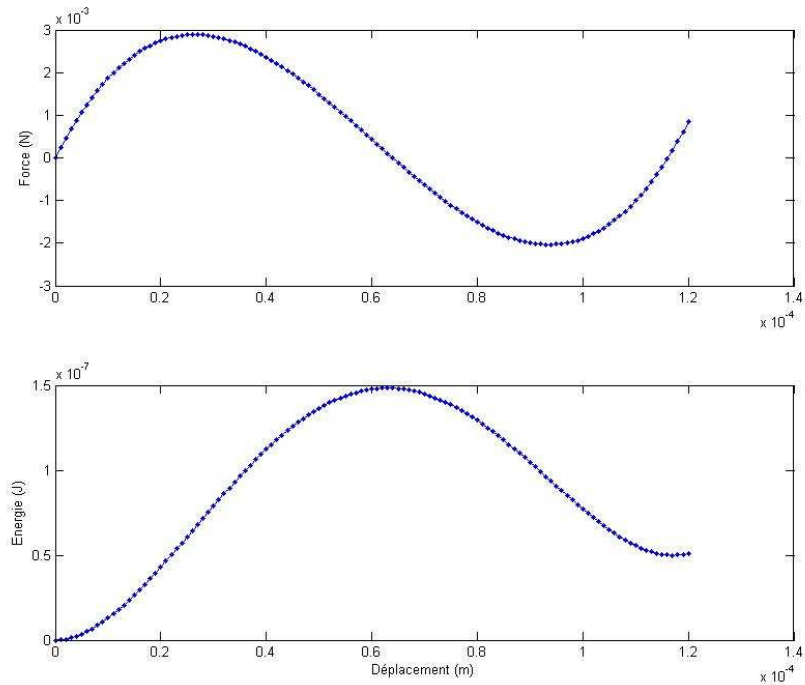
Fig. 3.16. The force-displacement and energy-displacement relations.

We can observe that the choice of the compliant joints results into the bistable behaviors, but their deformation energy can not be released; there is about 30% of residual deformation energy. Unlike the energy in the elastic beams which can be totally released, this energy in the compliant joints increase with the displacement of the bistable mechanism. In some cases, the elastic beam's deformation energy take fewer fractions in the total energy than the compliant joint's deformation energy, which will make the second stable position very close to the unstable position. In Fig. 3.17, the initial height h leads to different bistable behaviors. It shows, when h<35 µm, that the unstable position (local maximum energy point) is very close to the second stable position (local minimum energy point), which may cause the loss of the second stable position.
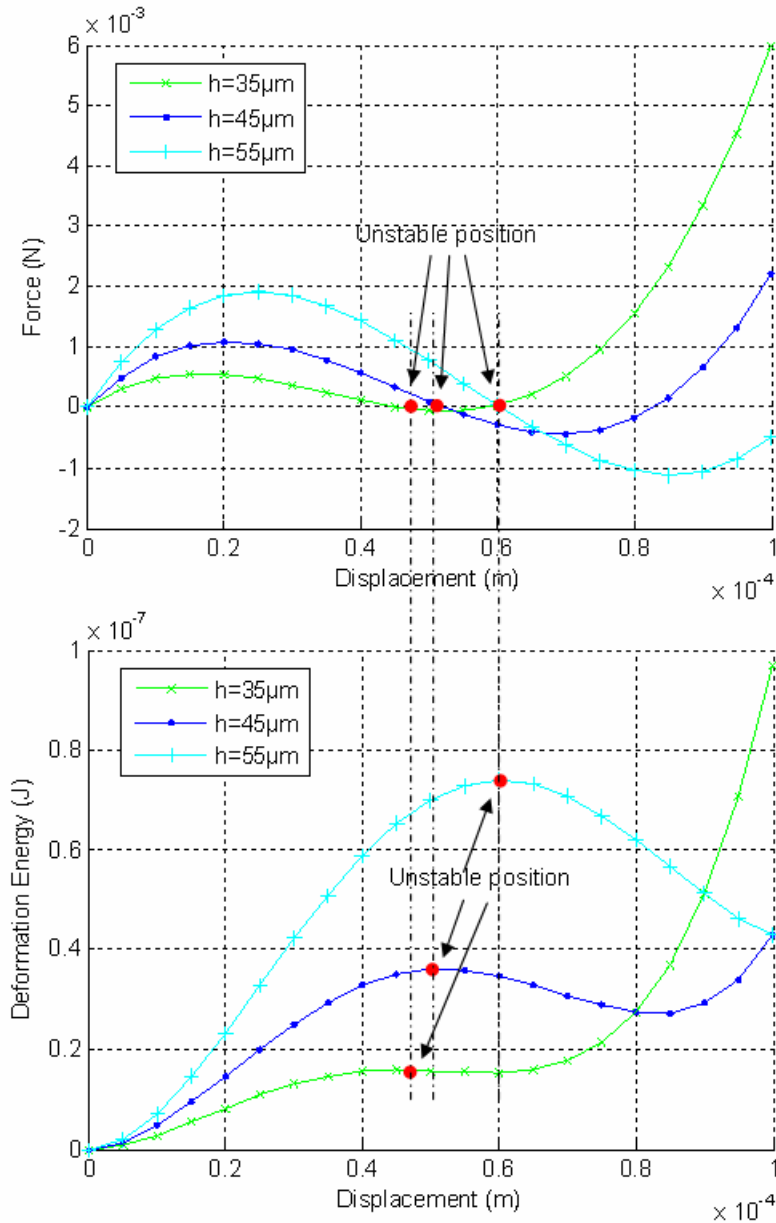
Fig. 3.17. The F-D and E-D relation due to different initial heights.

To ensure a good bistability, the energy kept in the elastic beam should be bigger or at least equal to the energy kept in the compliant joint.

$$Max(E_e) \geq Max(E_j) \tag{3.19}$$

This condition can ensure that the maximum deformation energy is twice the residual energy.

For the elastic beam, the compressed length and the deformation energy are:

$$\Delta L = \sqrt{L^2 + H^2} - \sqrt{L^2 + (H-Y)^2} \tag{3.20}$$

$$E_e = 2 \cdot \frac{1}{2} \cdot k_e \cdot \Delta L^2 \tag{3.21}$$

When *Y=H,* we obtains the maximum value.

$$MaxE_e = 2 \cdot \frac{1}{2} \cdot k_e \cdot \Delta L^2 = k_e \cdot (\sqrt{L^2 + H^2} - L)^2 \tag{3.22}$$

For the compliant joint, the changed angle is:

$$\Delta\theta = \tan^{-1}(\frac{H}{L}) - \tan^{-1}(\frac{H-Y}{L}) \tag{3.23}$$

When *Y=2H*, the maximum value is obtained.

$$MaxE_j = 4 \cdot \frac{1}{2} \cdot k_j \cdot \Delta\theta^2 = 8k_j \left(\tan^{-1}(\frac{H}{L}) \right)^2 \tag{3.24}$$

So, according to 3.19, we obtain:

$$k_e \cdot (\sqrt{L^2 + H^2} - L)^2 \geq 8k_j \left(\tan^{-1}(\frac{H}{L}) \right)^2 \tag{3.25}$$

Usually, H<<L,

$$k_e \cdot (\frac{H^2}{2L})^2 \geq 8k_j \frac{H^2}{L^2} \tag{3.26}$$

$$\frac{k_e}{k_j} \cdot \geq \frac{32}{H^2} \tag{3.27}$$

The ratio of stiffness between the elastic elements and compliant joints should be bigger than $\frac{32}{H^2}$ (H: the initial height) to ensure a good bistability.

So, to build a bistable mechanism, a compliant joint and an elastic beam are required. In the real situation, the two components can be designed freely.
For example, the elastic beam can be a single beam with a constant section, and a spring mechanism as in Fig. 3.18.
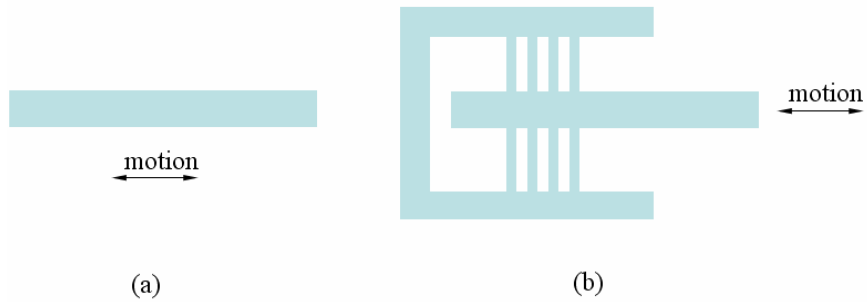
Fig. 3.18. (a) An elastic beam. (b) A spring mechanism.

The compliant joints can be realized with shapes shown in Fig. 3.19.
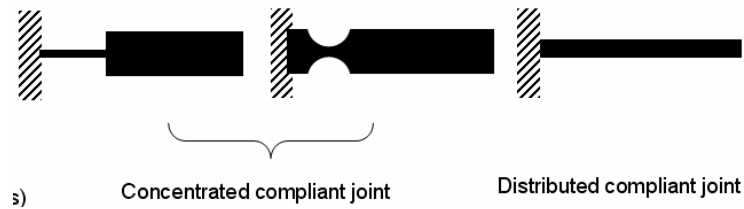
Concentrated compliant joint   Distributed compliant joint
Fig. 3.19. Examples of compliant joints.

A bistable mechanism is built as shown in Fig. 3.20. The symmetric configuration is built to obtain unidirectional motion (y).
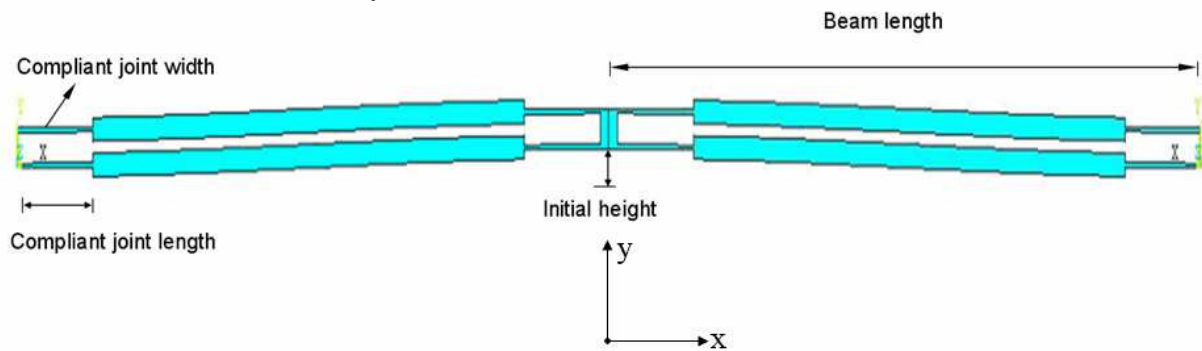
Fig. 3.20. The designed bistable mechanism.

Their stiffness can be calculated by:

$$kj = \frac{EI}{0.1L}, \quad ke = \frac{EA}{0.8L}, \text{ then } \frac{k_e}{k_j} \approx 2.34 \times 10^{10}$$

77

Tab. 3.3. The criterion values.

H (µm)	35	40	45
$\dfrac{32}{H^2}$	2.61×10^{10}	2.00×10^{10}	1.58×10^{10}

In this case, the initial height should be bigger than 40 µm to obtain good bistability. In fact, the compliant joint performance depends on their width and length. A thinner and longer compliant joint tends to perfect joint, but we should find the tradeoff between the compliance and the reliability.

3.2.5 Conclusion

This section proposed a generic model dedicated to the design of the bistable module. This generic model allows us to obtain the same performance as the various bistable mechanisms by designing the stiffness of the spring and the initial height.

Based on this generic module, a highly reliable bistable mechanism could be designed. Due to the fabrication difficulties of the ideal joints, the compliant joints are used to build a monolithic bistable mechanism.

In order to obtain bistable behaviors for the mechanism with the compliant joints, there are two important factors which should be taken into account: the stiffness of the elastic elements and the compliant joints, and the initial height. The dimensions of bistable mechanism are defined by the geometry. The spring with lower stiffness is much better as the compliant joint. The final dimension will be defined in the next chapter.

3.3 Design of the microactuators

We need to choose and design microactuators that offer enough mechanical energy to switch the bistable mechanism from the stable positions to the unstable position (after overcoming unstable position, the bistable structure goes itself to the other stable position). In order to design the suitable actuators, there are two factors that should be considered: the material and the machining method.

Generally, there are two cases: the use of the same material and the use of different materials. The second one requires machining or assembling the second material, which would lead to complicated microfabrication process. In this section, we propose several actuation principles.

3.3.1 Integrated actuation based on smart materials

Smart materials, such as piezoelectric, electrostrictive, and magnetostrictive materials present good performance which can be interesting to actuate bistable mechanisms.

According to the last section, during the switching of the bistable mechanism, the elastic element is firstly compressed and then recalled (see Fig. 3.21). This can be made by using the active materials due to the change of length under electric field (see Fig. 3.22). So, the deformation of the elastic element can be realized directly using the smart material.
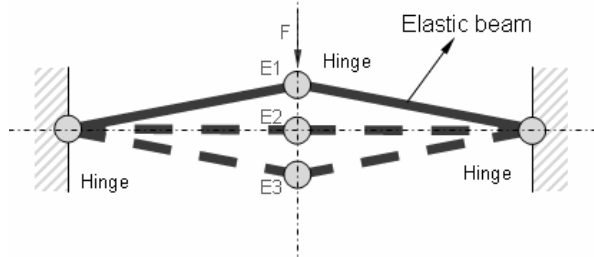
Fig. 3.21. The elastic beam is compressed from first stable position to second stable position.

$$\Delta L = V \, d_{31} \, L$$

$$\Delta W = V \, d_{31} \, W$$
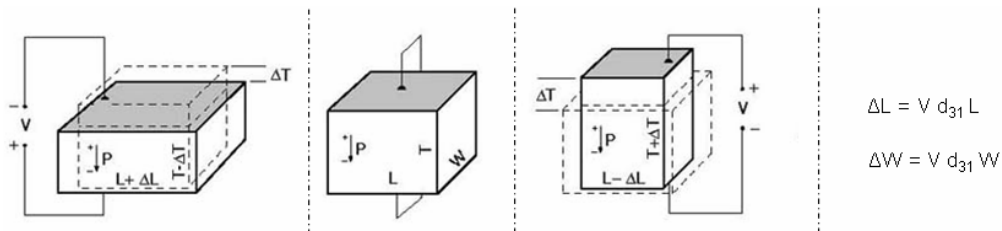
Fig. 3.22. Bi-directional actuation of piezoelectric materials

We propose a bistable mechanism integrating the microactuators. Considering the different active materials, the piezoelectric material is firstly taken into account. A proposed design is shown in Fig. 3.23. The bistable mechanism is made in piezoelectric material on which the electrodes are deposited on both the front and back sides.
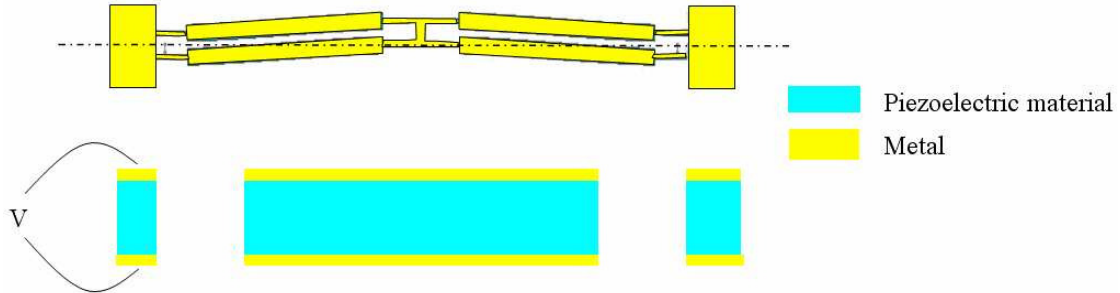
Fig. 3.23 Bistable mechanism integrating the actuators

According to the piezoelectric coupled equation:

$$\{S\} = [s^E]\{T\} + [d^t]\{E\}$$

(3.28)

Where S is the strain, s is the compliance, T is the stress and *[d]* is the matrix for the converse piezoelectric effect. The superscript E indicates a zero or valued constant electric field.

The strain-charge for a material, such as a polarized piezoelectric ceramic (tetragonal PZT or BaTiO3) may also be written as (ANSI IEEE 176):

$$\begin{bmatrix} S_1 \\ S_2 \\ S_3 \\ S_4 \\ S_5 \\ S_6 \end{bmatrix} = \begin{bmatrix} s_{11}^E & s_{12}^E & s_{13}^E & 0 & 0 & 0 \\ s_{21}^E & s_{22}^E & s_{23}^E & 0 & 0 & 0 \\ s_{31}^E & s_{32}^E & s_{33}^E & 0 & 0 & 0 \\ 0 & 0 & 0 & s_{41}^E & 0 & 0 \\ 0 & 0 & 0 & 0 & s_{55}^E & 0 \\ 0 & 0 & 0 & 0 & 0 & s_{66}^E \end{bmatrix} \begin{bmatrix} T_1 \\ T_2 \\ T_3 \\ T_4 \\ T_5 \\ T_6 \end{bmatrix} + \begin{bmatrix} 0 & 0 & d_{31} \\ 0 & 0 & d_{32} \\ 0 & 0 & d_{33} \\ 0 & d_{24} & 0 \\ d_{15} & 0 & 0 \\ 0 & 0 & 0 \end{bmatrix} \begin{bmatrix} E_1 \\ E_2 \\ E_3 \end{bmatrix}$$

(3.29)

The deformation of piezoelectric material is induced by the electric field and the external force.
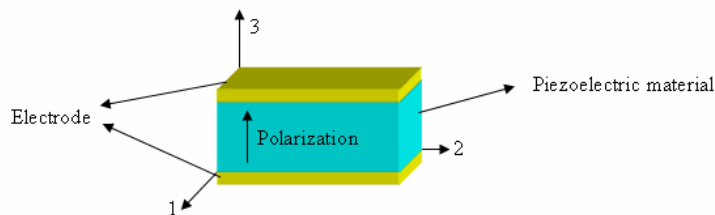
Fig. 3.24. The defined direction (*1,2,3)* for deformation.

80

This calculation model can be considered in Fig. 3.25.
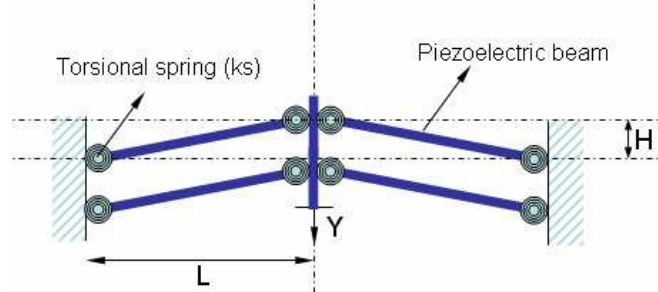
Fig. 3.25. Calculation model of piezoelectric bistable mechanism.

Because we make a thin-long beam in the direction of 1 under electric field E_3, we take into account the strain in the direction of 1. Based on the Eq. 3.29, we have the equation:

$$S_1 = s_1 T_1 + s_{12} T_2 + s_{13} T_3 + d_{31} E_3 \tag{3.30}$$

Since there is no external force, there are no stresses (T1, T2 and T3). According to 3.30, the compressed length of the beam can be estimated as below,

$$\Delta L = \int_0^L s_1 = \frac{d_{31} U L}{d} \tag{3.31}$$

As shown in Fig. 3.26, from the initial position to the unstable position, the piezoelectric elastic beam is compressed:

$$\Delta L = \sqrt{L^2 + h^2} - L \approx \frac{h^2}{2L} \tag{3.32}$$
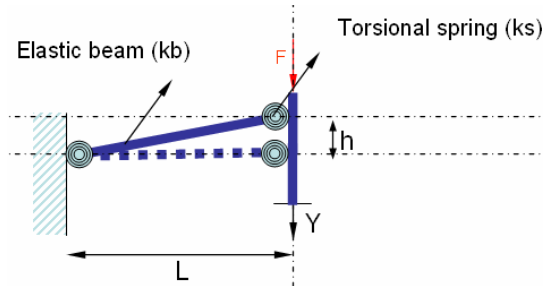
Fig. 3.26. The model of the compressed piezoelectric material.

The required actuation voltage is: $U = \dfrac{\Delta L \cdot d}{d_{31} L} = \dfrac{h^2 \cdot d}{2 \cdot L^2 \cdot d_{31}}$ $\tag{3.33}$

In fact, in order to actuate the bistable mechanism, torsional springs should be considered in the model because they require more energy to be actuated. Here we give a simple model to understand the principle.

By taking d=100 µm, L=4 mm, d_{31}=200 pC/N, we obtain the result given in Fig. 3.27.
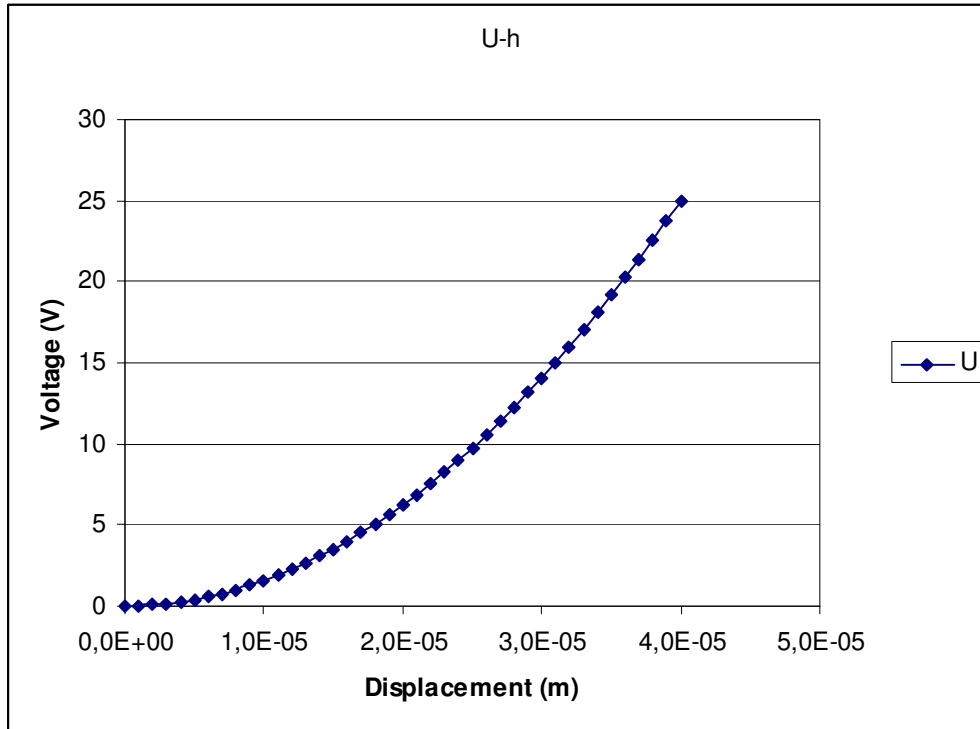
Fig. 3.27. The applied voltage Vs the displacement.

According to this calculation, 25V applied on piezoelectric actuator can produce about 40 µm displacement, which can switch the bistable mechanism. The piezoelectric material may be machined using laser micromachining or special MEMS process.

Using the same design, electrostrictive material or magnetostrictive material can be used to build this kind of bistable mechanism. The magnetostrictive material takes the advantage of the wireless actuation, and only the magnetic field should be created to actuate the bistable mechanism (see Fig. 3.28).
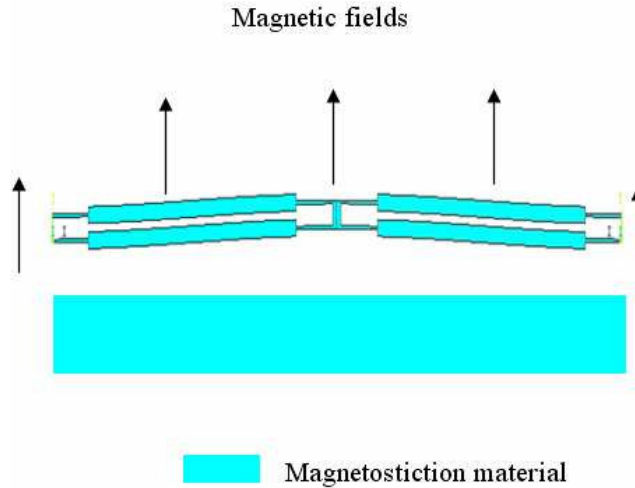
Fig. 3.28. The magnetostriction bistable mechanism

Considering the Terfenol-D material, according to the coupled equation:

$$\varepsilon = \frac{\sigma}{E_y^H} + qH \qquad (3.34)$$

ε : Strain
σ : Stress (Pa)
E_Y^H : Young modulus (Pa)
q : Coupling factor (m/A)
H : Magnetic field density (A/m)

According to the eq. 3.34, the compressed length of the magnetostriction material is:

$$\Delta L = \int_0^L \varepsilon = qHL \qquad (3.35)$$

As the basic model, it needs that the compressed length of elastic spring is:

$$\Delta L = \sqrt{L^2 + h^2} - L \approx \frac{h^2}{2L} \qquad (3.36)$$

So, the required actuation magnetic field is:

$$H = \frac{h^2}{2qL^2} \qquad (3.37)$$

For example, we use these values $q=15\times10^{-9}$, L=4 mm, Fig. 3.29 can be obtained.
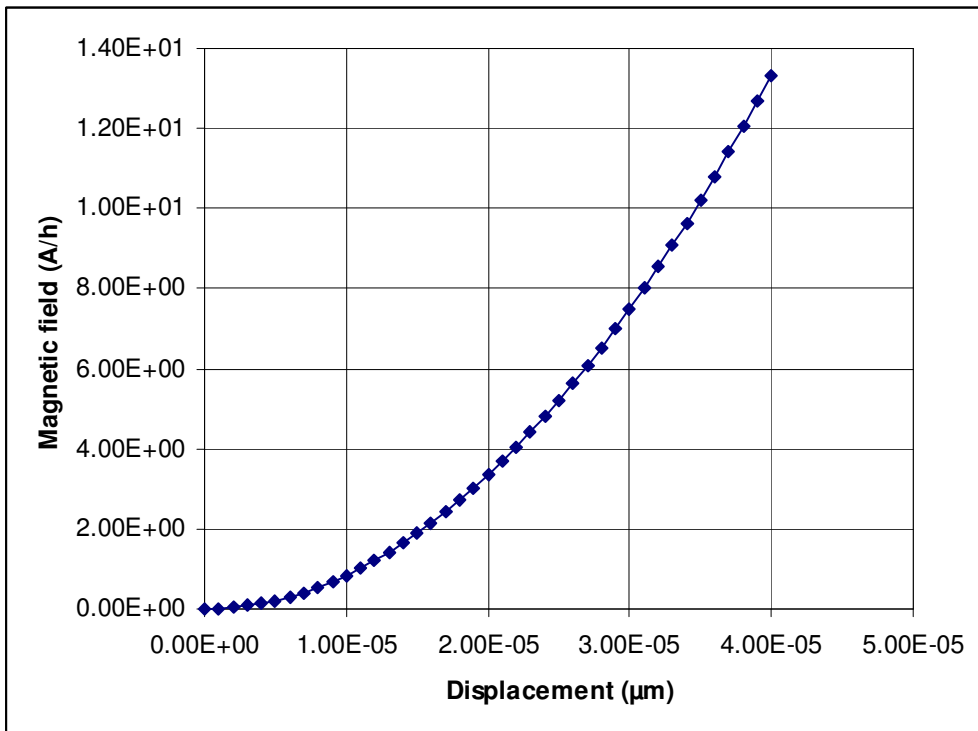
Fig. 3.29. The applied magnetic field Vs the displacement.

According to this calculation, 300 A/m magnetic field densities applied on the actuator permits to switch the bistable mechanism. This magnetic field can be created by an external electromagnetic coil. But, special micromachining process should be developed to micromachine material.

Therefore, the use of active materials allows actuating the bistable mechanism by itself. It presents many advantages: reduction of the fabrication process, and compact dimension. However, these active materials need to be machined by special process. New processes should be developed.

3.3.2 External actuation based on thermal actuators

Thermal actuation is also a solution to switch the bistable mechanism, as shown in Fig. 3.30. It is a typical U-shape actuator. The U-shape uses the asymmetric dilatation to induce an in-plane displacement. This actuation can be divided into two processes: the electro-thermal processes, secondly and the thermal-mechanism process.

Fig. 3.30. U-shape thermal actuator.

3.3.2.1 Thermal-mechanical model
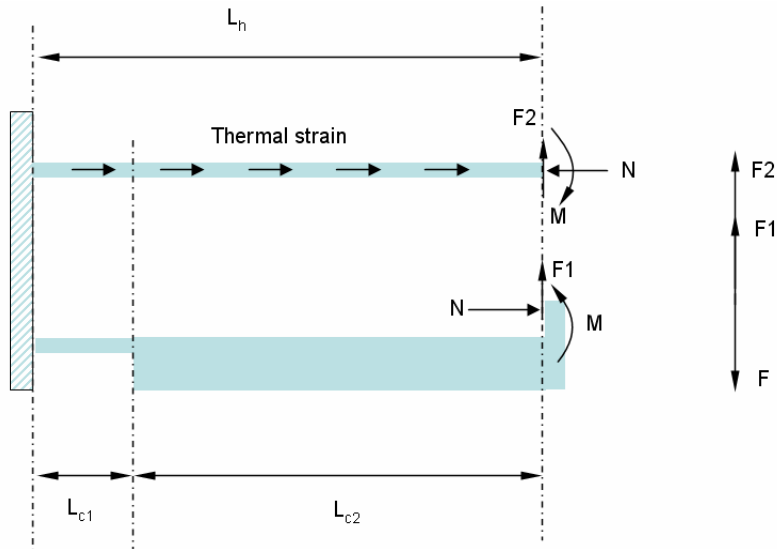
Fig. 3.31. The model of thermal actuator.

Symbols of dimension are in the Fig. 3.31. *E* is the young's modulus, *I* is the moment of inertia. For the hot beam, the force-displacement and moment-angle equations are:

$$\begin{pmatrix} y \\ \theta \end{pmatrix} = \begin{bmatrix} \dfrac{L_h^{\,2}}{2EI_h} & \dfrac{L_h^{\,3}}{3EI_h} \\[2mm] \dfrac{L_h}{EI_h} & \dfrac{L_h^{\,2}}{2EI_h} \end{bmatrix} \begin{bmatrix} M \\ F_2 \end{bmatrix} \tag{3.38}$$

85

For the cold beam, the force-displacement and moment-angle equations are:

$$\begin{pmatrix} y \\ \theta \end{pmatrix} = \begin{bmatrix} \dfrac{L_{c1}^2}{2EI_c} + \dfrac{L_{c1}L_{c2}}{EI_{c1}} & -\dfrac{L_{c1}^3}{3EI_c} - \dfrac{L_{c1}^2 L_{c2}}{2EI_{c1}} \\ -\dfrac{L_{c1}}{EI_{c1}} & \dfrac{L_{c1}^2}{2EI_{c1}} \end{bmatrix} \begin{bmatrix} Nd_0 - M \\ F_1 \end{bmatrix} \tag{3.39}$$

In the vertical direction, the total forces are:

$$F = F_1 + F_2 \tag{3.40}$$

$$\alpha\Delta T L_h - \frac{NL_h}{EA_h} - \frac{NL_c}{EA_c} = \theta \cdot t_0 \tag{3.41}$$

There, α is coefficient of thermal expansion and ΔT is the increased temperature.

There are 6 unknowns and 6 equations, we can calculate out the solution:

$$D = \frac{(-94L_h FI_h + 141t\alpha TEAI_h - 47t^2 AL_h F + 50L_h FI_c - 675t\alpha TEAI_c)L_h^2}{6E(-625I_c^2 + 1150I_h I_c + 250I_c At^2 + 47I_h^2 + 94I_h At^2)} \tag{3.42}$$

The displacement without force ($F=0$) is given by:

$$D = \frac{(141I_h - 675I_c)t\alpha TEAL_h^2}{6E(-625I_c^2 + 1150I_h I_c + 250I_c At^2 + 47I_h^2 + 94I_h At^2)} \tag{3.43}$$

The blockage force ($D=0$):

$$F = \frac{3t\alpha TA(47I_h - 225I_c)}{L_h E(94I_h + 47t^2 A - 50I_c)} \tag{3.44}$$

The comparison between the calculated model and the FEA simulation is given in Fig. 3.32.
By taking L_h=4 mm, L_{c1}=500µm, W_h=30µm, W_c= 120µm, we obtain the result given in Fig. 3.27.
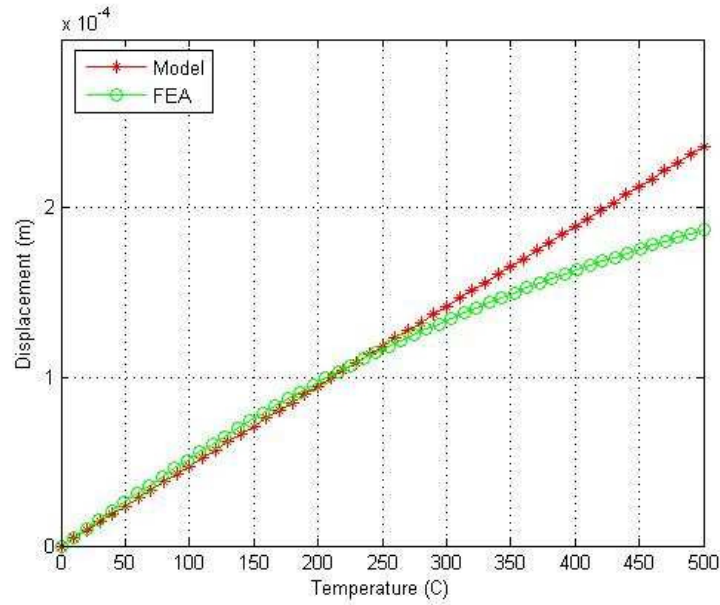
Fig. 3.32. Temperature-displacement comparison between model and FEA.

We can observe that the model gives a solution accurate enough when the temperature is below 300 °C.
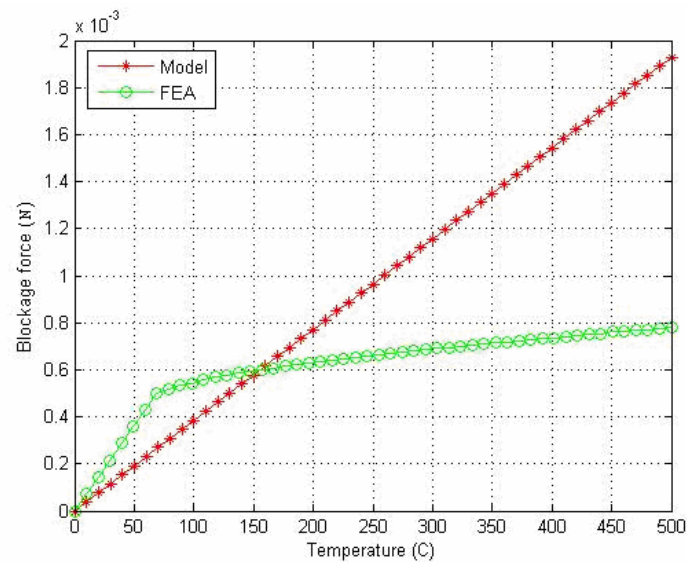
Fig. 3.33. Temperature-blockage force comparison between model and FEA.

87

According to the Fig. 3.33, the blockage force is obtained by limiting the tip's displacement. Since in this linear model the buckling effect is not taken into account, the thermal actuator can not give a linear force after buckling. In fact, the buckling effect takes place in the compressed hot beam and causes the reduction of the stiffness.

Therefore, to design this kind of microactuator, the buckling effect of hot beam should be taken into account. It should have an enough stiffness to avoid the buckling effect during actuation of bistable mechanism.

3.3.2.2 Electro-thermal model

Since the beam is heated by the electric current, it is necessary to estimate the transformation from electrical energy to thermal energy.
According to the previous calculation, we need to heat the hot beam until $300^{\circ}C$ to obtain enough force to actuate the bistable mechanism.
The resistance of hot beam is:

$$R = \frac{\rho l}{S} = 2\frac{2\times10^{-4}\times4\times10^{-3}}{2000\times10^{-12}} = 400\Omega \tag{3.45}$$

Where ρ is the resistivity, l is the length, S is the section area.
The resistance of cold beam is:

$$R = \frac{\rho l}{S} = \frac{2\times10^{-4}\times3.5\times10^{-3}}{12000\times10^{-12}} + \frac{2\times10^{-4}\times0.5\times10^{-3}}{2000\times10^{-12}} = 108\Omega \tag{3.46}$$

In the hot beam, the kept energy while increased to $300^{\circ}C$ is:

$$E = C \times M \times \Delta T \tag{3.47}$$

$$E = 705\times2.78\times10^{-8}\times300 = 5.88mJ \tag{3.48}$$

where
C: Thermal capacity of silicon ($705J\cdot kg^{-1}\cdot K^{-1}$)
M: Mass of hot beam (27.8 µg)
ΔT: Increased temperature (300K)

In the cold beam, the kept energy is fourth time lower.
$E_c = 1.53mJ$
So, the total energy induced is:
$E_{total} = 7.21mJ$

Since there is almost no other kind of energy loss (convection, and radiation) [QIU 04], the applied voltage can be estimated.

$$U = \sqrt{\frac{R \cdot E_{total}}{t}} = \sqrt{\frac{508 \cdot 7.21 \times 10^{-3}}{10^{-2}}} = 20V \qquad (3.49)$$

Thus, an applied voltage of 20V during 10ms will heat enough to actuate the bistable mechanism.
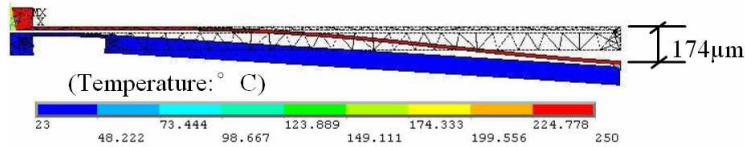
Fig. 3.34. Electro-thermal-mechanical simulation result.

To verify the estimation, an electro-thermal-mechanical simulation is performed with ANSYS. The result is shown in Fig. 3.34. A voltage of 20V can produce 174 µm displacements, which is enough to switch the bistable mechanism.

3.3.3 Electrostatic actuators

There are two kinds of electrostatic actuators, the parallel plate and the comb drive. Since the parallel plate presents the pull-in effect which leads to small distance, here we consider only the comb-drive. Comb drive electrostatic actuators can give a constant force and large displacement.
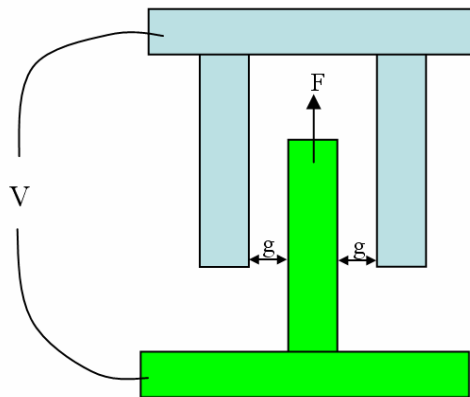
Fig. 3.35. A single finger of comb-drive.

$$F = \frac{nt\varepsilon_0\varepsilon_r V^2}{2g} \qquad (3.50)$$

89

where
V = applied electric voltage
ε_r = relative permittivity of dielectric
ε_0 = permittivity of free space (8.85 pF/m)
n = number of electrode pairs
t = thickness of electrodes
g = gap between electrodes

In order to estimate the number of the fingers required to actuate the bistable mechanism, the fabrication process is taken into account. The Bosch DRIE process limits the minimum width of a beam to 5µm. A thickness of 100 µm is used. The constant force can be obtained:

$$F = \frac{1 \times 100 \times 10^{-6} \times 8.85 \times 10^{-12} \times 100^2}{5 \times 10^{-6}} = 1.77 \mu N \qquad (3.51)$$

In order to actuate the bistable mechanism, a force of 1mN is needed, so the number of fingers is:

$$N = \frac{1000}{1.77} \approx 565 \qquad (3.52)$$

This will take a length of L:

$$L = 565 \times 20 \times 10^{-6} = 1.13 cm \qquad (3.53)$$

This dimension is too long to fit in the bistable module.

3.3.4 Conclusion

The various actuation principles show different performance which are summarized in Tab. 3.4.

Tab. 3.4. Comparison of different kinds of possible actuator.

Actuator	Structure	Micromachining	Dimension
Active material	Integrated with the bistable mechanism	Active material	Change with bistable mechanism
Thermal actuator	U-shape	Silicon	Medium
Electrostatic actuator	Comb-drive	Silicon	Large

Active materials present good performance. Their dimensions are not limited and compact dimensions. Furthermore, wireless actuation is also possible. However, we can not fabricate this design, because our clean room does not provide these active material microfabrications, the development of new process is required that is not possible in the context of this thesis.

In that condition, we decided to use external actuation. Since the dimensions of electrostatic actuators take a large of space, the thermal actuator is chosen in this work.

3.4 Stop blocks design

3.4.1 Overall design

As we have seen above, we need two stable positions, each of them having a blockage force. Two stop blocks have to be designed to ensure the two final positions and blockage forces. The first one can be integrated in the structure of the module as a bump in the frame that maintains the whole system. This bump is defined to limit in the desired position the displacement of the bistable structure.

The second one is more complicated to design. In chapter 2, we have noticed that no solution have been proposed in the MEMS literature to enable such a double wish. In fact, a solution would exist if we are able to pre-constrain the structure during the microfabrication process. Such a solution should be inspired from [CHA 08] but the process is very difficult to perform and the obtained pre-stress is far from the desired blockage force. So, we have to design a mechanical solution based on compliancy to obtain the second stop block.

3.4.2 Detailed design of the compliant stop block

The designed stop block is shown in Fig. 3.36. We use deformable beams that are forced slip into the stop block. Once it is actuated, it is limited by the stop block. This compliant stop block requires a large stiffness in the direction of shuttle's motion, and a relative small stiffness in the perpendicular direction in order to deform.

(a) Before activation

(b) After activation
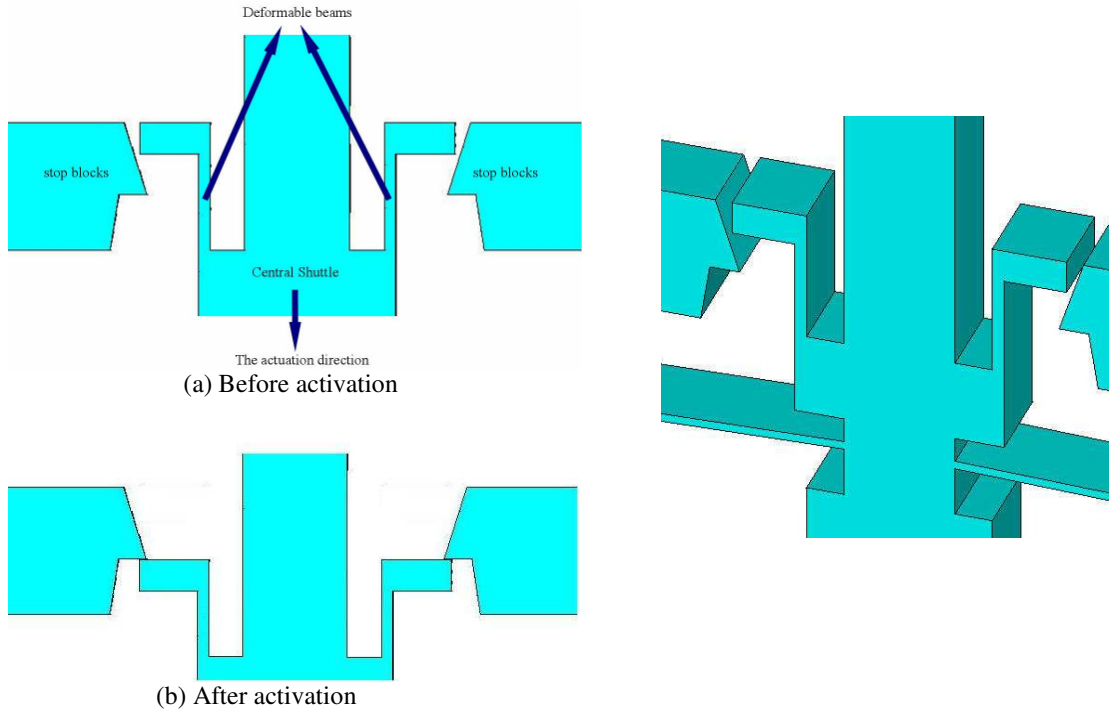
Fig. 3.36. The designed stop block.

In order to ensure the successful activation into the first stop block, the deformable beam should be designed carefully.

The deformable beams have a displacement δ, L is the length of deformable beam, E is the Young's module and the I is the moment of inertia. The cantilever end deflection δ to applied stress σ:

$$\delta = \frac{3\sigma(1-\upsilon)}{E}\left(\frac{L}{t}\right)^2 \tag{3.54}$$

Where ν is the Poisson's ratio, E is the Young's modulus, L is the beam length and t is the cantilever thickness (see Fig. 3.37). To avoid the material fracture, we give a value of maximal stress of 300Mpa.

Since the activation process can be built a model of contact analysis, a FEA is done by using the commercial software ANSYS. We give dimensions of L=310µm and t=15µm to perform this simulation.
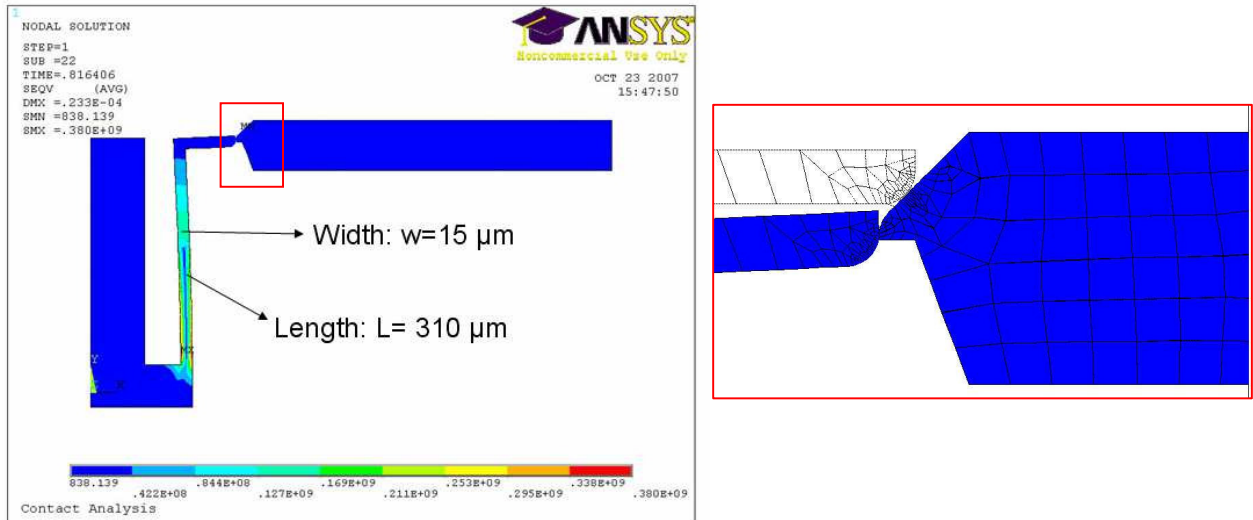
Fig. 3.37. The activation simulation of the stop block.

The simulation shows that it can be activated by an external force (see Fig. 3.37). The contact surface does not give a great friction when the deformable beams have a lower stiffness in the normal direction. Compliant stop block takes use of the curved surface to create blocked positions. Firstly, the beams contacts the surfaces due to an external force, then slip following with the curved surface, lastly get into the blocking position and we stop applying this external force. The design of this deformable beam should be done carefully to avoid the fracture. Their dimension can be defined according to the fracture criteria.

3.5 The bistable module

Based on the design of the bistable structure, the thermal actuators and the stop blocks, a complete view of a bistable module is given in Fig. 3.38.
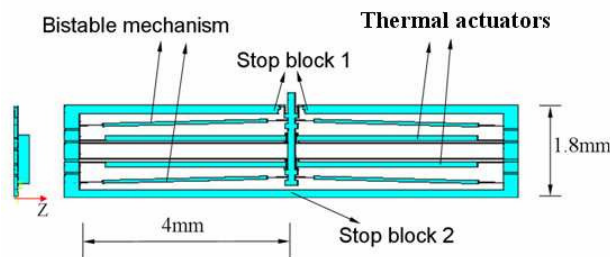
Fig. 3.38. An entire bistable module.

93

Two pairs of thermal actuators are used, and the two locations of the stop blocks are defined in the Fig. 3.39.
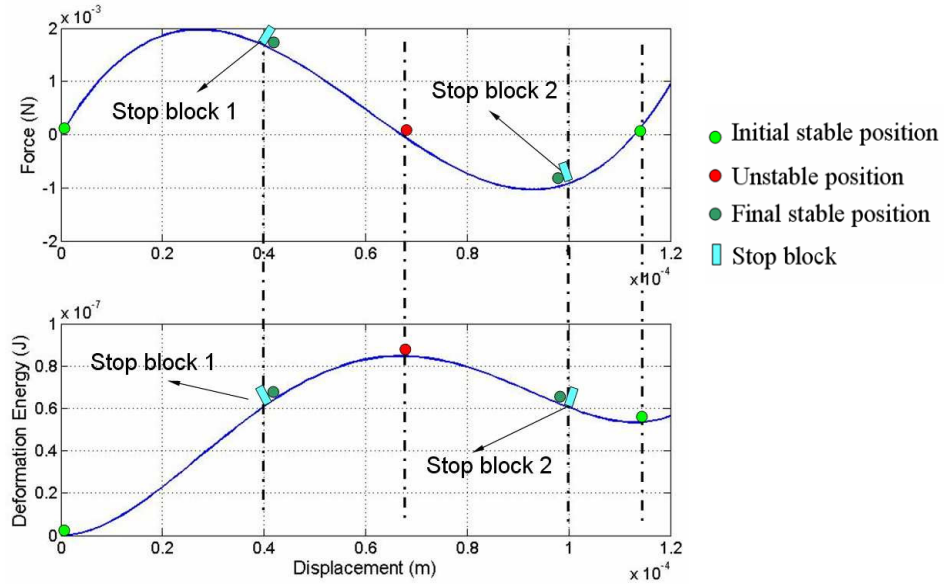
Fig. 3.39. The location of the two stop blocks.

Since the microfabrication gives errors, dimensions of fabricated bistable modules will differ with the designed dimensions. According to the fact that we suppose microfabrication give 2% errors, we give estimations with a coefficient 0.98 and 1.02 on the dimensions (see Fig. 3.40).
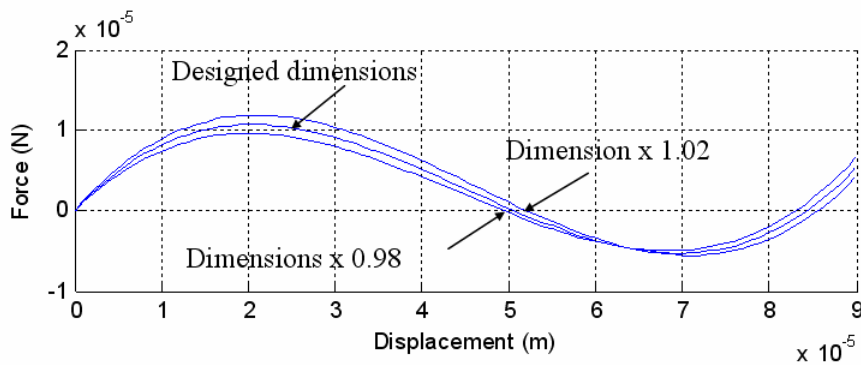
Fig. 3.40. Force versus displacement curve with or without errors.

Three dimensions give different unstable positions (see Tab. 3.5).

Tab. 3.5. Unstable position of three dimensions.

Three dimensions	Unstable position	Error
Designed dimensions	50.7µm	0
Dimensions x 0.98	49.2µm	-1.5µm
Dimensions x 1.02	52.1µm	1.4µm

This fabrication error causes uncertainty in the unstable position. The design of the stop block must ensure that the unstable position is between the two stop blocks. Therefore, for the first time, we define the stop blocks with three different distances (see Fig. 3.41). This configuration can tolerant with +-0.02 error about the fabrication.
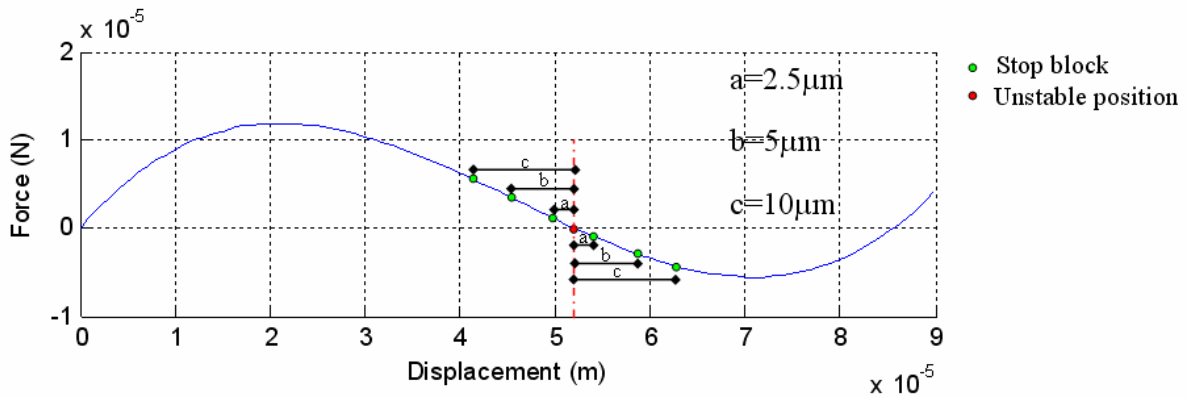
Fig. 3.41. Three locations of the stop blocks.

Three distances for stop blocks give each a blockage force 1.25µN (a), 2.6µN (b), 5.2µN (c). The fact is that the blocked force becomes small while it gets close to the unstable position. So, to obtain a sufficient blockage force for microrobotics applications, we need to choose a distance great enough.

The two pairs of actuators are used to move in each direction. Fig. 3.42 shows that the activation of A2 actuators will pull the bistable mechanism from stable position 1 to stable position 2. For getting the stable position 1, we activate the A1 actuators. Due to the stop blocks, we have two accurate positions.
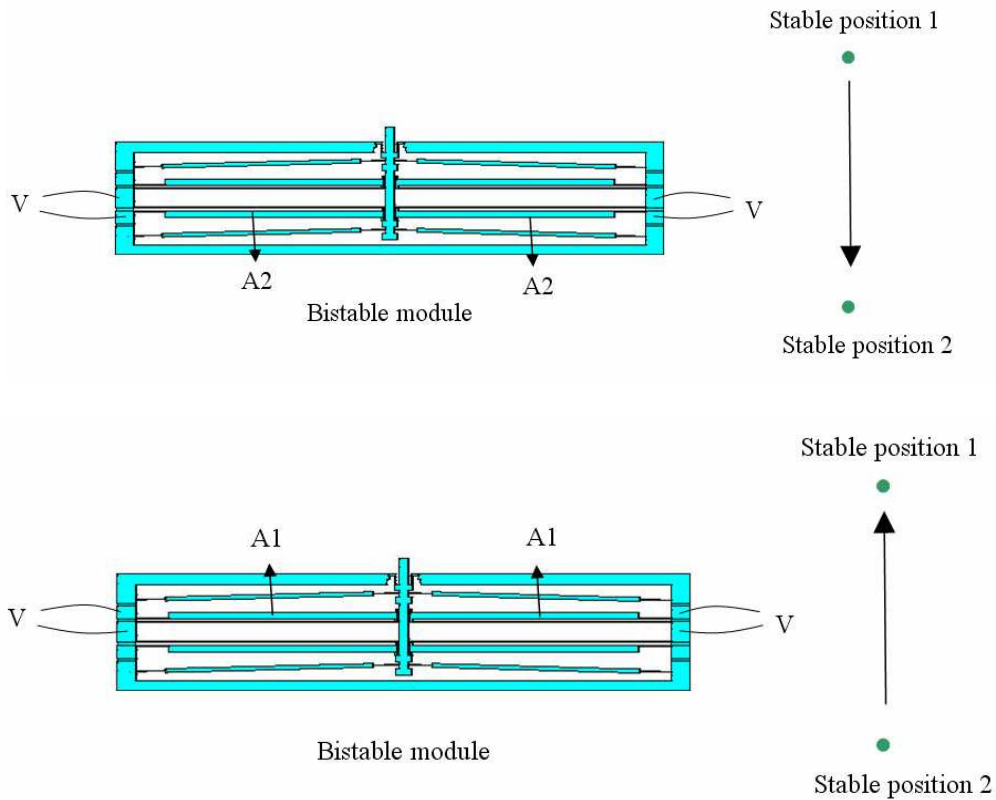
Fig. 3.42. Two pairs of thermal actuators for two stable positions.

3.6 Cascaded bistable modules

3.6.1 Design example

If N bistable modules are cascaded, we obtain a microrobot axis consisting in a serial chain allowing getting 2^N states. In the plane of this overall structure, there are two possible forces Fx and Fy (see Fig. 3.43).
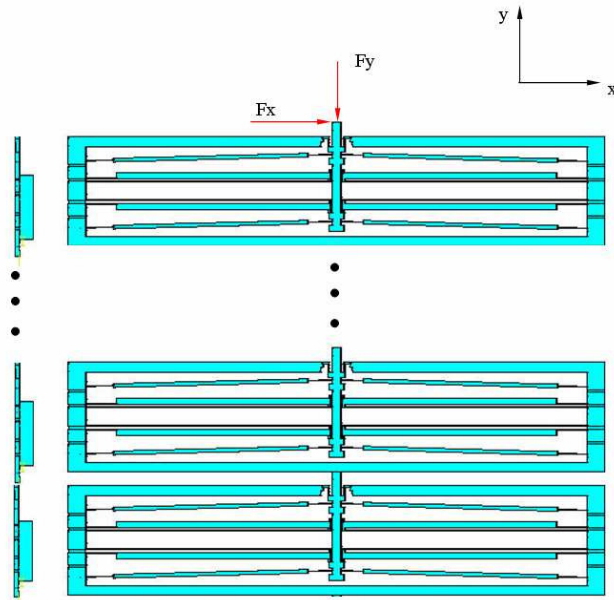
Fig. 3.43. N cascaded bistable modules.

The Fy force is in the direction of the actuation of the bistable mechanism, which depends on the states of the bistable mechanism.
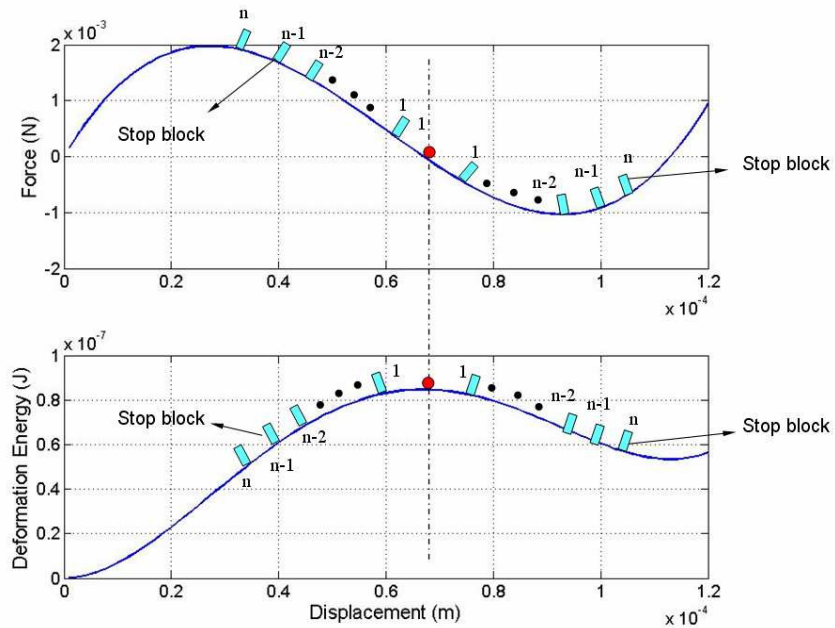
Fig. 3.44. Locations of the stop blocks in the cascaded bistable modules.

97

Since stop blocks are placed in different position, different blockage forces are obtained shown in Fig. 3.44, and the minimum blockage force is generated by the first stop block location.

3.6.2 Out-of-plane analysis

N cascaded bistable modules are considered in this section (see Fig. 3.45). Since the two curved-beams will support all the structure in the first bistable module, it is necessary to study the gravity influence on the structure.
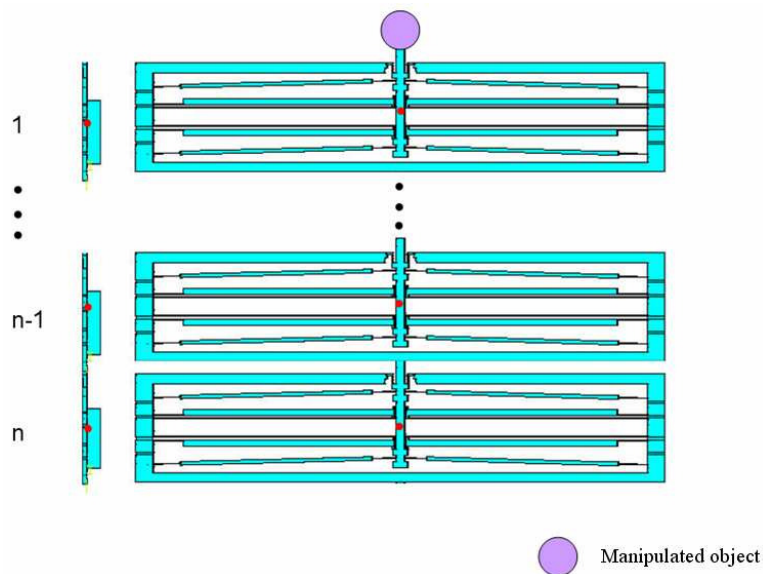
Fig. 3.45. N cascaded bistable modules with an object.

In order to find the out-of plan stiffness caused by gravity, we performed a calculation model presented in Fig. 3.46.

In this calculation model, the two bistable curved beams are considered as two springs with stiffness of k, and the actuators and the frame are considered as a rigid beam. Only the spring causes a flexion. The gravity center of every bistable module is located in the middle of the two springs.
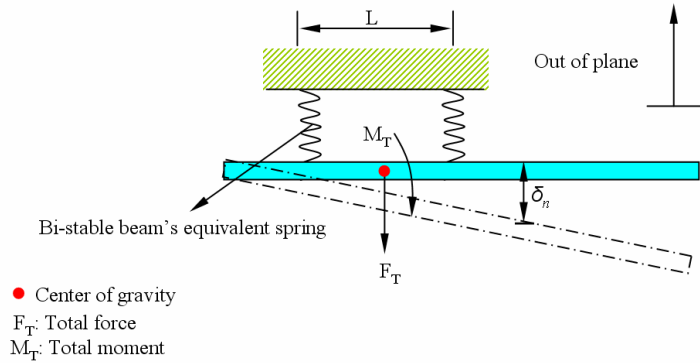
Fig. 3.46. The equivalent out-of plane model of a bistable module.

For N bistable modules, we simplify the model as in Fig. 3.47. The total moment $M_T = (\dfrac{M\,(n^2 - n)}{2} + M_G)$ and total force $F_T = (nF + G)$ are the equivalent moment and force of the n bistable modules which are applied on the first bistable module. The out of plane flexion is given by:

$$\delta_n = \frac{F_T}{k} + \frac{M_T}{0.5L^2 k}(L + L_1) = \frac{nF + G}{k} + (\frac{F(n^2 - n)(L + L_1)}{2} + \frac{G(0.5L + (n-1)(L + L_1))}{2})\frac{(L + L_1)}{0.5L^2 k}$$

(3.55)
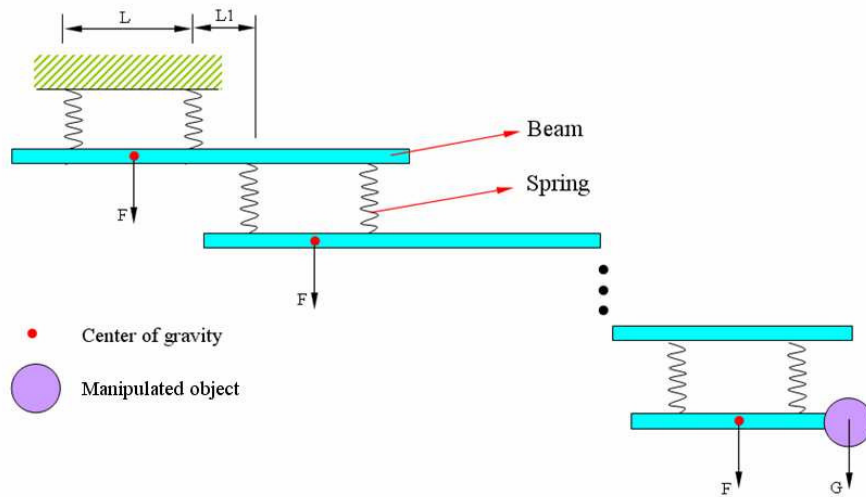
Fig. 3.47. Model of n cascaded bistable modules.

99

The total displacement of manipulated object G is given by:

$$\delta_T = \sum_{n=1}^{n} \frac{F_T}{k} + \frac{M_T}{0.5L^2 k}(L+L_1) = \sum_{n=1}^{n} \frac{nF+G}{k} + (\frac{F(n^2-n)(L+L_1)}{2} + \frac{G(0.5L+(n-1)(L+L_1))}{2}) \frac{(L+L_1)}{0.5L^2 k}$$

$$\text{(3.56)}$$

The spring is a variable section cantilever beam, of which stiffness k can be determined by a classic cantilever model:

$$k = 2 \times \frac{EI}{l^3} \times \frac{1}{\dfrac{0.1^3 + 0.1^3}{3} + \dfrac{0.9 \times 0.1^2}{2} + \dfrac{0.8^3 + 0.1 \times 0.8^2}{10}} = \frac{38EI}{l^3}$$

$$\text{(3.57)}$$

Where E is the Young's modulus, I is the moment of inertia and l is the length of the cantilever beam.

Each bistable module has a mass of 2.128mg (Dimensions are obtained using the same as the example). We simulate the deflection of cascaded structure at the tip caused by a silicon sphere with a diameter of 300µm (mass: 0.0325mg). The comparison of the tip's flexion between the model and the FEA is presented in Tab. 3.6 for cascaded bistable modules with 1 to 4 modules.

Tab. 3.6. Tip's flexion comparison between the model and the FEA.

n	Model (µm)	FEA (µm)
1	0.24	0.22
2	2.11	1.9.1
3	16.8	14.4
4	41.6	38.2

The tip's flexion is accumulated with the increase of the bistable modules. The analysis shows that there isn't much stress in the first bistable module. Nevertheless, there is a large flexion on the tip of the structure. According to eq. 3.56 and eq. 3.57, we obtain:

$$\delta_n \propto \left(\frac{1}{k}\right) \propto \left(\frac{1}{I}\right) \propto \left(\frac{1}{h^3}\right) \qquad \text{(3.58)}$$

where I is moment of inertia and h is the thickness of the structure.
According to the eq. 3.58, the tip's flexion could be reduced with the increase of the thickness of the structure. In our case, the tip's flexion is 1.6µm with a thickness of 100µm, which can be neglected.

In fact, increasing the thickness can increase not only the out-of-plane stiffness, but also the in plane stiffness.

3.6.3 Electric connections

When several module bistables are cascaded, the electric connections have to be taken into account. We propose a connection approach (see Fig. 3.48), the movable party and the fixed party is connected by metal wire. Metal wire can be realized by process of wire bonding. In order to avoid connection forces too great, the metal wire should have an enough length (see Eq. 3.59).

$$F = \frac{3EI\delta}{L^3} \tag{3.59}$$
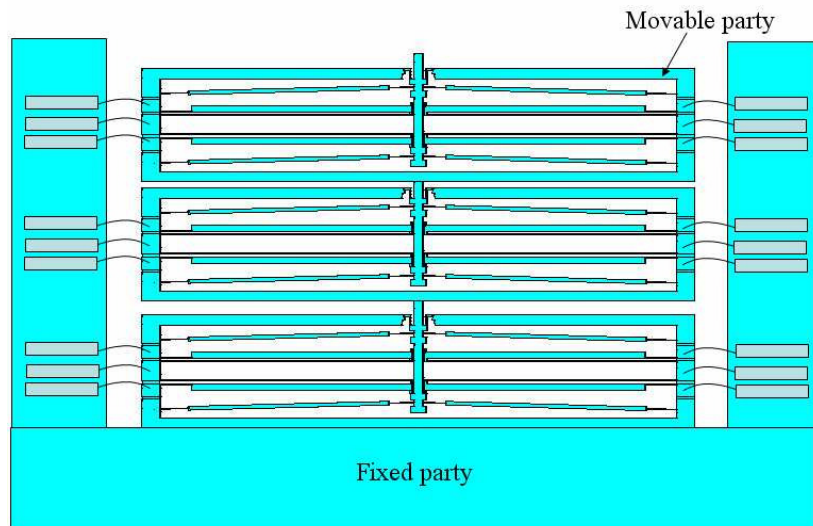
Fig. 3.48. Schematic of wire connections.

3.7 Conclusion

This chapter presented the design of a whole bistable module. Firstly, a synthesis of bistable mechanism has been made. By comparing the different mechanisms a generic bistable model has been proposed. Based on this basic model, the bistable behavior has been studied. A criterion is proposed to ensure a good bistability.

In the second section, various actuators have been studied to actuate these bistable mechanisms. The smart materials present good performance and it would be very interesting to integrate both the bistable mechanism and the actuators. Moreover, the use of the magnetostrictive materials would allow wireless actuation. Although this solution shows many advantages, the new

microfabrication process of active materials requires to be developed. Considering the valuable time, we propose to use two pairs of thermal actuator to switch the bistable mechanism.

In the third section, the stop blocks have been designed. The stop blocks permit to give a blockage force in each of the stable positions. This stop block is designed using the compliant beam. A first activation is necessary to make the shuttle into the stop block. The use of microfabrication gives a monolithic structure, but it is difficult to realize the blocked force in such structure. This proposed compliant stop blocks allow us to create blockage force by activation.

Finally, an entire bistable module has been designed with the bistable mechanism, the actuators and the stop blocks. Two analysis of the proposed structure has been made. The first was an out-of-axis analysis of the displacement that lead to conclusion that the structure enables a very good guiding. The second is the analysis of the out of plane displacement of a cascaded system consisting in modules in series. In fact, the bistable module has to be designed to support cascaded structure

The following chapters will describe the microfabrication of the bistable module and its static and dynamic analysis.

Chapter 4 Microfabrication of bistable modules

"Learning without thinking is useless; thinking without learning is dangerous."

– Confucius

(551 B.C. – 479 B.C.)

4.1 Introduction

We have previously presented the design of an entire bistable module. In order to fabricate the bistable modules by using microfabrication technologies, we need to define their dimensions adapted the MEMS fabrication process. In this chapter, we treat the constraint induced by the MEMS fabrication process to obtain the final design of the bistable structures.

As presented in chapter 2, a bistable module is a structure or mechanism with two stable positions, which can be switched between these two stable positions, no external energy is required to maintain these two stable positions.
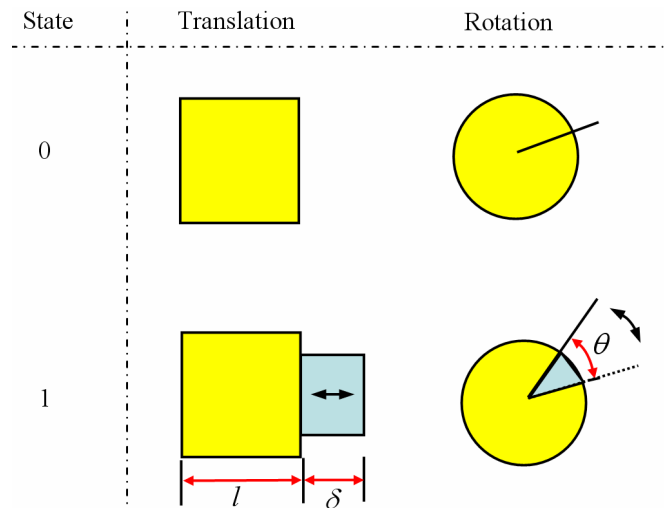
Fig. 4.1. Remind of a bistable module.

In the chapter 3, we designed a bistable module which is shown in the Fig. 4.2. This bistable module includes two pairs of thermal microactuators, bistable mechanism and stop blocks. This design allows us to obtain two blocked, repeatable positions.
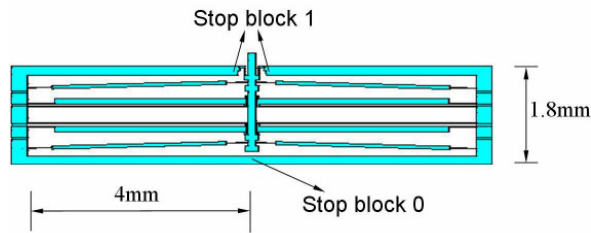
Fig. 4.2. Designed bistable module.

4.2 MEMS and microrobotics

In order to introduce the MEMS process for our microrobot microfabrication, we give a MEMS microfabrication review in this section.

Microrobots can be fabricated by traditional machining and assembly; these microrobots usually have dimensions of centimeter. In order to fabricate much smaller with higher accuracy and precision, MEMS fabrications should be introduced for microrobot fabrication. MEMS are the acronym of MicroElectroMechanical Systems, which is intended to integrate more functionality into a single silicon chip (acoustic, electronic, mechanical, and optical functionalities). The use of the MEMS fabrication allows us to make small and precise devices.

The MEMS Microfabrication is the set of design and fabrication tools that machine and form structures and elements at the microworld. In general, microfabrication is such a process that selectively etches away parts of the silicon wafer or adds new structural layers to form the mechanical and electromechanical devices. These main processes include deposition, lithography, and etching.
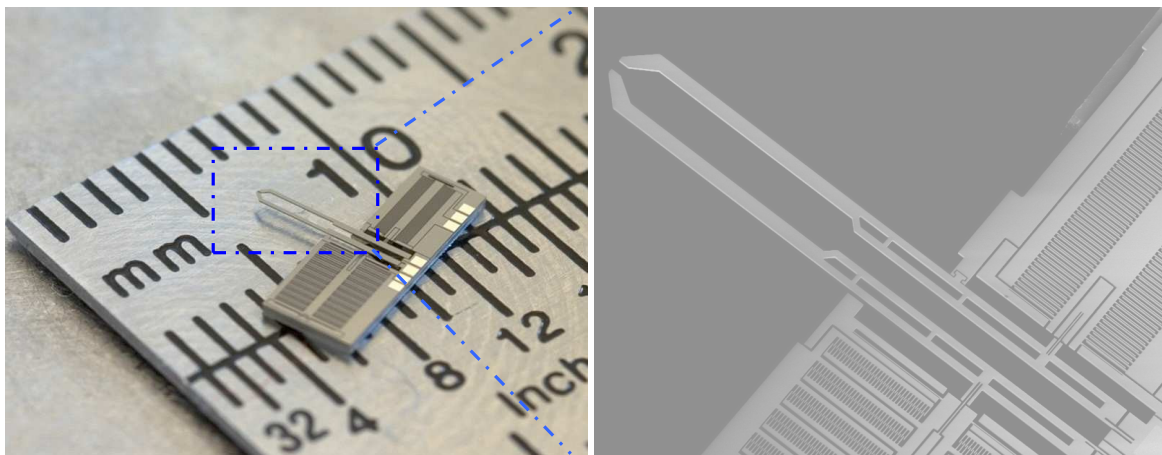
Fig. 4.3. A fabricated microgripper by FEMTO TOOLS [FEM].

A microgripper is fabricated in silicon wafer with classic MEMS fabrication (see Fig. 4.3),

which is a product of the FEMTO TOOLS. This microgripper has the integrated sensor and actuator. It can be used to manipulate fragile objects by controlling the force.

Shown in the Fig. 4.4, it is a bio-inspired design by SilMach [SIL]. Wings of a dragonfly are fabricated on a silicon wafer. It has a weight of 20mg for the length of 6cm. it could fly with the integration of actuators, power system and electronic circuits.
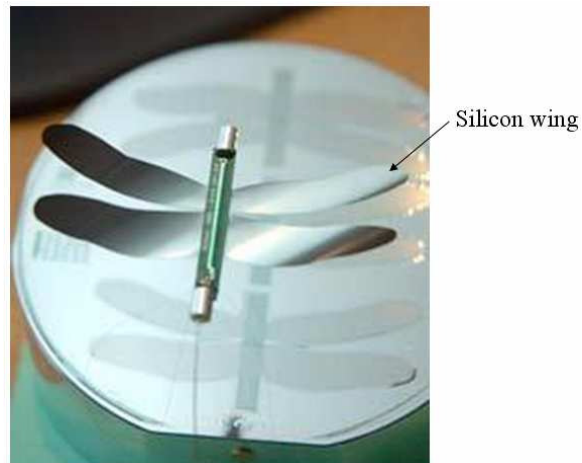
Fig. 4.4. A dragonfly was made by silicon (SilMach) [SIL].

Another example is the mobile microrobot presented in chapter 1. It is actuated by electrostatic force, and two kinds of motion (translation and rotation) can be generated. This roobt can be controlled wireless.
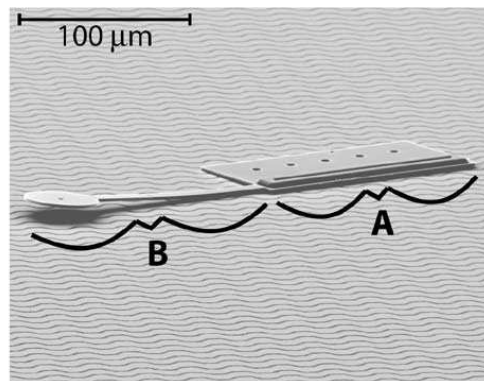
Fig. 4.5. A mobile microrobot. A: scratch drive actuator, B: cantilevered steering arm (B) [DON 06].

In fact, there are two major MEMS fabrication technology: Bulk and surface microfabrications. Wafer bonding can be used as the post process of bulk micromachining. LIGA (lithographe, galvanoformung, abformung) has been used in high-aspect ratio applications.

4.2.1 Surface microfabrication

Surface micromachining is based on the deposition and etching of different structural layers on top of substrate. Surface micromachining starts with a silicon wafer or other substrate and grows layers on top. These layers are selectively etched by photolithography and either a wet etch involving an acid or a dry etch involving an ionized gas, or plasma. Fig. 4.6 shows a typical surface micromachining process.

Firstly, a sacrificial layer is deposited and pattered (see Fig. 4.6 a,b). Secondly the structure layer is deposited and patterned (see Fig. 4.6 c). Lastly the sacrificial layer is cleaned to release the structure layer (see Fig. 4.6 d).
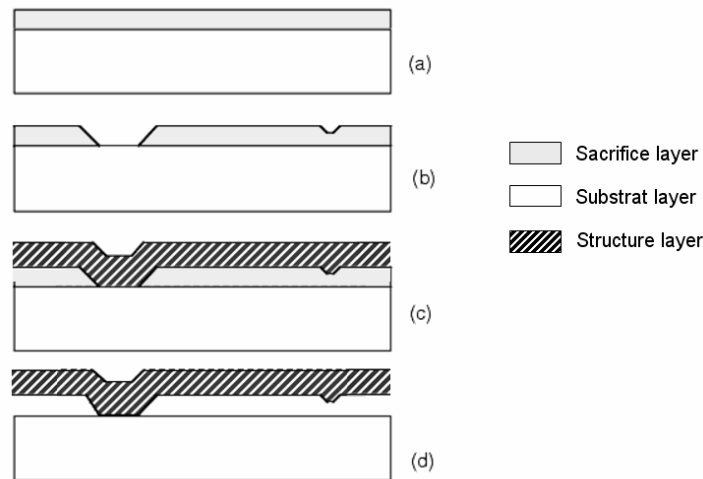
Fig. 4.6. A typical surface micromachining process.

As the structures are built on top of the substrate and not inside it, the substrate's properties are not as important as in bulk micromachining, and the expensive silicon wafers can be replaced by cheaper substrates, such as glass or plastic. Another advantage is a multi layer structure can be built by this surface micromachining. Nevertheless, as thin film is deposited, it is difficulty of built thick structures.

4.2.2 Bulk microfabrication

Bulk micromachining defines structures by selectively etching inside a substrate, usually silicon. Whereas surface micromachining creates structures on top of a substrate, bulk micromachining produces structures inside a substrate. Usually, silicon wafers are used as substrates for bulk micromachining, as they can be anisotropically wet etched, forming highly regular structures. Wet etching typically uses alkaline liquid solvents, such as potassium hydroxide (KOH) or tetramethylammonium hydroxide (TMAH) to dissolve silicon which has been left exposed by the photolithography masking step.
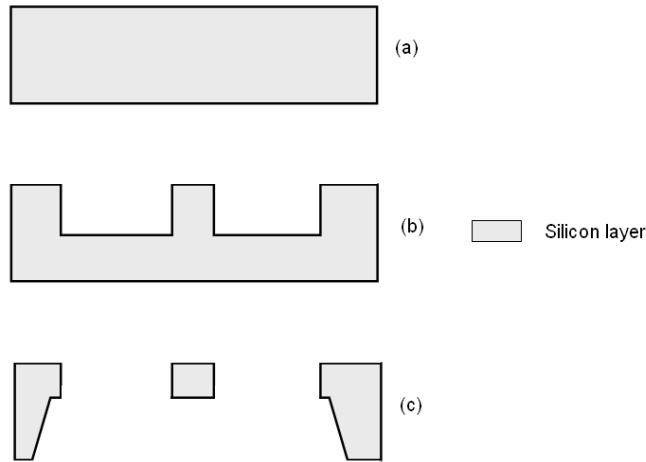
Fig. 4.7. A typical bulk machining.

Bulk micromachining starts with a silicon wafer or other substrates which is selectively etched, using photolithography to transfer a pattern from a mask to the surface (see Fig. 4.7). This silicon layer is etched by deep reactive ion etching (DRIE) in the front side (see Fig. 4.7 b), and then the back side is etched potassium hydroxide (KOH) to free the structure (see Fig. 4.7 c).

Bulk micromachining has the limits to form complex three dimensional microstructures because of the single layer. One of the solutions is to bond the different elements through the separate fabrication of a complex system.

Wafer bonding is a technique that enables virtually seamless integration of multiple wafers. Wafer bonding for MEMS can be categorized into three major types: anodic bonding, intermediate layer bonding-assisted bonding and direct bonding.

Anodic bonding is usually established between a sodium glass and silicon for MEMS. A voltage is applied between the glass and silicon, and at the same time, the heater also provides the bonding temperature around 180~500 ^{0}C.

Intermediate layer assisted bonding requires an intermediate layer that can be metal, polymer, solders, glass, etc., to fulfill the bonding between wafers.

Direct bonding is also called silicon fusion bonding, which is used for silicon wafer to silicon wafer bonding. This type of bonding is based on the chemical reaction between OH-groups present at the surface of native silicon or grown oxides covering the wafers.

The typical product of wafer bonding is the silicon on insulator (SOI) wafer (Fig. 4.8). A SOI wafer has three layers which include one thin silicon dioxide layer in the middle and the two

silicon layers outside.
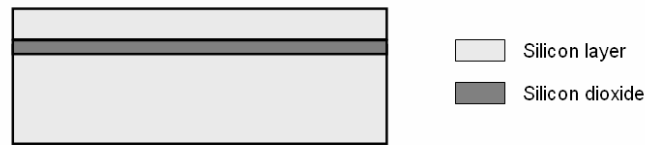
Fig. 4.8. A SOI wafer.

This bonding technique is extensively used in building complex structures consisting of several wafers, but is also used in packaging of Microsystems.

4.2.3 LIGA

LIGA (see Fig. 4.9) is an acronym for lithography, electroforming and micromolding (in German, lithographe, galvanoformung, abformung), which is a process developed by a team at the Institute for Nuclear Process Engineering (Institut für Kernverfahrenstechnik IKVT) at the Karlsruhe Nuclear Research Center.

LIGA was one of the first major techniques to allow manufacturing of high-aspect-ratio structures with lateral precision below one micrometer.

The LIGA process is not possible with silicon-based micromachining techniques. Nevertheless, it is possible to make more complex microstructures. Various plastics, metal ceramics or combinations of these can be used by this LIGA process to fabricate difficult and complex structures.

(a) Exposure
(b) Electroplating
(c) Finishing to height
(d) Stripping and removal of substrate
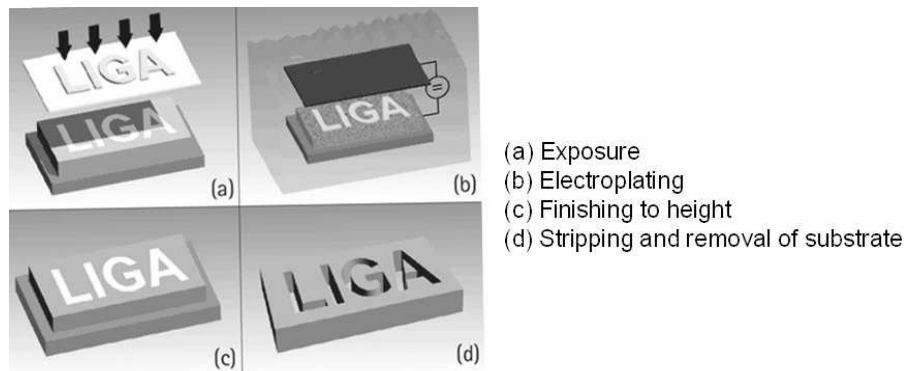
Fig. 4.9. Example of the LIGA process [MIC].

The MEMS fabrication technique could be potential choices for our microrobot fabrications. They offer many advantages such as small dimension, high accuracy, bulk production, and low cost etc. In fact, MEMS technology has the ability to integrate sensors, actuators, and electronics into a small silicon piece, which could be a solution to make full autonomy microrobots in the future.

4.3 Final design of the bistable module

4.3.1 Influences of the microfabrication process

Due to the diversity working principles involved in MEMS. Some possible failure mechanisms for MEMS have been identified as shown in the following items. Most of them are MEMS specific problems, notably.

➢ Mechanical fatigue

➢ Mechanical fracture

➢ Stiction

➢ Vibration and shock

Mechanical fatigue is the material failure when a material is subjected to cyclic loading. This effect is an accumulation of damage due to cycling loading. Although the cyclic stress is below the material ultimate strength, the structure will crack and even fail. The fatigue behavior of polysilicon is generally modeled with a stress versus life or known as an S-N curve as shown in Fig. 4.10.
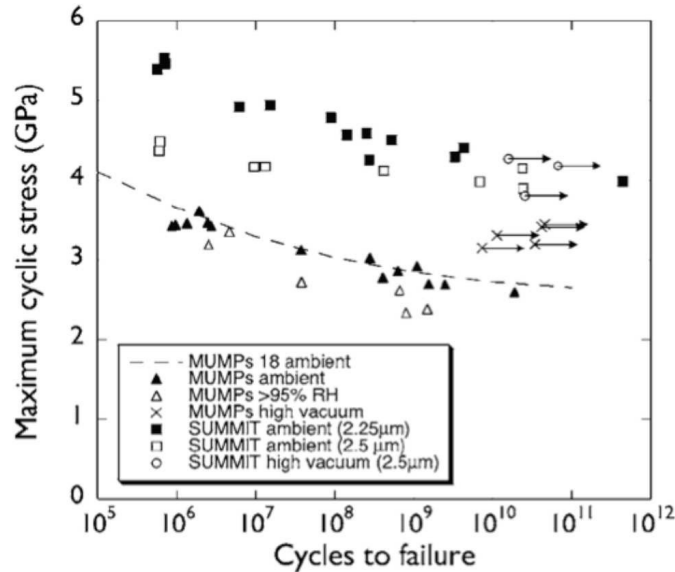
Fig. 4.10. A typical S-N curve of polysilicon [ALS 07].

We can observe that the cycling load reduces the material fracture stress. Eventually, the material cracks at a stress lower than its original material strength. However, if the material is loaded at a lower stress level, the fatigue effect could be reduced greatly. Therefore, in the design of MEMS devices, mechanical fatigue effect are taken into account and a lower stress level are designed to increase the working life.

Mechanical fracture is the breaking of an object into two, or more, parts when the stress in the structure exceeds the fracture limit. Since MEMS devices are fabricated by brittle material (silicon), the fracture of mechanical structure leads to a catastrophic failure. Generally, the movable structure undergoes great displacement and stress. The fracture of a brittle material is a stochastic parameter which requires statistical information [BAG 03] [TSU 98]. When a large number of seemly identical structures are tested, it has been found that the fracture strength actually scatters around a certain mean value. The probability of fracture actually follows the Weibull distribution function [WEI] [GRE 97]. The design of MEMS devices should put the maximal stress well below the mean fracture strength to ensure reliability.
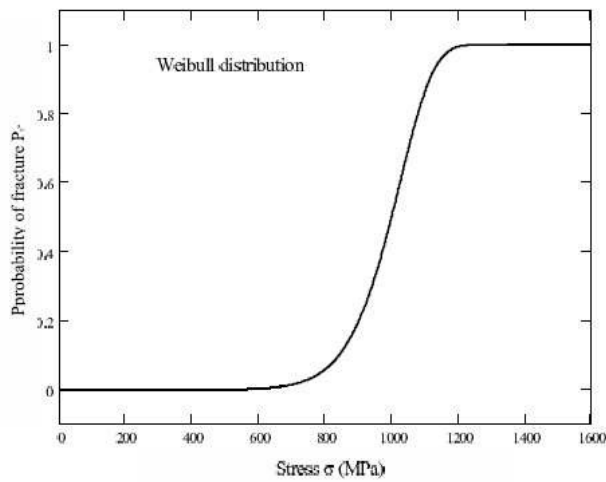
Fig. 4.11. Weibull distribution of the probability of fracture versus stress [WEI].

Stiction is an effect that two surfaces have an adhesion contact. It is difficult to separate the two surfaces due to the fragile nature of the microstructure. This phenomenon is called a stiction failure in MEMS. This effect happens usually during MEMS fabrication due to the capillary force. The capillary forces between the microstructure and substrate cause the two surfaces to adhere together. In fact, this effect occurs mainly in the surface micromachining. Various techniques [SPEN 02] [SPEN 03] have been suggested to prevent the stiction problem. Some techniques include roughening and skewing the surfaces, using getters, and leaky dielectrics have been proposed.

MEMS devices are often exposed to vibrating and shocks environment during their fabrication and in-field usages. They should have the ability to undertake the large acceleration impact. This shock can lead to lift-off or even fracture of a microstructure [TAN 00]. Moreover, when the vibration frequency is close to the resonant frequency of the MEMS device, it can induce large vibration amplitude and lead the device to failure. This problem should be concerned when we design MEMS devices.

4.3.2 Bistable module layout

There are many factors to be considered at the same time. To define suitable dimensions of the bistable module for microfabrication, we propose a design plan shown in Fig. 4.12.

Firstly, the material is chosen, and then the fabrication process is determined according to the choice of material, after that, the dimension of microactuator is defined; lastly, the dimensions of the bistable mechanism are defined.
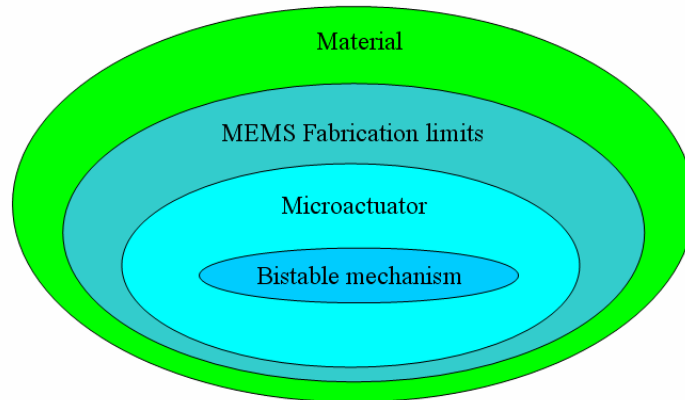
Fig. 4.12. Steps to define the dimensions of bistable mechanisms.

4.3.2.1 Material and fabrication process definition

The bistable mechanism can be fabricated by any elastic material. However, the thermal microactuator requires that the material has a low resistivity to ensure a low working voltage. The resistivity of semi-conductor material silicon can be changed by doping, so silicon with low resistivity is thus used.

Since the whole bistable module is in the same silicon layer, to avoid short circuits, the actuators need to be separated from the other parts of the bistable module. However, for keeping the integrity of bistable module, the backside layer is also used. So there are two layers at least to fabricate this bistable module.

As previously introduced, there are two choices to machine the micromechanical component: the surface microfabrication technology and the bulk microfabrication technology. The thickness should be more than 100µm to neglect out-of-plane displacement according to the previous calculation,. So, the surface microfabrication technology can not be used. At the same time, the bistable module needs two layers: the device layer and the handle layer. Although the use of bulk microfabrication and the wafer bonding can be a solution, since the silicon on insulator (SOI) wafer offers three layers: device layer, sacrificial oxide layer and handle layer, it could reduce the fabrication process. So the SOI wafer and the bulk

microfabrication process will be used to fabricate the bistable modules. As shown in Fig. 4.13, the handle layer is used to support all the structure, and the bistable module is fabricated in the device layer.

(a)

(b)
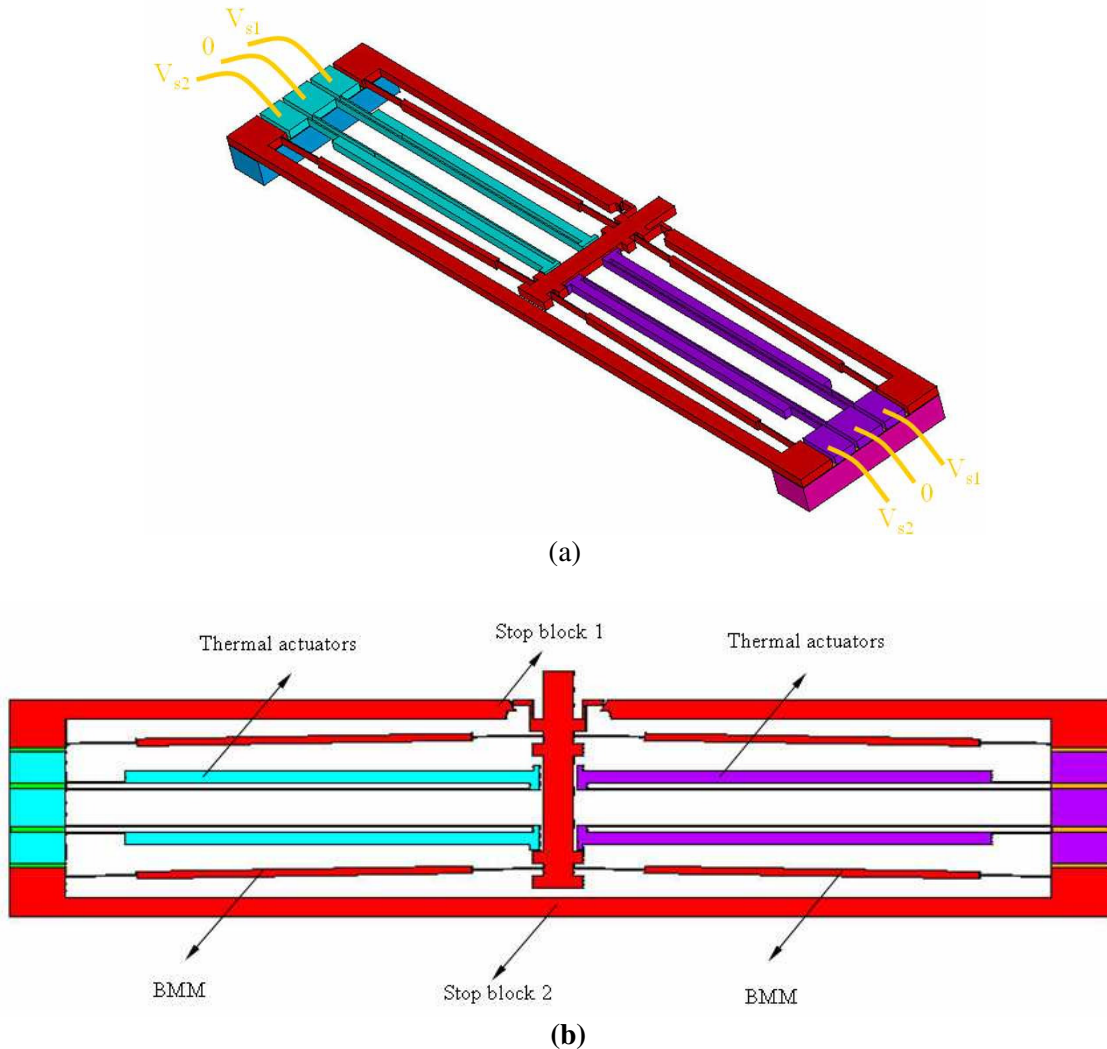
Fig. 4.13. (a) 3D view of the bistable module. (b) plane of the bistable module.

4.3.2.2 Design of microactuator

According to the chosen material and MEMS fabrication process, we will define the dimensions of the microactuator. The goal is to build a microactuator with the maximum mechanical output energy under the previous considerations. A mechanical power output of a microactuator is determined by its motion range and stiffness. The maximal power output is limited by fabrication and the working environment. We are trying to build an optimal thermal actuator which can offer more mechanical energy output. The dimensions (see Fig. 4.14) of thermal actuator are defined according to the work of S.Murater [MUR 05]. In its work, he

proposed the following principles to obtain more displacement:

- The ratio l_c / l_h is equal to 0.8, where l_h is length of hot beam, and l_c is length of cold beam.

- The length of hot beam is as long as possible (l_h maximum). Until their stiffness is too small to be fabricated.

- The width of cold beam is as small as possible (w_c minimum). Until the entire weight is so big that it produces too much out-of-plane displacement.

- The width of the hot beam is as small as possible (w_h minimum). Until it reaches the fabrication limits, and may lead to the bulking problem.

- g (gap between hot and cold beam) can be optimized according to the above parameters.
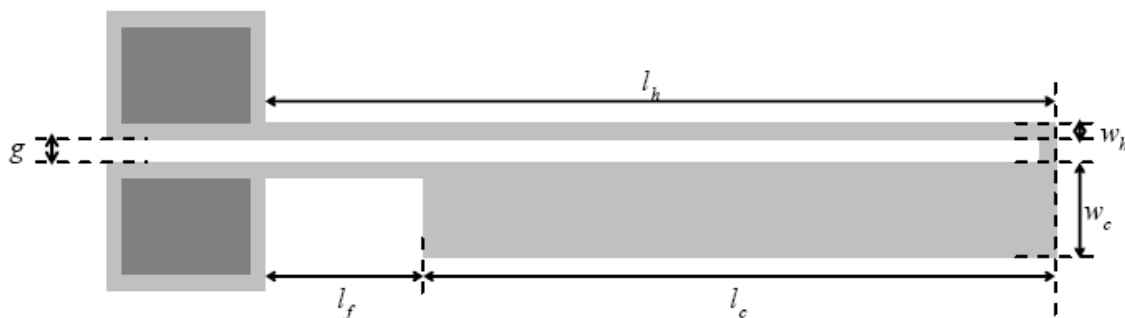
Fig. 4.14. Dimensions of thermal actuator [MUR 05].

Based on these principles, the dimensions can be given. However, to define dimensions under the MEMS fabrication limits consideration of two main factors permits to resolve the fabrication problems: their maximum stress and their first frequency. The maximum stress has to be taken into consideration to avoid the fatigue and the fracture problems; the first frequency has to be designed to avoid vibration and shock problems.

In thermal microactuator, these two factors can be adjusted by the geometry of the actuator. In fact, there are many possibilities that can satisfy all the limits. We propose a thermal actuator with the dimensions given in Fig. 4.15. These dimensions have a maximum stress of 200 Mpa and a first frequency of 2.98 Khz. This design gives a theoretically working life of 10 million cycles.
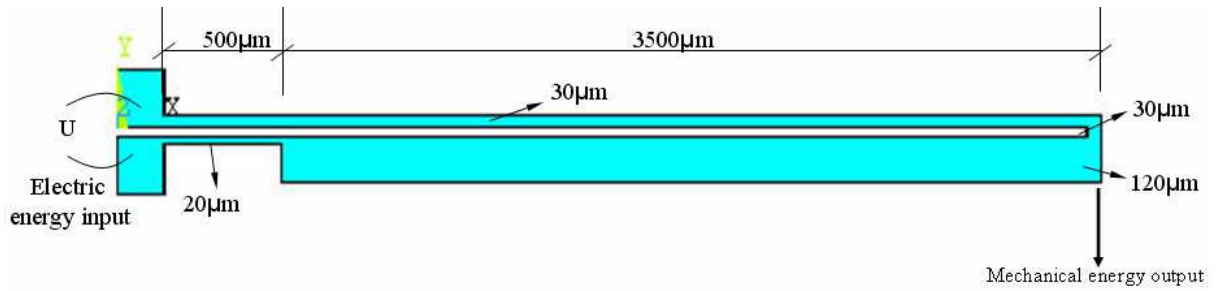
Fig. 4.15. Dimensions of thermal actuator.

From the work of S.Murater [MUR 05], the free displacement of thermal actuator has a linear relation with the applied voltage's square. The mechanical energy output can be defined by 3.1.

$$E_{mech} = \frac{1}{2} kD^2$$
(3.1)

Where

k : Stiffness of thermal actuator
D : Tip displacement of thermal actuator
E_{mech} : Mechanical energy
U : Applied voltage

Therefore, we can obtain a relation between the voltage input and the mechanical energy output:

$$E_{mech} \propto D^2 \propto U^4$$
(3.2)

In fact, this mechanical energy can be increased due to the heat accumulation in the hot beam. it is limited by the maximum temperature. We proposed a maximum temperature of 300°C to avoid too much heat in the whole structure.

As shown in Fig. 4.16, this thermal actuator offers 15µN force and 62nJ mechanical energy in the condition of 300°C with 1µm thickness.
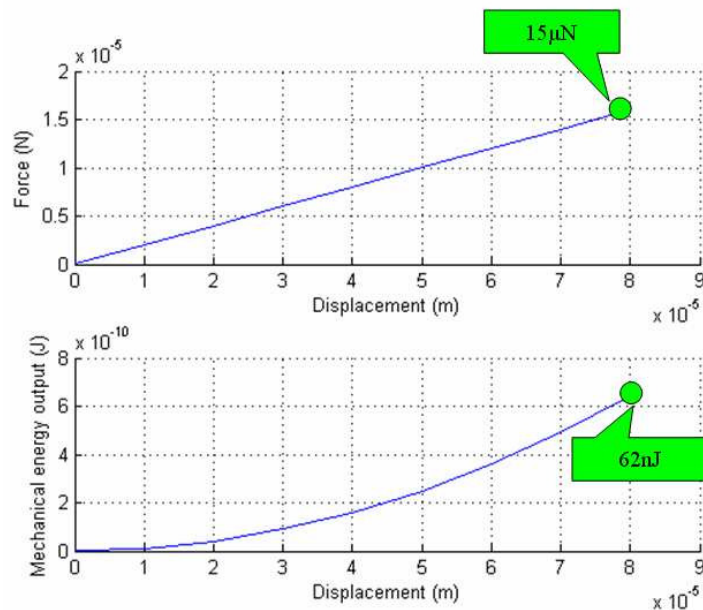
Fig. 4.16. Force and mechanical energy output of thermal actuator.

4.3.2.3 Design of bistable mechanism

According to the performance of thermal actuator, the adapted bistable mechanism can be designed. Indeed, smaller bistable mechanisms can be switched easier. Nevertheless, from the aspect of fabrication, smaller dimensions may lead to failure due to too small stiffness. Therefore, taking into account both the fabrication process and the thermal microactuator, the dimensions of the bistable mechanism should be big enough to avoid the fabrication problems and small enough to be actuated by microactuators.

As talked in the chapter 3. 1, the ratio of stiffness between the elastic element and compliant joint should be bigger than $\dfrac{32}{H^2}$ (H: the initial height) to ensure a good bistability. The bistable behavior can be insured with these dimensions (see Fig. 4.17).

The dimensions, including the compliant joint width, length, initial height and beam length can be defined preliminary by fabrication limits and the requirement of microactuators. These dimensions give a maximum stress of 100Mpa and first frequency of 3.69 KHz. This design gives a working life of 10 million cycles.
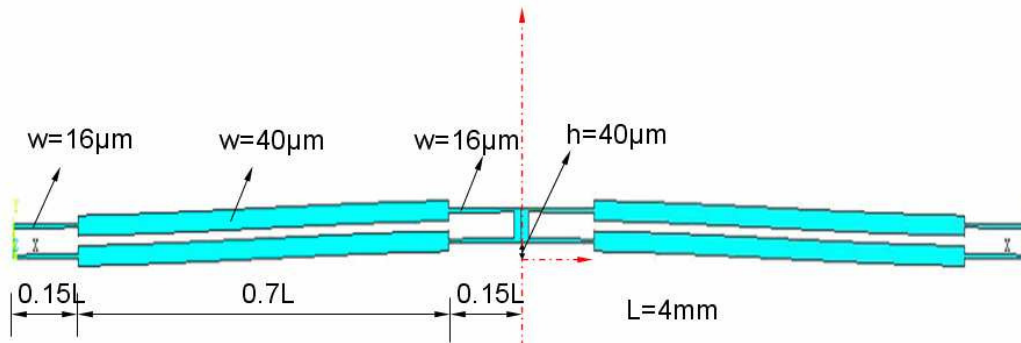
Fig. 4.17. Dimension of bistable mechanism.

This bistable mechanism (with a 1µm thickness) requires that the maximal force is 1µN and the total mechanical energy is 50nJ. (see Fig. 4.18)
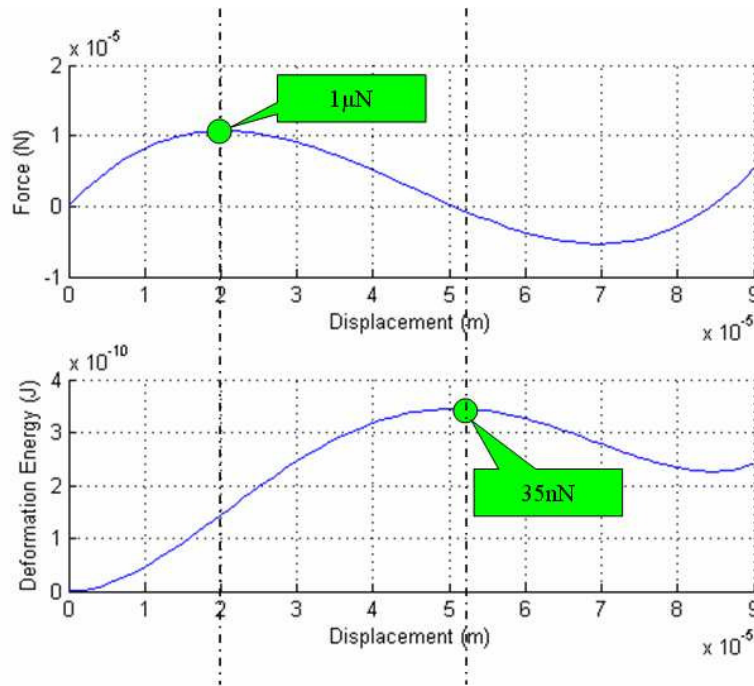
Fig. 4.18. Required force and energy for the bistable mechanism.

In the Tab. 4.1, we detail the main fabrication problems and their solutions.

Tab. 4.1. The fabrication problem and solutions

	Solutions	
Problem	**Thermal actuator**	**Bistable mechanism**
Mechanical fatigue	Maximal stress: 200Mpa	Maximal stress: 100Mpa
Mechanical fracture	Maximal stress: 200Mpa	Maximal stress: 100Mpa
Stiction	Avoid the use of the surface micromachining	

116

Vibration and shock	First frequency is bigger than 2.98Khz	First frequency is bigger than 3.69Khz

We obtain a whole module with dimensions shown in Fig. 4.19.
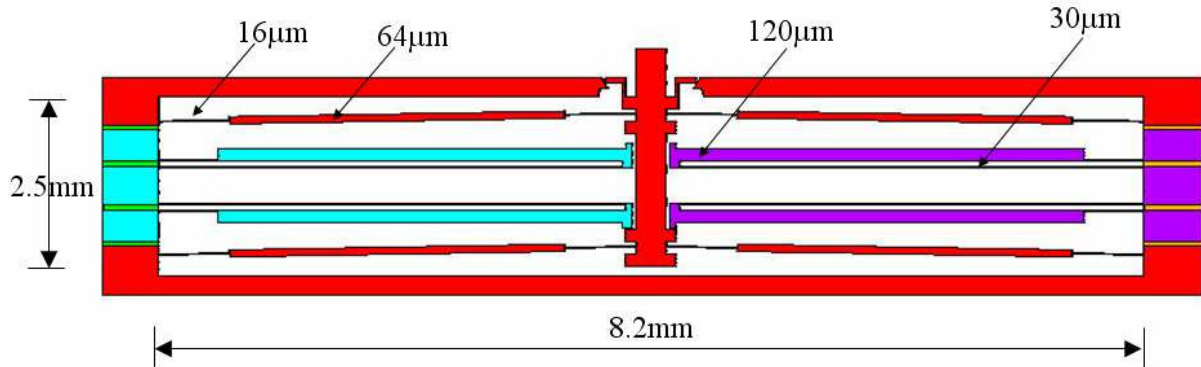
Fig. 4.19. Globe view with dimensions.

The design of thermal actuator and bistable mechanism needs the consideration not only the aspect of their own performance (bistable behavior, electro-thermal-mechanical behavior) but also the fabrication limits. A designed structure with lower maximal stress and a higher first frequency can avoid fabrication problems (mechanical fatigue, mechanical fracture, vibration and shock). The other fabrication problem (ex, Stiction) should also be taken into account. Indeed, specific MEMS devices require that we research all the solutions. Sometimes, we need to redesign the structure when we encounter new fabrication problem.

In the following sections, we will present the microfabrication process of bistable module. This microfabrication is made by the standard clean room process. Firstly, the various processes are investigated and developed. Then, the etching of each layer is detailed in the following.

4.4 SOI micromachining

To micromachine the SOI wafer (see Fig. 4.20), three layers should be considered, the device layer, the handle layer and the sacrificial layer. The silicon layers (device layer and handle layer) can be etched by DRIE or KOH, and the sacrificial layer is cleaned by HF.

Fig. 4.20. Structure of SOI Wafer.

This SOI wafer has a device layer of 100μm thickness, a handle of 300μm thickness and a

117

sacrificial oxide layer of 1µm thickness.

In fact, the whole process depends on the etching order of each layer. We enumerate all possible processes in table 4.2 for the SOI wafer and investigate each of them.

Tab. 4.2. The possible micromaching processes of SOI.

Process	Step 1	Step 2	Step 3	Problems
1	Device layer	Handle layer	Sacrificial layer	The sacrificial layer is broken
2	Device layer	Sacrificial layer	Handle layer	Difficult to clear sacrificial layer.
3	Handle layer	Sacrificial layer	Device layer	Result in under etching
4	Handle layer	Device layer	Sacrificial layer	The sacrificial layer is broken

In the process 1, the device layer is firstly totally etched. After that, the handle layer is etched until the stop layer. Finally, sacrificial layer is cleaned by hydrofluoric (HF) acid. Since the sacrificial layer is very thin, it can be broken during the final etching period of the handle layer. Nevertheless, If we put a protection layer after the etching of the device layer, this can avoid the broken of sacrificial layer. Finally, we clean the protection layer.

In the process 2, the device layer is firstly totally etched. After that, the sacrificial layer is cleaned by hydrofluoric (HF) acid. Finally, the handle layer is etched. Since the etching line is very small, the liquid HF can not clean the sacrificial layer. The use of vapor HF can clean sacrificial layer, however, the deep handle layer makes the etching speed variable, it is difficult to predict the exact time of etching. So, this process leads to an unavoidable under-etching.

In the process 3, the handle layer is firstly etched. After that, the sacrificial layer is cleaned from backside. Finally, the device is etched. Since there are big cavities in the backside, the liquid HF can clean this layer. There is no stop layer, so it results into an under-etching of device layer.

In the process 4, the etching starts from the handle layer. After that the device layer is etched, and finally the sacrificial layer is cleaned. The same problem occurs as the process 1, that is, the sacrificial layer can be broken during the final etching period of the device layer.

As a summary, the process 2 and 4 can not be adopted in the fabrication of bistable module. Fortunately, the process 1 and 3 can provide the completed structures, which are attempted in process of fabrication. Results show that the process 3 will lead to more under-etching, but the process 1 can totally avoid this phenomenon. So, the process 1 will be applied in the

following sections.

Before these steps, the 1µm pad must be deposited to apply the electric current to the thermal microactuator.

4.4.1 The power pads

The thermal microactuator is made from the low resistivity silicon. |In order to apply the electric current into the silicon, metal pads is made. To avoid voltage loss in the contact pads, aluminum is used as the contact pad material according to experiences.

The 1µm aluminum layer is sputtered by Alcatel SCM450 for about 10min (see Fig. 4.21-1). More vacuum level leads to more pure aluminum deposition. Pumping for at least 180min can make a good vacuum level. After aluminum deposition, a layer of photoresist S1815 is spin-coated, patterned and developed (see Fig. 4.21-2, 3). Then, the aluminum is etched by acid which takes about 35min (see Fig. 4.21-4).

Finally, it is put in vacuum and high temperature condition (400°C) for an hour to allow the diffusion of the aluminum atoms into silicon layer (see Fig. 4.21-5). The temperature and the duration have been optimized to ensure a lower contact resistance. These conditions allow obtaining a small contact resistance between 6 and 10 ohms.
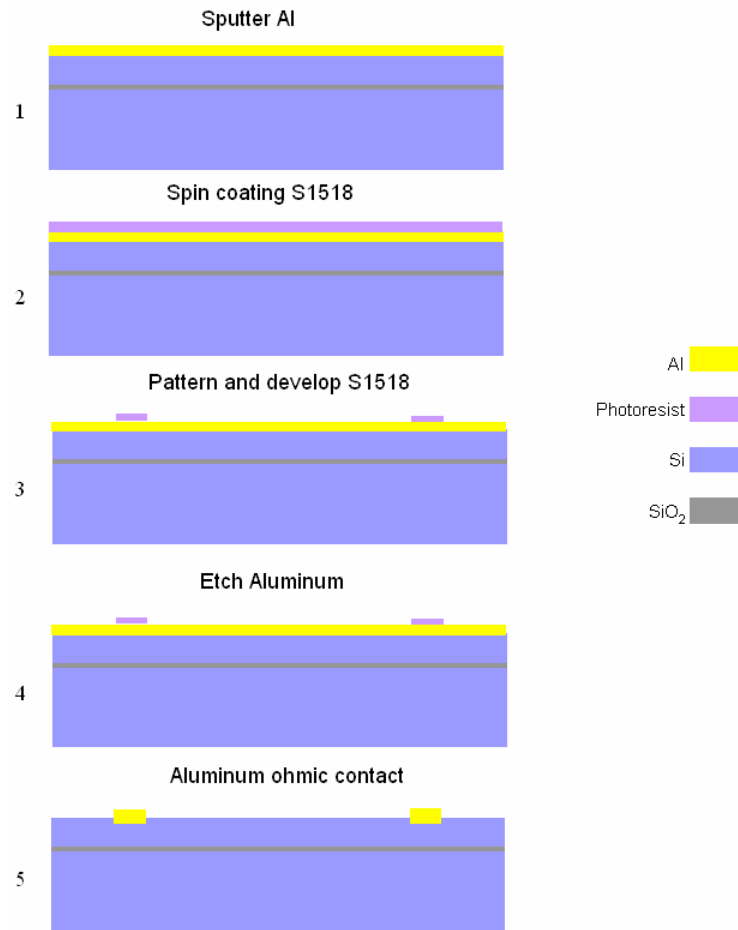
Fig. 4.21. Process to make the contact pads.

4.4.2 The etching of the device layer

After the contact pads have been made, the device layer will be etched by DRIE. The DRIE is used to etch the silicon for obtaining a flat etching side. The classic etching side is shown in Fig. 4.22. These effects can be reduced.

Tab. 4.3 DRIE etching sidewall.

A	Under etching
B	Verticality
C	Scalloping
D	Notching
E	Grass
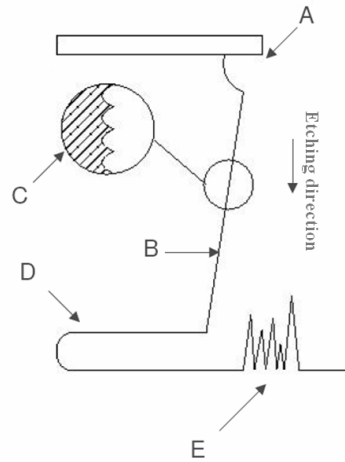
Fig. 4.22. Classic etching sidewall of DRIE.

To reduce these effects, an optimized recipe has been developed in our clean room, the following takes use of this developed recipe.
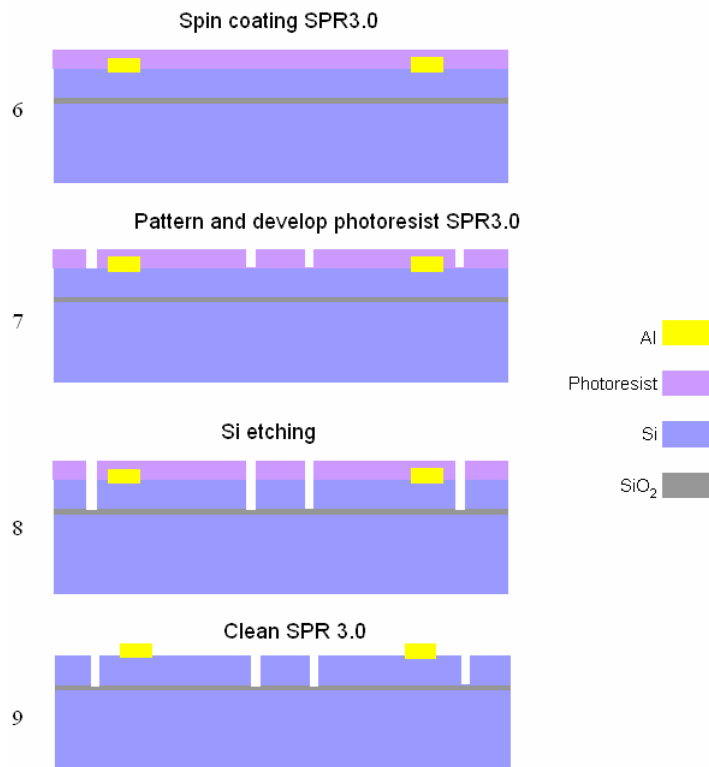
Fig. 4.23. Etching of device layer.

Firstly, a layer of 2.8µm photoresist (SPR220.3.0) is spin-coated at 3000 rpm on the device layer, exposed under the 300mJ/cm^2 dose and then developed to reveal the pattern as illustrated in Fig. 4.23- 6. The development of this SPR220.3.0 has to be carefully watched

121

because this process is fast. The time of development should be limited to 8-10 seconds to avoid over-developed. To guaranty the same etching speed in the surface, an etching line of 20µm all over the wafer is designed in the mask. The Si etching is done in Alcatel 601E machine as the Fig. 4.23- 8. This etching is stopped by the layer (SiO$_2$).

4.4.3 The etching of the handle layer

After the etching of the device layer, the handle layer is be etched. Before that, a layer of photoresist is sputtered to cover the etched structure for protecting the structure during the handle layer etching, which is shown in Fig. 4.24- 10.
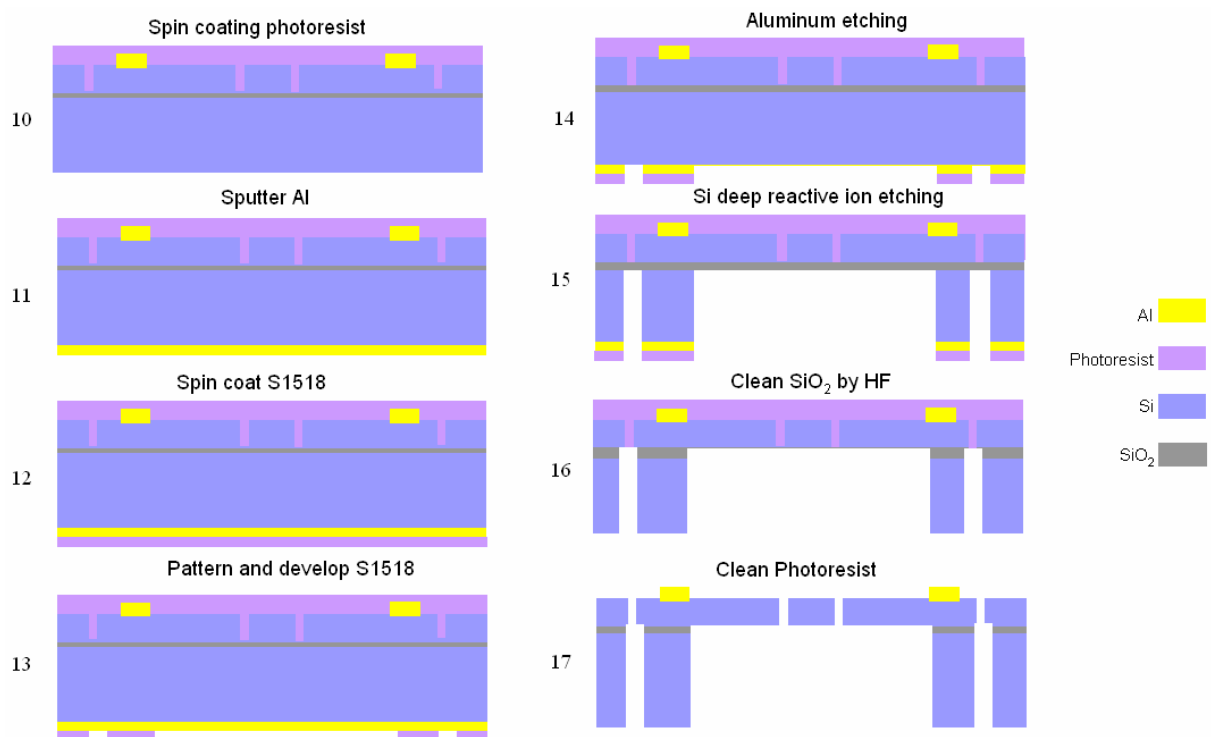
Fig. 4.24. Etching of handle layer.

An aluminum mask is sputtered to etch the 300µm handle layer by radio-frequency (RF) configuration of DRIE in figure Fig. 4.24- 11. A typical photoresist is spin-coated, patterned and developed (see Fig. 4.24-11, 12 13). After that, the aluminum is etched by acid. Then, the silicon of handle layer is etched by DRIE (Fig. 4.24- 15) until stopped by the sacrificial layer. This handle layer has a thickness of 300µm. Our etching speed is about 5µm/min. In order to allow the etching heat to be transferred, a break time is set for each 20min. The oxide layer is cleared by HF from the backside in Fig. 4.24-16, at last we put the wafer into acetone to clear the photoresist as shown in Fig. 4.24-17.

4.5 The fabricated bistable modules

We obtain the bistable modules after performing all steps. Some SEM photos about the fabricated bistable modules are shown in Fig. 4.25.

(a)

(b)

(c)

(d)

(e)

123

(f)
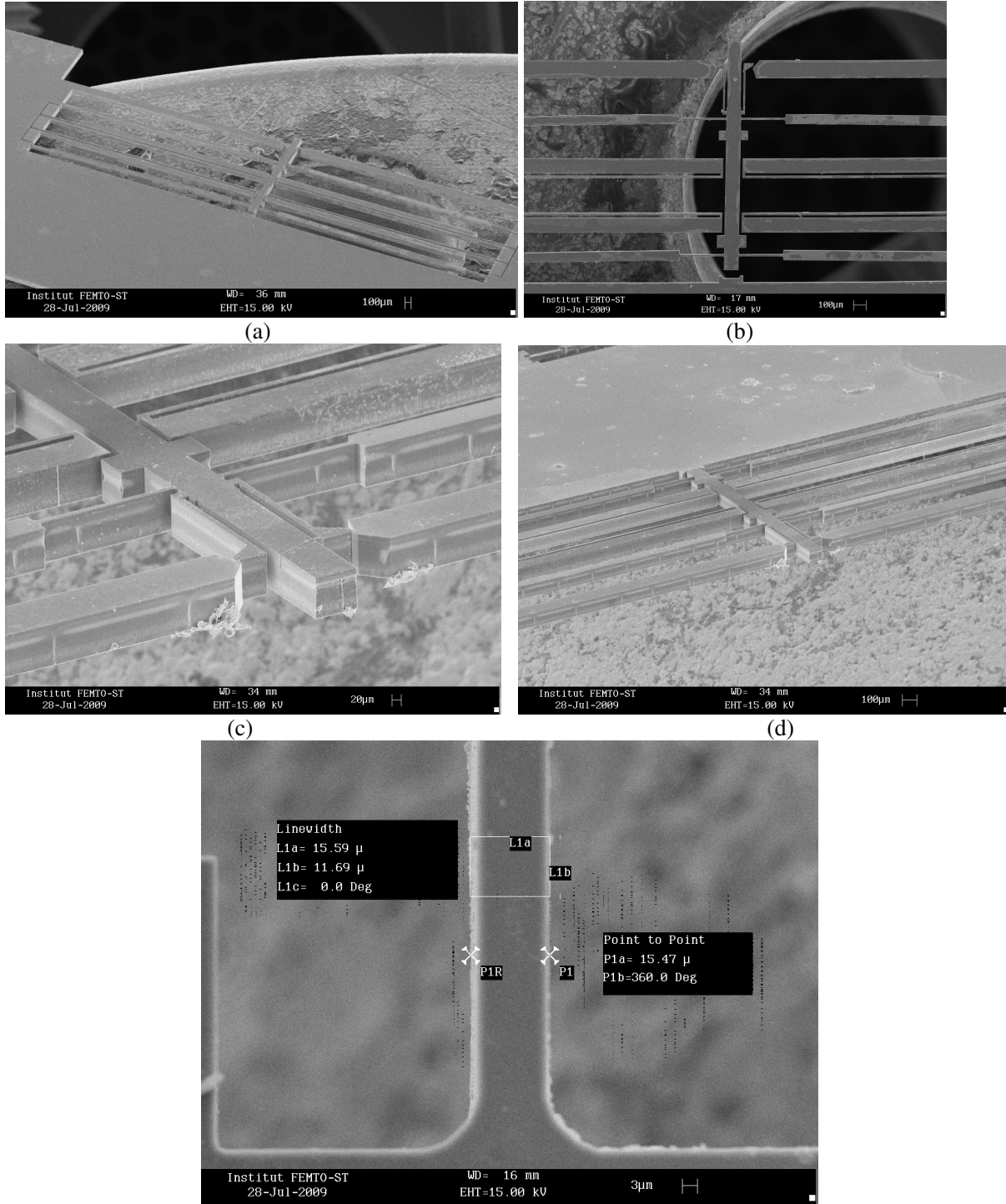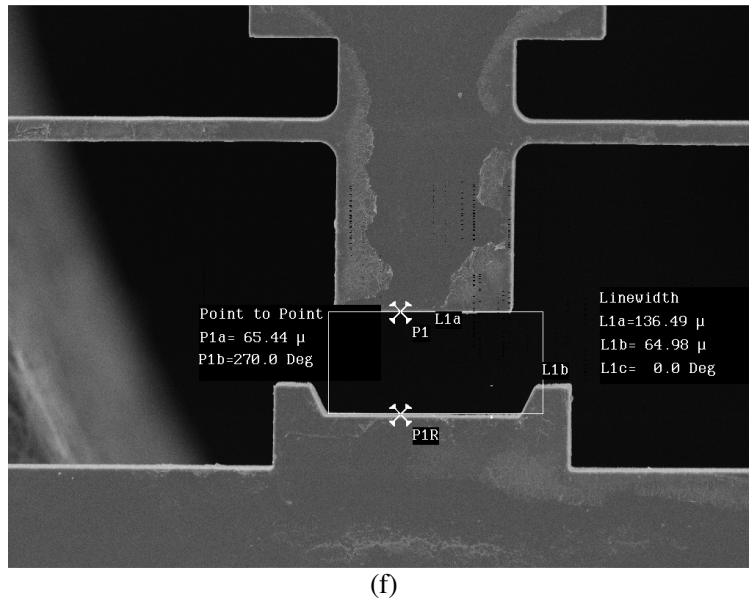
Fig. 4.25. (a,b,c,d)Scanning electron microscope (SEM) pictures of microfabricated module. (e) The width measurement of bistable beam using the SEM picture. (f) Measurement of the distance between the bistable mechanism and the second stop block using the SEM picture.

As shown in Fig. 4.25-e, the width of the bistable beam is 15.5µm while designed dimension is 15µm. The distance between the bistable mechanism and the second stop block is 64.98µm while the designed dimension is 65µm (see Fig. 4.25-g).

Measurements show that there is only small error between the measurement and the designed dimensions. This fabrication process allows us to obtain the desired structure. The performance of bistable module will be tested in the next chapter.

However, there are tiny photoresist residues in the surface of the bistable mechanism (see Fig. 4.25) which are residues of the protection layer of photoresist. This tiny residue does not influence the structure, so we did not try to clean it totally.

4.6 Conclusion

MEMS Microfabrication is a set process for specific MEMS device. The process should be investigated and developed. Each process requires much time to be developed. Four possible processes have been studies to fabricate the bistable modules.

According to the studies, the use of the process 1 can obtain the desired structure (see Tab. 4.4).

Tab. 4.4. The process summary to fabricate the bistable module.

Step	Process	Mask	Comments
1	Deposition of aluminum (device layer)		
2	Spin-coating the photoresist S1518		
3	Lithography	1	Pattern the electric connection to the thermal actuators. The recruit gives a good electric contact.
4	Development		
5	Etching acid		
6	recruit at 400°C		
7	Spin-coating the photoresist SPR220-3.0		
8	Lithography	2	The etching the device layer utilizes the DRIE in low frequency.
9	development		
10	Etching (DRIE)		
11	Deposition of aluminium (handle layer)		
12	Spin-coating the photoresist S1518		
13	lithography	3	The etching of the handle layer permits to free the structure by an aluminum mask.
14	development		
15	Etching (DRIE)		

In order to perform the in-plane test for the next, we need to fabricate the off-chip bistable modules. Three solutions have been tried: the saw cut, electrical discharge machining and the fracture line.

The first approach takes use of the saw to cut the wafer into small pieces. The direct cut will make the suspended structures failure due to the vibrations. However, if we glue the wafer on a plastic paper, it is difficult to take it off.

The second approach takes use of the electrical discharge machining, this technique permit to machine the object in the plane. The difficult is that it does not have an accurate alignment and fixation system. We do not have time to design a suitable system.

The third approach takes use of the fracture line. We create intentionally fracture party connecting the bistable module and the wafer. After the process is finished, we take the bistable module off the wafer by breaking this fracture connection. This solution permits us to obtain whole bistable modules off the wafer. The fracture line need be designed repeatedly to adapt to the process.

As discussed in the process 1, after the etching of the device layer, the structure is already separated with the wafer. The use of the protection layer can be embedded bistable module. These bistable modules can be taken off when we clean the protection layer. Using this approach, three different stable positions of bistable module are fabricated (see Fig. 4.1). The locations of the stop block are 5µm, 10µm and 20µm, respectively. Using the off-chip bistable module, we will perform the static and dynamic tests in the next chapter.

This proposed process gives a yield until 90%. Most of the structure can be used because of

the use of a protection layer. Some photos are shown in Fig.4. 26 and Fig.4. 27.
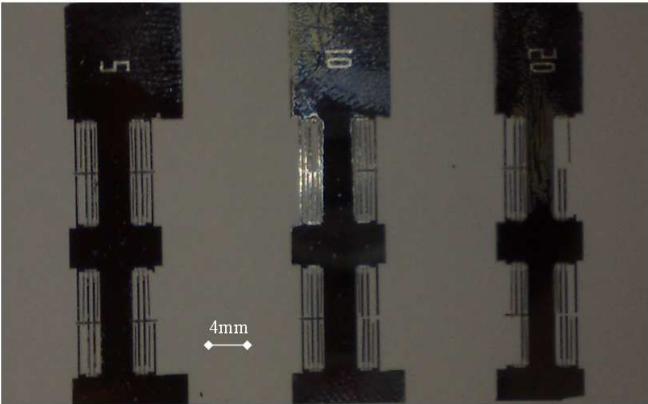
Fig.4. 26. Fabricated bistable modules.

Furthermore, the use of the same fabrication process, we fabricated two cascaded and three cascaded bistable modules (see Fig.4. 27).

| (a) | (b) |
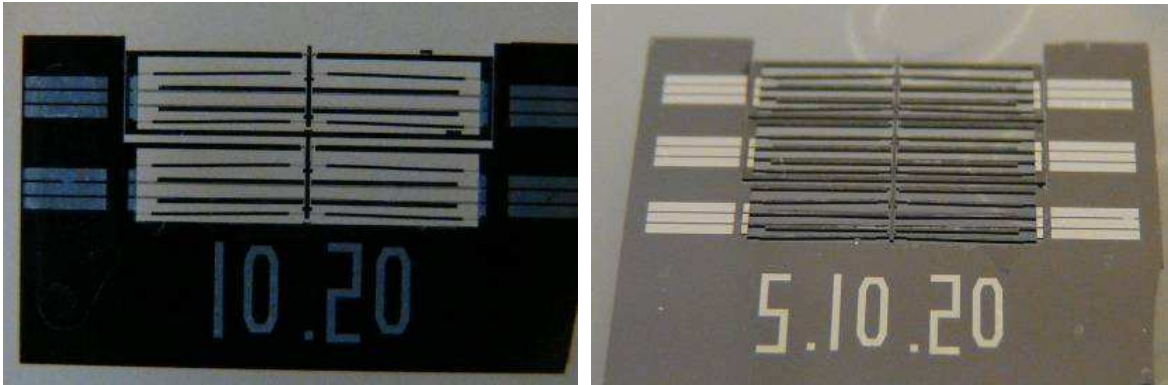
Fig.4. 27. (a) Two cascaded bistable module, (b) Three cascaded bistable modules.

Chapter 5 Characteristics of bistable module

"Imagination is more important than knowledge. For knowledge is limited, whereas imagination embraces the entire world, stimulating progress, giving birth to evolution."

Albert Einstein

(1879 – 1955)

5.1 Introduction

As seen previously, the digital microrobot consists of bistable modules link to offer discrete workspace. Each point of workspace is reachable through an open-loop control strategy because it needs a particular configuration of each module must have two stable and repeatable positions. The switch of the module for a position to the other is done by our open loop control strategy.

In this chapter, we will study the behavior of a module and the way it reaches a stable position. That is why we will study the characteristics of the bistable modules. We first describe the process to activate a module and then the static and dynamic characteristics. The static characteristics show the force versus displacement of the bistable mechanism using an accurate force sensor, and the voltage versus displacement of thermal actuator. The dynamic characteristics show the behavior of switching the bistable mechanism. In the last section, a control strategy is proposed to master the entire switching procedures.

5.2 Activation process

The stop block is designed to limit the motion of the bistable mechanism and give blockage force in each of the stable positions. The Fig. 5.1 gives the designed stop block for the side where a compliant structure is needed as described in the previous chapter. Two deformable beams are designed to create this stop blocks.

127
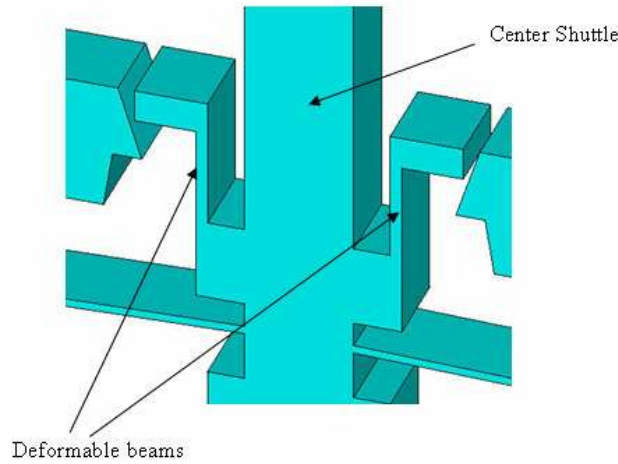
Fig. 5.1. The designed stop block.

The activation that consists in inserting the center shuttle between the two stable positions is performed by using an external force. We use a probe to slowly push the center shuttle of bistable mechanism into the stop blocks. Since the two deformable beams deform symmetrically, the direction of the force should be aligned with the center shuttle. In the meantime, the out-of-plane force should be null. The experimentation set-up is shown in Fig. 5.2.

The bistable module and the probe are mounted on an anti-vibration table. The probe is fixed on an x-y-z stage, which can be moved with micrometric resolution. An optical microscope is put on the scene allowing us to operate the activation process. The activation needs that the probe pushes the center shuttle with a different distance (40 um, 50 um and 60 um) for each of three stop blocks.
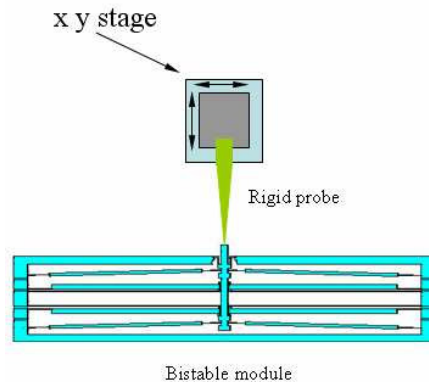
Fig. 5.2. Activation of bistable module using a probe.

Fig. 5.3 shows the results before and after activation. Despite the contact area (classic DRIE sidewall) presents rather great roughness, all of the activation of bistable mechanism was successful.

(a)   (b)

(c)
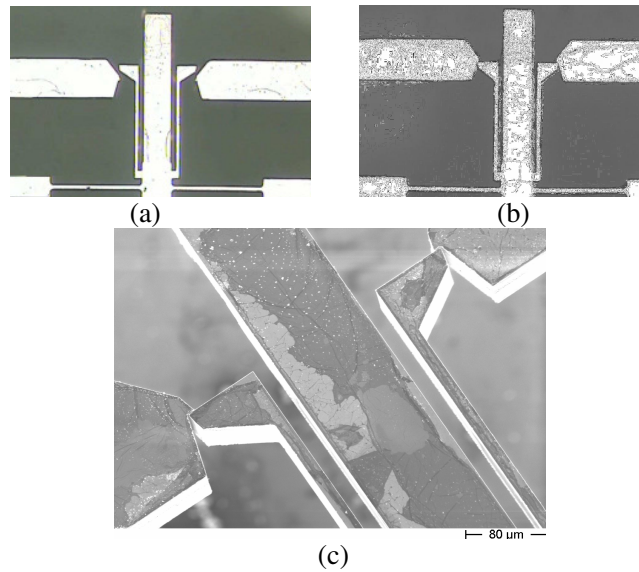
Fig. 5.3. (a) Before activation. (b) After activation. (c) SEM photo of 3D stop block after activation.

5.3 Static characteristics

The static characteristics describe the static response of the entire bistable module (including the bistable mechanism and the thermal micro-actuators). For the bistable mechanism, the force-displacement relation is measured, which shows the bistable behavior. For the thermal micro-actuators, the voltage-displacement relation is measured.

5.3.1 Force-displacement relation of a bistable module

In order to measure this relationship, a commercial force sensing probe is used [FEM] (see Fig. 5.4). It is mounted on an x-y positioning table. The force information and the displacement are recorded. The result curve is shown in Fig. 5.5.

A finite element analysis (FEA) is also made by using the commercial FEA software ANSYS. The results from the FEA and the static experimentation are presented in Fig. 5.5. The results show that the experimentation matches the FEA very well.
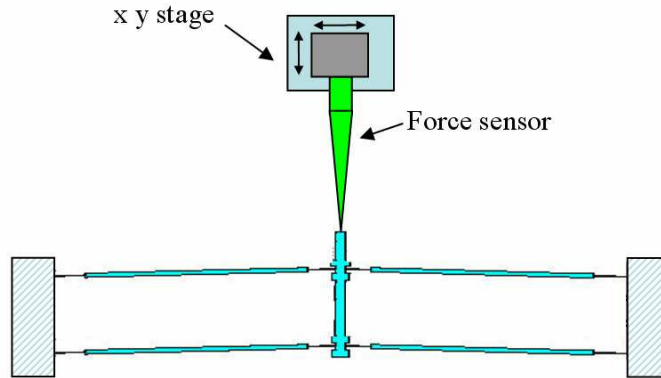
Fig. 5.4. Experimental set-up (a commercial force sensing probe (ST-S270 from FEMTO TOOLS [FEM] with a sensitivity of 899.2 μN/V).

As a typical bistable mechanism, it presents first a positive stiffness, which increases with the actuation force. After going through the position at maximum actuation force, it presents a negative stiffness, which means that the actuation force decreases until zero. In fact, it is an unstable position for the bistable mechanism. After passing through this position, it goes to the other stable position without external force.
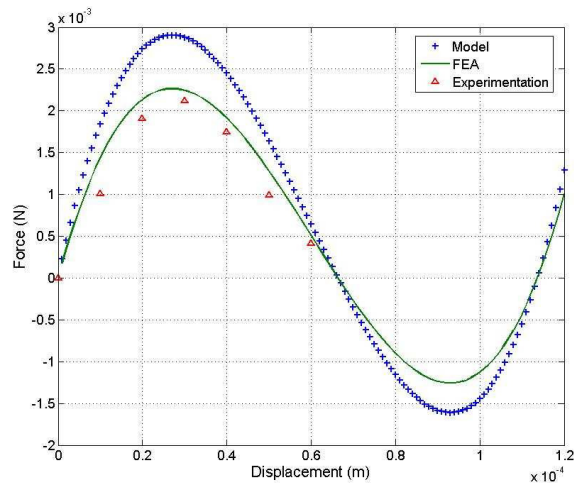
Fig. 5.5. Force (F) Versus displacement (Y) characteristic.

The result shows that the model gives 20% error comparing with the FEA and the experimentations. That is because the stiffness of the compliant joints and the compressed beam can not be defined precisely. We use the classical beam theory to obtain the stiffness. However, the FEA and experimentation meet very well. Although the fabrication gives the final dimension errors, they result in a 5% error in this force-displacement relation, which does not make any changes on the bistable behavior.

130

5.3.2 Blockage force evaluation

The blockage force can be evaluated using the same force sensor as previously (ST-S270 from FEMTO TOOLS [23] with a sensitivity of 899.2µN/V). An optical microscope is installed on the scene to observe the measurement. We move the force sensor to push the blocked bistable mechanism, at the moment when the bistable mechanism moves we can obtain the blockage force.

Tab. 5.1. The measured blockage force (see Fig. 5.6).

Stop block	Type 1 (a=2.5µm)	Type 2(b=5µm)	Type 3(c=10µm)
Measured blockage force	212µN	540µN	1310µN
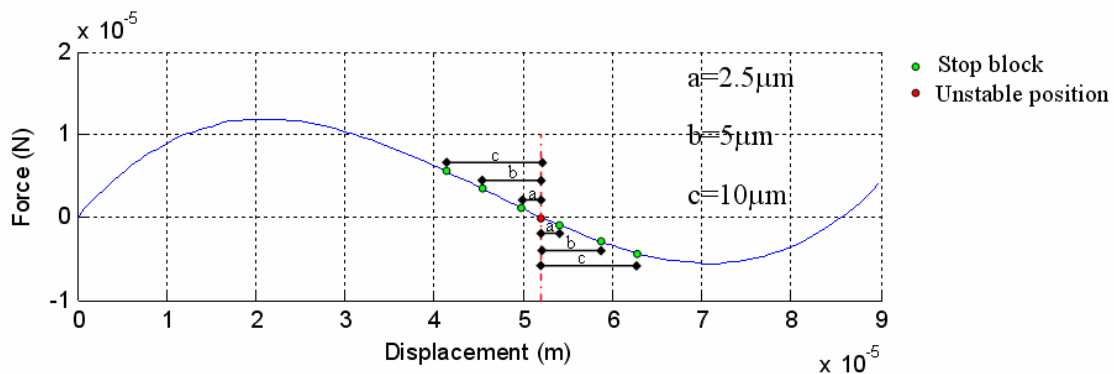
Fig. 5.6. Three locations of the stop blocks.

The blockage force gives stable position with high repeatability. Unlike traditional microrobots which rely on the high quality of sensor system and closed-loop control to guarantee the repeatability, the use of stop blocks permits to mechanically limit positions and ensure the repeatability.

5.3.3 Voltage-displacement relation of thermal micro-actuators

The thermal actuator generates an in-plane displacement while the electric current passes through it (see Fig. 5.7).
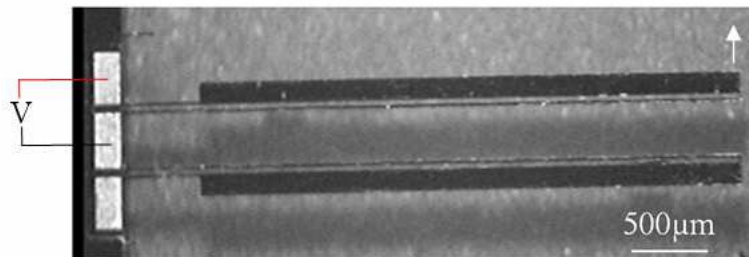
Fig. 5.7. A pair of thermal actuators.

A slow ramp voltage is applied to avoid the voltage impact. The result shows that the

131

displacement of the thermal actuator is not linear with the applied voltage (see Fig. 5.8). This simulation is made using electro-thermal-mechanical couple field analysis, which permits to take into account all three thermal mechanisms: conduction, convection and radiation.
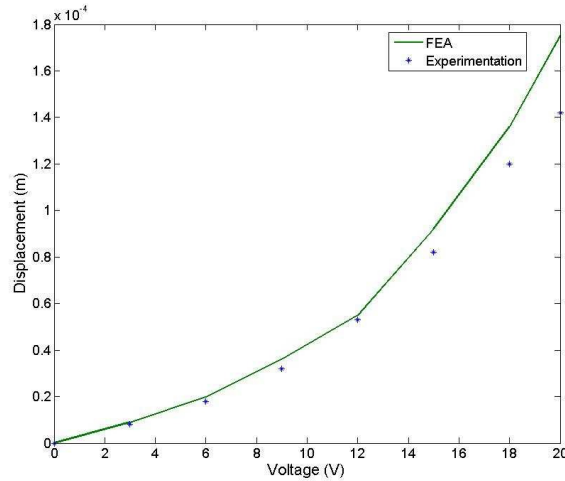
Fig. 5.8. Static behavior of the thermal actuator.

The result is shown in Fig. 5.8. We can observe that the FEA gives more error, when the voltage increases, that is because the resistivity of silicon changes with the temperature and we did not have this exact change curve. The displacement versus voltage tests shows that this actuator produces 160 µm displacement for 20 V. According to the estimation in the chapter 4, 80 µm displacement of the actuator is enough to switch this bistable mechanism.
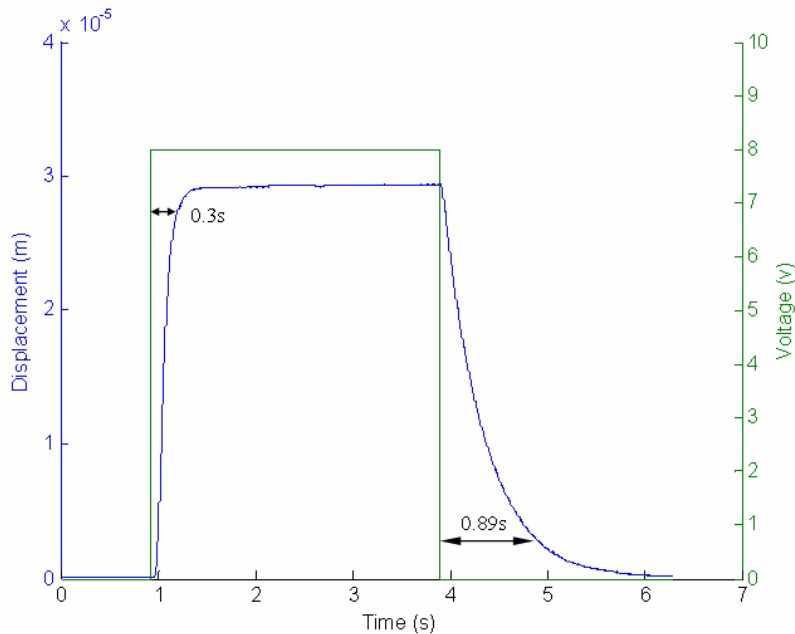
Fig. 5.9. Dynamic response of the thermal actuator.

132

Fig. 5.9 shows the response of the actuator to a square input voltage of 8V. The settling time is about 0.3s for a rising edge and 0.89s for a falling edge. Since the electro-thermal effect is fast, we obtain a short settling time for the rising edge. However, the energy dissipation is slower than the heating, so we obtain a longer time for the falling edge.

This performance allows us to continuously switch the bistable mechanism with a delay of about 0.89 s. This delay is caused by energy dissipation in the actuators. In fact, each switching takes about 12mJ thermal energy in the thermal actuator which needs to be transferred into the substrate to be cooled for the next switching.

5.4 Dynamic characteristics

5.4.1 Introduction

We have to study the behavior of the mechanism from a stable position to the other stable position and analyse according to microrobotics needs. These characteristics are important for microrobotics and micro-positioning applications. Micromanipulation tasks, such as pick-and-place, micro-positioning etc., are based on state changes. Dynamic characteristics show the duration, speed, accuracy, repeatability of state changes. We will study these characteristics in this section.

In this test, the bistable modules are prepared for an in-plane measurement. For this measurement, we use a high resolution (10 nm) interferometer from SIOS Technology to test the dynamic response of bistable mechanism. All the test devices are mounted in an anti-vibration table (see Fig. 5.10).
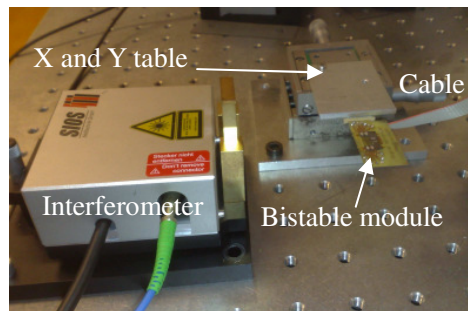
Fig. 5.10. Experimental set-up.
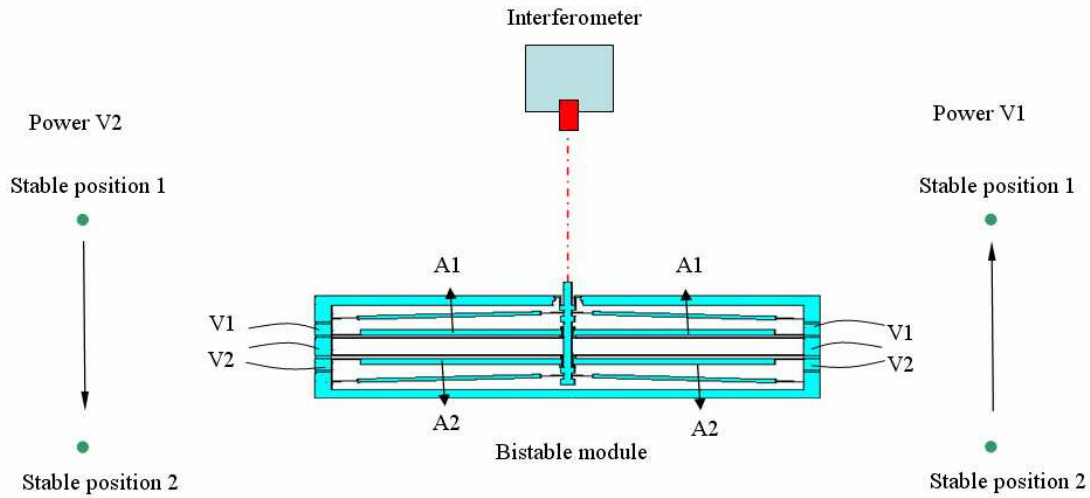
Fig. 5.11. Switching test using the high resolution interferometer.

Since the bistable module is activated, the bistable mechanism is in the blocked position (see Fig. 5.12). Two transitions of switching will be studied. For the transition to stop block 2, we power the actuators (A2). For the transition to stop block 1, we power the actuators (A1).
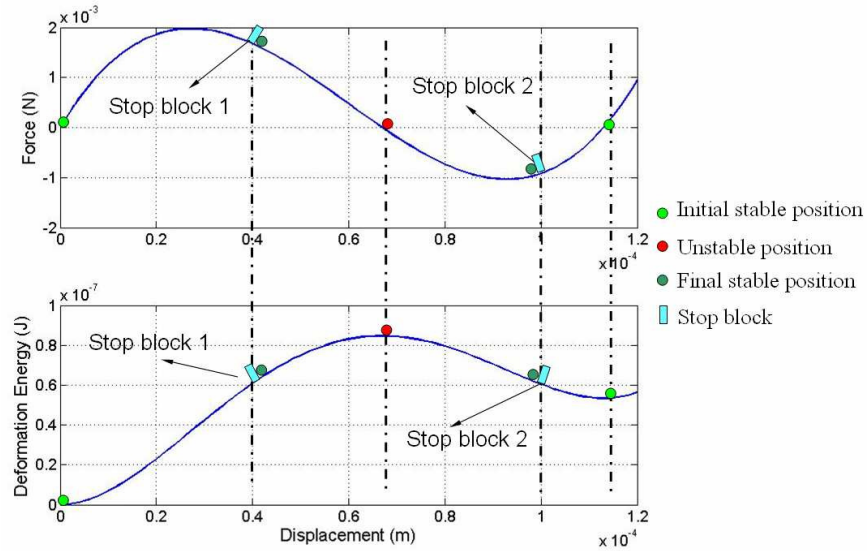
Fig. 5.12. Locations of the stop block.

5.4.2 Transition from stop block 1 to stop block 2

To switch from stable position 2 to stable position 1, the voltage is applied on the thermal actuators (A2) (considering the impact of thermal actuators, a ramp voltage is applied). The interferometer detects the motion of the bistable mechanism. The result is shown in Fig. 5.13.

134
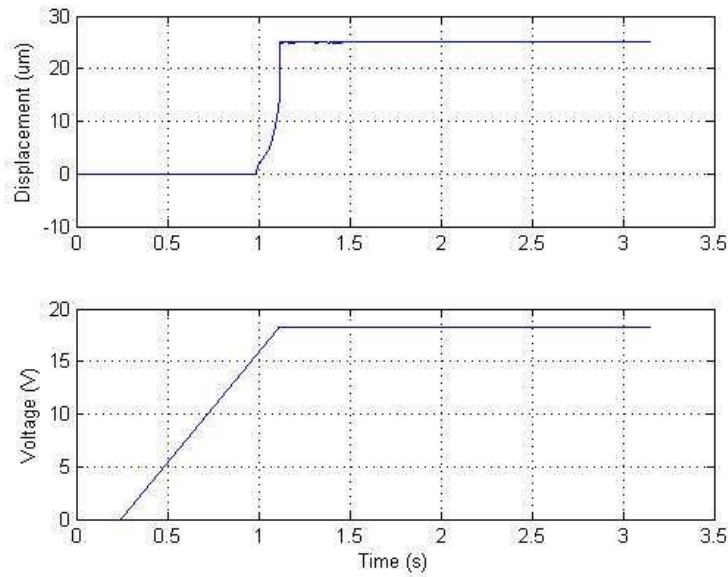
Fig. 5.13. Response from stable position 1 to the position 2.

Since there are gaps between the actuator and the bistable mechanism, they will be in contact after some time. The bistable mechanism can be switched when the applied voltage reaches 17V.
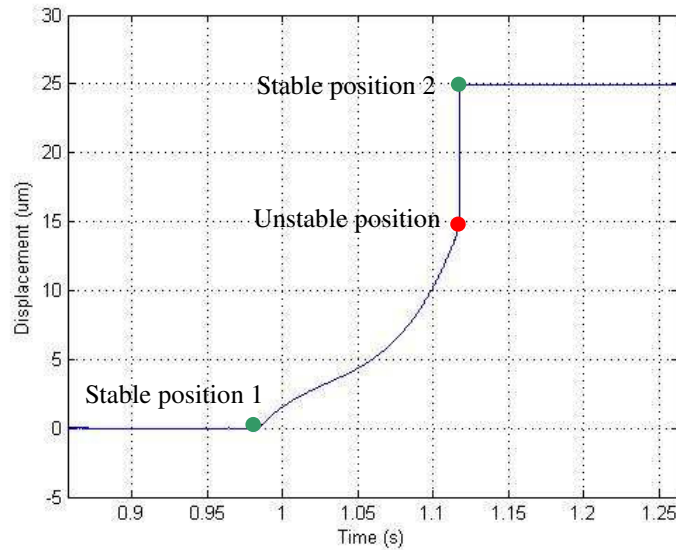
Fig. 5.14. Details of the transition to stable position 2.

In Fig. 5.14, the first phase from stable position 1 to unstable position is controlled by actuators. The duration is about 117 ms for a displacement of 25 µm. The unstable position can be located (red point). The second phase is faster. It requires only some nanoseconds to reach the stable position 2. This transition dose not presents overshoot and oscillation.

135

Since the final position is blocked by stop block, the accuracy and repeatability are ensured. A lot of test has been done which show the same result.

5.4.3 Transition from stop block 2 to stop block 1

A ramp voltage is applied to the thermal actuators (A1) to actuate the bistable mechanism from stable position 2 to stable position 1. Fig. 5.15 shows the results.
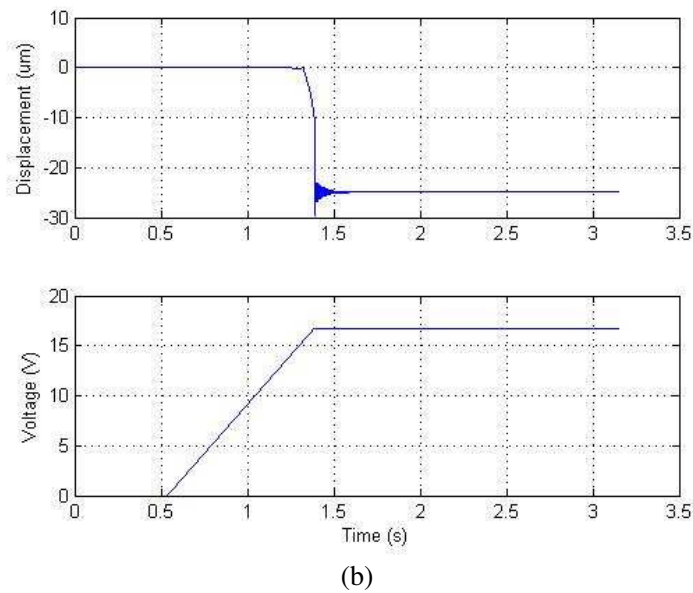
(b)
Fig. 5.15. Response from position 2 to position 1.

As previously, since there are gaps between the actuator and the bistable mechanism, they will contact after some time. The bistable mechanism can be switched when the applied voltage reaches 17 V.

In Fig. 5.16, the first phase (from the stable position 2 to unstable position) is similar to the transition (from the stable position 1 to unstable position). However, during the second phase from unstable position to the stable position 1, vibrations appear (see Fig. 5.16). This is because the stop block 1 is made up of deformable beams which present compliancy. The overshoot of this vibration is 4.5 μm. The unstable position can be located. The final position is no static error the same as the initial stable position 1.
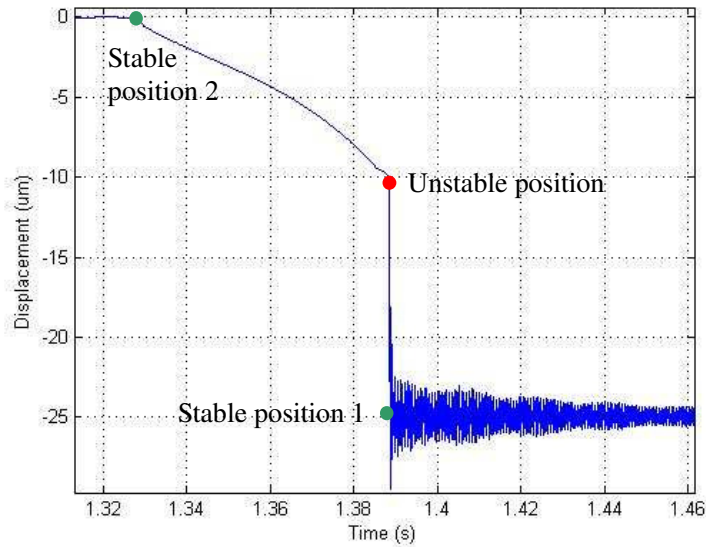
Fig. 5.16. Details of the transition to stable position 1.

We performed the same test on three types of locations of stop block. They present similar curve, we give a table to compare the different results (see **Tab. 5.2**).

Tab. 5.2. Experiment results of three locations of stop blocks.

Measured distance between stable states (µm)	Time from S1 to S2 (ms)	Switching voltage (V)	Unstable position FEA (µm)	Unstable position experiment (µm)
6.75	25.5	15.2	66	66.6
11.12	60.6	15.9	66	67.6
25.12	117.3	16.7	66	69.1

The actuation time between the two stable positions almost depends on thermal actuators because the free motion of bistable mechanism from the unstable position to stable position is so fast that it can be ignored (usually 100-300ns, see Fig. 5.16). This actuation time can be optimized by studying the control of thermal actuator.

5.5 Control strategy

According to the result of last section, the actuation of bistable mechanism from stable position 2 to stable position 1 shows vibration around the stable position, which is not suitable for microrobotics or micro-positioning. To control the switching and avoid the vibration, we propose an open-loop control strategy to obtain a damped transition.

137
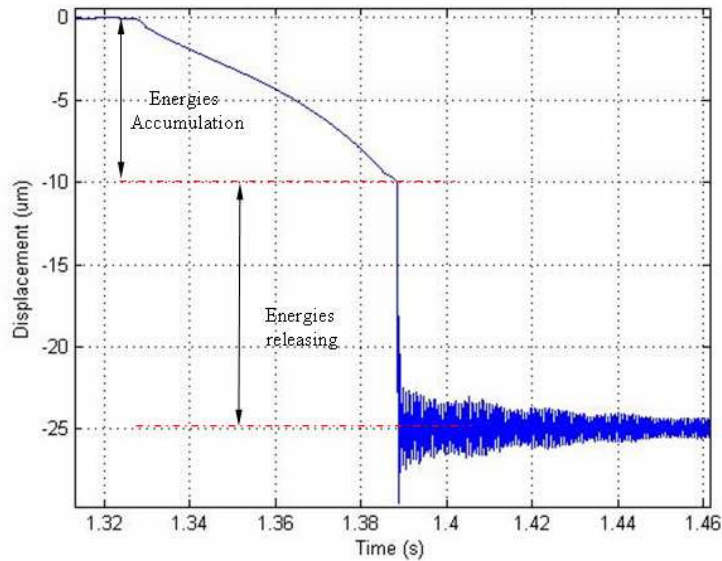
Fig. 5.17. Two phases of the switching of bistable mechanism.

The strategy is based on the use of two pairs of thermal actuators during switching operation. The idea is using one pair of thermal actuators (A2) to catch the bistable mechanism when it is just actuated from the unstable position by the other pair of actuators (A1) (see Fig. 5.18). The interferometer is used to detect the position of the bistable mechanism.
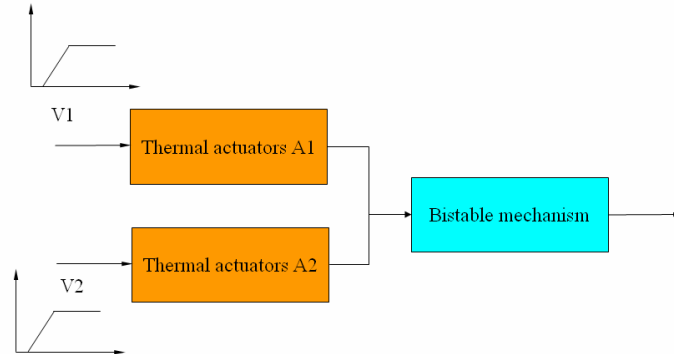
Fig. 5.18. A schematic of control system of bistable module.

First of all, the first phase is the accumulation of the deformation energy, which is controlled by actuator (A1). This phase carries out by applying a ramping voltage (see middle curve of Fig. 5.19). Since there are some gaps between actuators and the bistable mechanism, the time of touching is at 1.63s. When the unstable position reaches (the time is at 1.69s), the first phase is finished.

After then, it goes through the unstable position, and enters the second phase (the deformation energy releasing). In this phase deformation energy is releasing. The actuator (A2) is used to control this phase (see bottom curve of Fig. 5.19). The bistable mechanism is maintained by

the actuator (A2) until 1.83s, it is released, and reaches the second stable position (see top curve of Fig. 5.19).
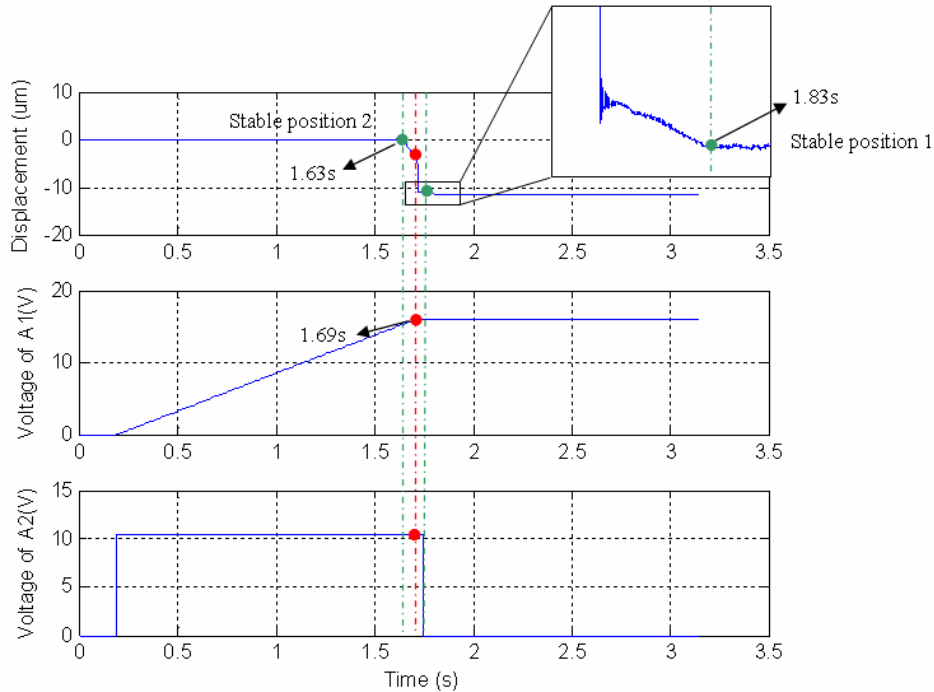
Fig. 5.19. Control sequenes (Voltage A2 and Voltage A1) and the response of bistable mechanism .

Fig. 5.20 shows the comparison between the transition with and without control. We can observe that the use of this control can reduce the vibration. The whole switching time is about 205ms, and it does not present overshoot and vibration.

In fact, each phase is controlled by each pair of actuators, so two phases of the switching can be controlled totally using two pairs of actuators. This control results show that the vibration of bistable mechanism is reduced significantly. At the same time, there is no overshoot when the final target position is considered. Therefore, with this control strategy, we can obtain the switching of bistable mechanism in two directions without vibrations.
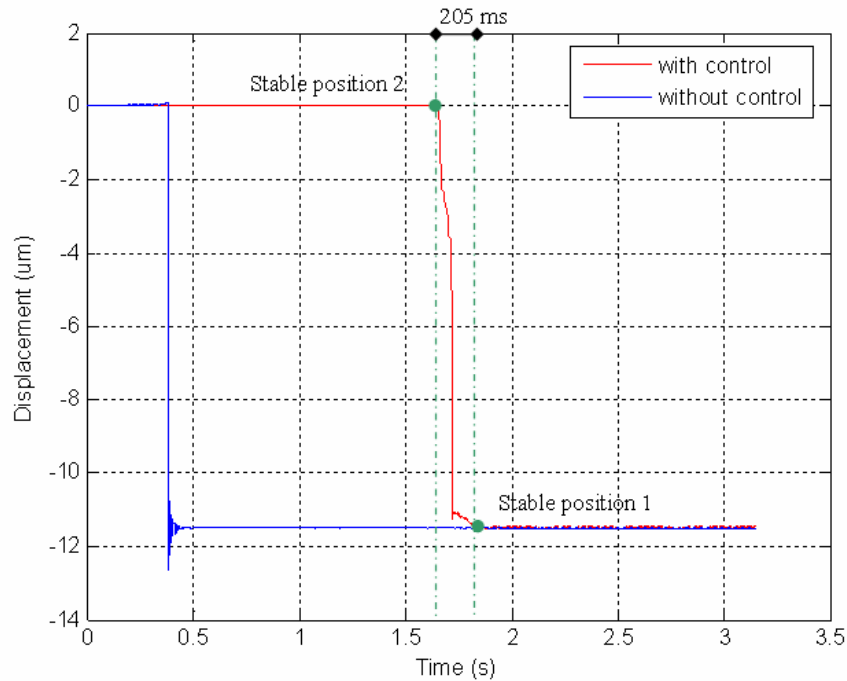
Fig. 5.20. Comparison between the transition with control and without control.

5.6 Conclusions

We have presented the static characteristics of bistable mechanisms that consist in the force versus displacement relation, three bistable mechanisms with blocked positions of 6.75 µm, 11.12 µm and 25.12 µm present bistable behaviors. Each one has a blockage force of 212 µN, 540 µN and 1310 µN. Static characteristics of thermal actuator include the voltage versus displacement relation. It produces 160 µm displacements for 20 V which is enough to switch the bistable mechanism. The step voltage test of thermal actuator shows a settling time of 0.3 s for a rising edge and 0.89 s for a falling edge.

We have shown the dynamic characteristics that the switching between these two stable positions. The dynamic motion of bistable mechanism for two transitions has been studied. For the transition to the stop block 2, it presents smooth transition with no overshoot and no vibration. For the transition to the stop block 1, it presents vibrations due to the compliant stop block.

To resolve this problem, a control strategy has been implemented. The main idea was to use two pairs of the actuator to reduce this vibration. These two pairs of thermal actuator are cooperated used to control the entire switching procedures. The use of this control can avoid the vibration and the overshoot.

Conclusion and perspectives

In our research work, we have proposed the development of a new kind of microrobots that can perform high accurate positioning without the need of high level control. This new generation of microrobots is called digital microrobots. The digital microrobot offers a new approach for the design of microrobots architectures based on elementary bistable modules. Each module has two mechanical stable and repeatable states driven by a simple binary signal. The position of the whole microrobot is controlled by a digital word representing the state of the modules. Digital microrobotics also takes the advantage of microfabrication technology and open-loop control.

This new concept shows many advantages:

- repeatability and accuracy are obtained thanks to the mechanical bistable performance of the modules;

- neither proprioceptive sensors nor bulky and expensive instruments are needed to control the microrobot;

- fast and large displacements can be obtained using the parallel control of the state of the modules;

- digital microrobots can be built in great quantities and potentially at low cost;

- low power consumption can be obtained as power is not needed to maintain the modules in a given state but only during the transition phases.

6.1. Contributions of this research

We have investigated the numerous proposals to realize bistable mechanisms. A basic bistable mechanism was proposed which permits to obtain a general model. According to this model, three positions including two stable positions and an unstable position can be predicted. Considering the real situations, two kinds of models are taken into account: the perfect joint connection and the compliant joint connection. The perfect joint connection can guarantee the symmetric force-displacement performance of bistable mechanism during the whole switching phase and all the deformation energies can be released after switching. However, it is difficult to fabricate this kind of joint in the microworld. The compliant joint is adopted in our design. The compliant joint connection uses beam deformation to create the rotation

motion. Since the energy in this compliant joint can not be released totally, the model is modified to consider this energy. In fact, this residual energy from the compliant joints may result in bad stable position. To solve this problem, we presented the following criterion: the maximal energy in the elastic beam is bigger than the maximal energy in the compliant joint. Good stable position can be ensured by this criterion.

To switch the bistable mechanism, various actuation principles have been studied such as piezoelectric materials, magnetostrictive materials, thermal actuators and electrostatic actuators. Active materials present good performance due to the integration of both the bistable mechanism and the actuators. This design permits to obtain compact structures. However, this proposition needs the microfabrication of the active materials which require the development of new processes. Thermal actuator is also a solution. The U-shape actuator is suitable for the microfabrication. However, the design of this actuator should be done carefully. If the actuation leads to the hot beam buckling and the stiffness of this actuator is reduced greatly, as a result, it can not provide big actuation force. Electrostatic actuators can also be used but they take more space compared to the previous actuators.

Unlike the traditional microrobots, in digital microrobots, the stable position is maintained by the mechanism. In order to reject perturbations, a blockage force is required. The stop blocks are designed to limit the motion range of the bistable mechanism and provide a blockage force in each of the stable positions. Stop blocks have been designed to offer blockage forces in each of the stable positions. The stable position can be maintained if the external charge does not exceed this force. The repeatability can be ensured due to this stop block and it is mechanically ensured.

Based on the three components (bistable mechanism, thermal actuator, stop blocks), an entire bistable module was designed. A process using SOI wafers is developed to fabricate thie bistable modules. This process consists of three masks for etching the three layers: aluminum layer, device layer and handle layer. Static and dynamic characteristics show that the switching of the bistable mechanism can be done by actuating the thermal actuators. Each stable position can be reached. We also proposed a control strategy to resolve the vibration problem in one of the switching positions.

6.2. Perspectives

This research opens a window for future studies on digital microrobotics. An entire bistable module has been designed, fabricated and tested and two blocked positions are obtained. This can be the basis of the design of complex architectures such as multi-DDL microrobots, pure rotation microrobots, etc. The architecture can be built according to various robot kinematics. Three kinds of approaches are possible: serial, parallel and hybrid (serial/parallel).

6.2.1 Serial mechanism based on bistable modules

The serial mechanism is achieved by connecting each module to the previous one. Fig. 6.1 presents an example of two DOFs mechanism.
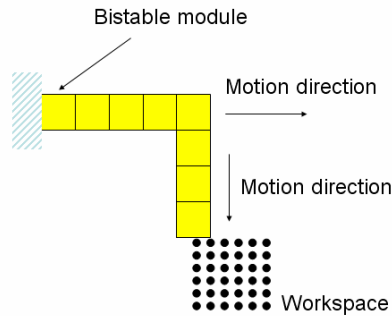
Fig. 6.1. Two DOFs plane serial mechanism.

This configuration leads to a discrete rectangle workspace and a simple control strategy. However, this serial mechanism also results into lower whole stiffness. In our proposed bistable module, the integration of thermal actuators is used to switch the bistable mechanism. These actuators need to be powered by external electric wire connections. In this serial mechanism these connections become very difficult to realize because they limit the motion of the serial mechanism. A wireless actuation approach is preferred and some solutions are conceivable in the future.

6.2.2 Digital microrobot based on parallel mechanisms

Parallel mechanism can be created according to the classic general parallel mechanisms. Bistable modules are mounted directly on the base. The kinematic chains connect these bistable modules to create a parallel mechanism. This kind of architecture avoids the connection problem described previously.

Fig. 6.2 shows a proposal for a parallel mechanism. Firstly, two bistable modules are connected by rigid bodies and compliant joints (see Fig. 6.2(a)). This mechanism gives plane rotation and translation and four states can be reached. Using the same connection, this mechanism can be extended to three bistable modules (see Fig. 6.2(b)). It gives $2^3=8$ states as shown in Fig. 6.2(c) by using the same extension, this parallel mechanism is extended to five bistable modules; this extension is theoretically unlimited. This configuration leads to $2^5 = 32$ stable positions. It offers three DOFs including two translations and one rotation.
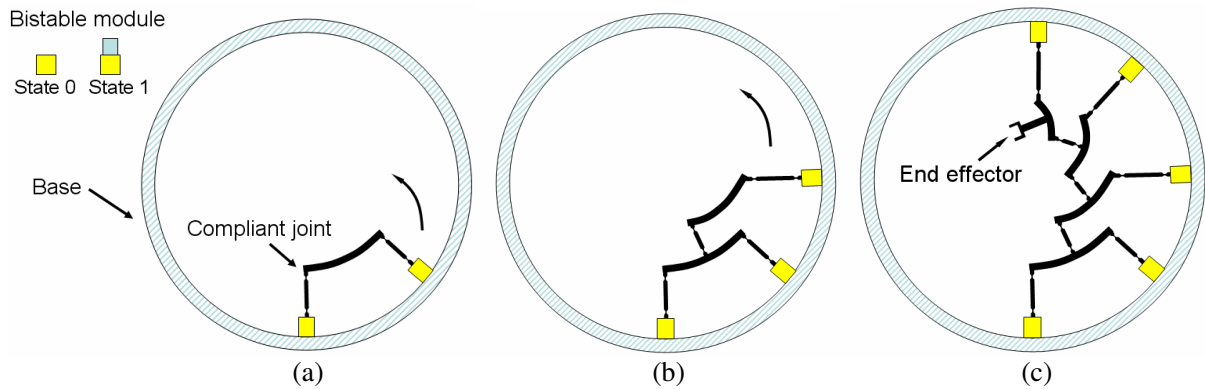
Fig. 6.2. (a) Two bistable modules (b) three bistable modules (c) five bistable modules.

6.2.3 Digital microrobot based on both serial and parallel mechanisms

Both of the serial and parallel mechanism presents advantages and drawbacks. If the digital microrobot is built using both the serial and parallel mechanisms, the difficulty from both of them will be reduced such as small stiffness (serial mechanism), small workspace (parallel mechanism), etc. We propose a structure based on a hybrid approach. Fig. 6.3 shows a platform which connects three discretely-actuated axes by rotation joints. This design gives a plane discrete workspace (x, y, θ).
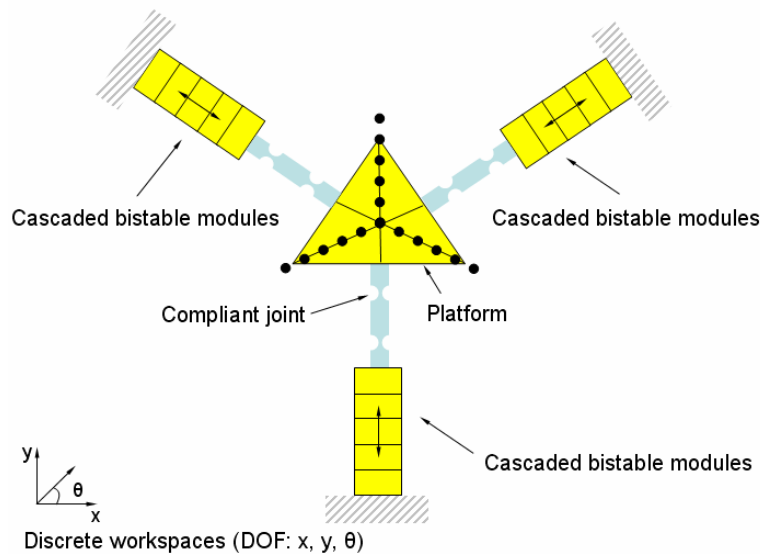
Fig. 6.3. A proposed design based on the serial and parallel mechanism.

144

References

[AGN 03] J. Agnus, thesis, étude, réalisation, caractérisation et commande d'une micropince piézoélectrique, 2003.

[AKA 04] F. Akasheh, T. Myers, J.D. Fraser, S. Bose and A. Bandyopadhyay, Development of piezoelectric micromachined ultrasonic transducers. Sens. Actuators A, 111(2–3), pp275–287, 2004.

[ALS 07] D. H. Alsem et al., very high-cycle fatigue failure in micron-scale polycrystalline silicon films: Effects of environment and surface oxide thickness, Journal Of Applied Physics 101, 013515, 2007.

[ARA 04a] F. Arai, K. Motoo, T. Fukuda and T. Katsuragi, High sensitive micro^louch sensor with piezoelectric thin film for micro pipetting works under microscope, Proc. of the IEEE Intcmational Conference on Robotics and Automation, pp1352-1357, New Orleans, 2004.

[ARA 04b] F. Arai, D. Daisuke, Y. Nonoda, T. Fukuda, H. lwata and K. Itoigawa, Integrakd microendeffe~tor for micromanipulation, louomal of IEEEIASME Transactions on Mechatronics, Vol. 3, no 1, March 1998.

[BAG 03] J. Bagdahn, W. N. Sharpe, and O. Jadaan, Fracture strength of polysilicon at stress concentrations, Journal of Microelectromechanical Systems, Vol. 12, No. 3, pp302-312, Jun, 2003.

[BAK 00] M. S. Baker, S.M. Lyon and L.L. Howell, A Linear Displacement Bistable Micromechanism, Proceedings of the 2000 ASME Design Engineering Technical Conferences, DETC2000/MECH-14117, 2000.

[BER 06] J. Bert, S. Dembele, N. Lefort-Piat, Trifocal transfer based novel view synthesis for micromanipulation," Book Series: Lecture Notes in Computer Science-Volume: 4291, pp411-420, 2006.

[BLO 89] F. R. Blom, S. Bouwstra, J. H. J. Fluitman and M. Elwenspoek, Resonating silicon beam force sensor, Journal of Sensors and Actuators, Vol. 17, pp513-5I9, 1989.

[BMM] Bio-MEMS & Microsystems. http://mems.eng.usf.edu//outreach/index.htm.

[CAM 03] D. Campolo, R. Sahai and R. S. Fearing, Development of piezoelectric bending actuators with embedded piezoclectric sensors for micromechanical flapping mechanisms, Proc of the IEEE International Conference on Robotics and Automation, pp3339-3346, 2003.

References

[CAO 07] A. Cao, J. Kim, L. Lin, Bi-directional electrothermal electromagnetic actuators, J.Micromech. Microeng. 975–982 (17) 2007.

[CAR 98] M.C. Carrozza, A. Menciassi, G. Tiezzi, P. Dario. The development of a LIGAmicrofabricated gripper for micromanipulation tasks, Journal of Micromechanics and Microengineering, 8 (2), pp141-143, 1998.

[CHA 08] B. Charlot, W. Sun, K. Yamashita, H. Fujita and H. Toshiyoshi, Bistable nanowire for micromechanical memory, J. Micromech. Microeng. 18 045005, 2008.

[CHA 09] N.chaillet and S. Regnier, 'la microrobotque' pp129, 2008.

[CHI 92] G. S. Chirikjian, Theory and Applications of Hyper-Redundant Robotics Manipulators, PhD Dissertation, CalTech, 1992.

[CHI 94] G. S. Chirikjian, A Binary Paradigm for Robotic Manipulators, Proc. of the IEEE ICRA'94, May 1994.

[CHI 95a] G. S. Chirikjian, Kinematics Synthesis of Mechanisms and Robotic Manipulators with Binary actuators, ASME J. Mech.Design, 121, 1995.

[CHI 95b] G. S. Chirikjian and J.W. Burdick, Kinematically Optimal Hyper-Redundant Manipulator Configurations, IEEE Trans.on Robotics and Automation, 11(6), pp123-136, Dec 1995.

[CHO 00] H. J. Cho, S. Bhansali and C. H. Ahn, Electroplated thick permanent magnet arrays with controlled direction of magnetization for MEMS application, Journal of Applied Physics, Volume 87, Issue 9, pp6340-6342, May 1, 2000.

[CL] Coulomb Law, http://en.wikipedia.org/wiki/Coulomb%27s_law.

[DON 06] B.R. Donald, C. G. Levey, C.D. gray. I. Paprotny , D. Rus, « An untethered, electrostatic, globally controllable MEMS micro-robot », Journal Of Microelectromechanical Systems, vol. 15, n°1, 2006.

[DONG 02] Y. Dong, Mechanical Design and Modeling of MEMS Thermal Actuators for RF Applications, in M.S.thesis, University of Waterloo, 2002.

[ENI 00] E.T. Enikov and B. Nelson, Three-dimensional microfabrication for a multi-degrec-of-freedorn capacitive force sensor using fibre-chip coupling, Journal of Micromech. And Microeng, Vol. 10, pp pp492-497, 2000.

[FAB 94] T. Fabula, H.l. Wagner and B. Schmidt, Triple-beam resonant silicon force sensor based on p:ezoelectric thin Glms, Journal of Sensors and Actuators Vol. A41-A42, pp375-380, 1994.

References

[FAT 07] S. Fatikow, T Wich, H Hulsen, T Sievers et M. Iahniseh: Microrobot system for automatic nanohandling inside a scanning electron microscope., IEEEIASME Transaction on Mechatronics, 12:2441 252, 111, June, 2007.

[FED 98] J.T. Feddema and R. W. Simon: Visual servoing and cad-driven microassembly IEEE Robotics and Automation Magazine, Vol. 5 (4): 181 24, 1998.

[FEM] Femto Tools, http://www.femtotools.com/.

[FRE 04] M. Freudenreich, U. Mescheder, G. Somogyi, Simulation and realization of a novel micromechanical bi-stable switch, Sens. Actuators A 114, pp451–459, 2004.

[FU 04] Y.Q. Fu, H.J. Du, W.M. Huang, Sam Zhang, M. Hua, TiNi-based thin films in MEMS applications: a review" Sensors and Actuators A 112, pp395–408, 2004.

[FUK 05] T. Fukushima, K. Asaka, A. Kosaka, T. Aida. Fully Plastic Actuator through Layer-by-Layer Casting with Ionic-Liquid-Based Bucky Gel, Angewandte Chemie International Edition Volume 44, Issue 16, 2410, 2005.

[GAU 08a] J.Y Gauthier, A. Hubert, J. Abadie,N. Chaillet, C. Lexcellent, Nonlinear Hamiltonian odeling of magnetic shape memory alloy based actuators. Sensors and Actuators a Physical, 141, pp536-547, 2008.

[GAU 08b] J.Y. Gauthier. thèse Modélisation des Alliages à Mémoire de Forme Magnétiques pour la conversion d'énergie dans les actionneurs et leur commande. Université de Franche-Comté, 2007.

[GIB 04] M. R. J. Gibbs, E. W. Hill and P. J. Wright, Magnetic materials for MEMS applications. Journal of Physics D: Applied Physics, Volume 37, Number 22, 21 ppR237-R244 (1), November 2004,

[GOM] T. Gomm, Development of In-Plane Compliant Bistable Microrelays, in M.S. Thesis, Brigham Young University, Provo, Utah, 2001.

[GRE 97] S. Greek, F. Ericson, S. Johansson, and J. Schweitz, In situ tensile strength measurement and Weibull analysis of thick film and thin film micromachined polysilicon structure, Thin Solid Films, Vol. 292, pp247-254, 1997.

[GROS 08] M. GROSSARD, thesis, Contribution à la conception optimale et la commande de systèmes mécatroniques flexibles à actionnement piézoélectrique intégré - Application en microrobotique, Université de Franche-comté, 2008.

[GUK 95] H. Guckel, T.R. Christenson, J. Klein, T. Earles, S. Massoud-Ansari, Micro Electromagnetic Actuators Based on Deep X-Ray Lithography, International Symposium on Microsystems, Intelligent Materials and Robots, Sendai, Japan, September 27-29, 1995.

References

[HAD 00] Y. Haddab, thèse, conception et réalisation d'un système de micromanipulation contrôlé en effort et en position pour la manipulation d'objets de taille micrométrique, 2000.

[HAD 09] Y. Haddab, Q. Chen, P. Lutz, Improvement of strain gauges micro-forces measurement using Kalman optimal filtering. IFAC, Mechatronics 19, 4, pp457-462, 2009.

[HAI 09] R.D. Haigha and R.W. Whatmoreb. On the processing conditions and interfacial chemistry of composite PZT thick films on platinised silicon substrates. Sensors and Actuators A: Physical, volume 151, Issue 2, pp203-212, 29 April 2009.

[HUG 91] P.C. Hughes, W.G. Sincarsin and K.A. Carroll, Trussarm-A Variable Geometry Truss Manipulator, J. of Intell. Mater. Syst., and Struct., Vol. 2, pp148-160, April 1991.

[HUM 99] J.V. Humbeeck, Non-medical applications of shape-memory alloys, Mater. Sci. Eng. A273–A275, 134–148, 1999.

[HWA 03] I. H. Hwang, Y.-S. Shim, J.-H. Lee, modeling and experimental characterization of the chevron-type bistable microactuator, J. Micromech. Microeng. 13 , pp948–954, 2003.

[IVA 09] A. Ivan, M. Rakotondrabe, P. Lutz, N. Chaillet, Quasistalic displacement self-sensing methcd for cantilevered piezoeleclric actualors, Review of Scientific instruments, vol. 80, no. 6, 2009.

[JEN 98], B. D. Jensen, Identification of Macro- and Micro-Compliant Mechanism Configurations Resulting in Bistable Behavior, M.S. Thesis, Brigham Young University, Provo, Utah, 1998.

[JIN 05] T. Jinni, Design and experiments of fully compliant bistable micromechanisms, in Mechanism and Machine Theory, 40, pp17–31, 2005.

[KAL 97] H. Kahn, W.L. Benard, M.A. Huff, A.H. Heuer, Titanium–nickel shape memory thin film actuators for micromachined alves, Mater.Res. Soc. Symp. Proc. 444, 227–232, 1997.

[KIM 04] D.H. Kim, B. Kim and H. Kang, Development of a piezoelectric polymer-based sensorized mierogripper for microassembly and micromanipulation, loumal of Microsystem Technologies, Vol. 10, pp275-280, 2004.

[KLE] Kleindiek, Germany. http ://www.nanotechnik.com/.

[KO 06] J.S. Ko, M.G. Lee, J.S. Han, J.S. Go, B. Shin, D.-S. Lee, A laterally-driven bistable electromagnetic microrelay, ETRI J. pp389–392, (28) 2006.

[KOTA 01] S. Kota, J. Joo, Z. Li. Design of Compliant Mechanisms: Applications to MEMS, Analog Integrated Circuits and Signal Processing-An International Journal, 29, Kluwer Academic Publications, pp7-15, 2001.

References

[KRY 08] S. Krylov, B.R. Ilic, D. Schreiber, S. Seretensky, H. Craighead, The pull-in behavior of electrostatically actuated bistable microstructures, J. Micromech. Microeng. 18 055026, 2008.

[KWON 05] H. N. Kwon, I..H.Hwang, J.-H. Lee, A pulse-operating electrostatic microactuator for bi-stable latching, J. Micromech. Microeng. 15, pp1511–1516, 2005.

[LAG 99] L.K. Lagorce, O. Brand and M.G. Allen, Magnetic Microactuators Based on Polymer Magnets, Journal of. Microelectromechanical Systems, 8:pp2–9, 1999.

[LANG 08] D. F. LANG PhD thesis, A study on Micro-gripping technologies, Technische Universiteit Delft, 2008.

[LMTS] EPFL/LMTS. http://lmts.epfl.ch/webdav/site/lmts/shared/images/DEAP_principle.jpg.

[LUH 07] R. Luharuka, J. P. Hesketh, Design of fully compliant, in-plane rotary, bistable micromechanisms for MEMS applications, Sensors and Actuators A: Physical, Volume 134, Issue 1, 28, pp231-238 February 2007.

[MAK 00a] E. Makino, T. Mitsuya, T. Shibata, Dynamic actuation properties of TiNi shape memory diaphragm, Sens. Actuators 79, pp128–135, 2000.

[MAK 00b] E. Makino, T. Mitsuya, T. Shibata, Micromachining of TiNi shape memory thin film for fabrication of micropump, Sens. Actuators 79, pp251–259, 2000.

[MEL] Mechanical Engineering Laboratory, Japan. http://unit.aist.go.jp/amri/group/finemfg/English/research/m-factory-e.htm.

[MEN 01]A. Menciassi, A. Eisinberg, G. Scalari, C. Anticoli, M.c. Carrozza, P. Dario Force feedback-based microinstrument for measuring tissue Properties and pulse in microsurgery, Proceedings of the IEEE International Conference on Robotics & Automation Seoul, Korea, May 21-26, 2001.

[MIC] Microworks, http://www.micro-works.de/liga.html.

[MIU 95] K. Miura, and H. Furuya, Variable Geometry Truss and Its Application to Deployable Truss and Space Crane Arm, Acta Astronautica, 12(7, 8), 1995.

[MOL 05] K. Molhave and O. Hansen, Electro-thermally actuated microgrippcrs with integrated force-feedback, Journal of Micromech. and Microeng., Vol I S. pp126S-1279, 2005.

[MUK 08] D. Mukhopadhyay, J. Dong, E. Pengwang and P. M. Ferreira. A SOI MEMS-based 3-DOF Planar Parallel-Kinematics Nanopositioning Stage. Sensors and Actuators A, 147, 340–351, 2008.

[MUR 05] S. Muratet, thèse, Conception, caractérisation et modélisation : Fiabilité prédictive de MEMS à actionnement électrothermique. Institut National des Sciences Appliquées de Toulouse, 2005.

References

[MURA 05] P. Muralt, N. Ledermann, J. Baborowski and N. Setter, Piezoelectric micromachined ultrasonic transducers based on PZT thin films. IEEE Trans. Ultrason. Ferroelect. Freq. Contr., 52(12), pp2276–2288, 2005.

[OKA 09] T. Okazaki, M. Tanaka, Y. Furuya. Magnetic-Field Driven Micro-Gas-Valve. Materials Transactions, 50(3), pp.461-466, 3/2009.

[OTS 99] K. Otsuka, X. Ren, Recent developments in the research of shape-memory alloys, Intermetallics 7, 511–528. 1999.

[PAK 03] J. Park and W. Moon, A hybrid-type micro-gripper with and integrated force sensor, Joumal of Microsystem Technologies, Vol. 9, pp511 -519, 2003.

[PLA 07] J. S.Plante, L. Devita and S. Dubowsky, A Road to Practical Dielectric Elastomer Actuators Based Robotics and Mechatronics: Discrete Actuation. Proceedings of the 2007 Conferences on Smart Structures, San Diego, California, (Invited Plenary), March 2007.

[QIU 04] J. Qiu, A Curved-Beam Bistable Mechanism, in Journal of MicroElectroMechanical Systems, vol. 13- 2, pp137-146, April 2004.

[QIU 05] J. Qiu, J.H. Lang, A.H. Slocum, A bulk-micromachined bistable relay with Ushaped thermal actuators, J. Microelectromech. Syst. 14, 2005.

[RAK 06a] M. Rakotondrabe, thèse, Développement et commande modulaire d'une station de microassemblage, 2006.

[RAK 06b] M. Rakotondrabe, Y. Haddab and P. Lutz, 'Design, development and experiments of a high stroke-precision 2DoF (linear-angular) microsystem', IEEE - ICRA, (International Conference on Robotics and Automation), pp669-674, Orlando FL USA, May 2006.

[RAK 09a] M. Rakotondrabe, Y. Haddab and P. Lutz, Quadrilateral modelling and robust control of a nonlinear piezoelectric cantilever, IEEE - Transactions on Control Systems Technology (T-CST), Vol.17, Issue 3, pp528-539, May 2009.

[RAK 09b] M. Rakotondrabe, C. Clévy and P. Lutz, Complete open loop control of hysteretic, creeped and oscillating piezoelectric cantilever, IEEE - Transactions on Automation science and Engineering (T-ASE), DOI 10.1109/TASE.2009.2028617, 2009.

[RAL 00] S. Ralis, B. Vikramaditya and B. J. Nelson: Micropositioning of a weakly calibrated microassembly system using coarse–to-fine visual serving strategies. IEEE Transactions on Electronics Packaging Manufacturing, Vol. 23 (2): 123 1 131, 2000.

[RHO 85] M.D. Rhodes and M.M. Mikulas, Deployable Controllable Geometry Trusses Beam, NASA TM 86366, 1985.

[ROB 98] H. Robertshaw and C. Reinholtz, Variable Geometry Trusses, Smart materials, Structures, and Mathematical Issues, pp105-120, 1998.

References

[ROB 99] R.Y. Robert, Mechanical digital-to-analog converters, in Proc. of the int. conf. on solid-state sensors and actuators. Transducers'99, sendai, japan, pp998-1001, June 1999.

[ROB] Robotics, http://en.wikipedia.org/wiki/Robotics.

[ROT 92] R.C. Roth, The Elastic Wave Motor - A Versatile Terfenol Driven, Linear Actuator With High Force and Great Precision - Actuator 92,rd International Conference on New Actuators, Bremen, Germany, p.138, 1992.

[SAD 00] D. J. Sadler, T. M. Liakopoulos and C. H. Ahn, "A Universal Electromagnetic Microactuator Using Magnetic Interconnection Concepts", IEEE Journal of Microelectromechanical Systems, volume 9, Issue 4, pp460 – 468, DOI: 10.1109/84.896766, Dec 2000.

[SHA 98] M. Shahinpoor, Y. Bar-Cohen, T. Xue. Ionic Polymer-Metal Composites (IPMC) As Biomimetic Sensors and Actuators, Proceedings of SPIE's 5th Annual International Symposium on Smart Structures and Materials, San Diego,CA. pp3324-27, 1-5 March, 1998.

[SIL] Silmach, http://www.silmach.com/.

[SIM 76] Simitses, George J, An introduction to the elastic stability of structures, 1976.

[SPEN 02] W. M. V. Spengen, R. Puers, and I. D.Wolf, A physical model to predict stiction inMEMS, Journal of Micromechanics and Microengineering, Vol. 12, pp702-713, 2002.

[SPEN 03] W. M. V. Spengen, R. Puers, and I. D.Wolf, On the physics of stiction and its impact on the reliability of microstructures, Journal of Adhesion Science and Technology, Vol. 17, No. 4, pp563-582, 2003.

[SUJ 04] V.A. Sujan, S. Dubowsky, Design of a lightweight hyper-redundant deployable binary manipulator, Journal of Mechanical Design, Vol. 126 pp.29-39, 2004.

[SUN 02] Y. Sun, B. Nelson, D. P. Potasek and E. Enikov, A bulk microfabricated multi-axis capacitive cellular force sensor using transverse comb drive Journal of Micromech. And Microeng., Vol. 12, pp 832-940, 2002.

[SUT 01]   J. Suthakorn and G.S. Chirikjian, A New Inverse Kinematics Algorithm for Binary Manipulators with Manu Actuators, Advanced Robotics, 15(2), 2001.

[TAM 09a] B. Tamadazte, S. Dembele, N. Lefort-Piat, A Multiscale Calibration of a Photon Video Microscope for Visual Servo Control: Application to MEMS Micromanipulation and Microassembly, Sensors & Transducers Joumal, vol. 5, pp37-52, 2009.

[TAM 09b] B. Tamataze, Vision 3D et Commande par asservissements visuels pour la micromanipulation et le micro-assemblage de MEMS, These, Université de Franche-Comté, 2009.

References

[TAN 00]   D. M. Tanner, J. A. Walraven, K.S. Helgesen, L.W. Irwin, D. L. Gregory, J. R. Stake, and N. F. Smith, MEMS reliability in a vibration environment, IEEE 38th Annual International Reliablity Physics Symposium, San Jose, California, USA, pp139-145, 2000.

[TDD] Terfenol-D Data Sheet: http://www.etrema-usa.com/documents/Terfenol.pdf.

[TIM] S. P. Timoshenko, Book, Theory of Elastic Stability.

[TMW]The Microinjection Workshop.
http://members.cox.net/microinjectionworkshop/index.html.

[TSU 98] T. Tsuchiya, O. Tabata, J. Sakata, and Y. Taga, Speciment size effect on tensile strength of surfacemicromachined polycrystalline silicon thin films, Journal of Microelectromechanical Systems, Vol.7, No. 1, pp106-113, Mar. 1998.

[VIK 99] B.Vikramaditya and B. J Nelson: Visually served micropositioning for robotic micromanipulation. Microcomputer Applications, 18, pp23-31, 1999.

[WAD 90] B.K. WADA, JPL, Pasadena, CA, Adaptive structures - An overview, JOURNAL OF SPACECRAFT AND ROCKETS, 0022-4650 vol.27 no.3 (330-337), 1990.

[WAG] D. Wagg, Ian Bond, Paul Weaver, Michael Friswell, Adaptive structures: engineering applications Book.

[WANG 07] Z.H. Wang, J.M. Miao and W.G. Zhu Piezoelectric thick films and their application in MEMS, Journal of the European Ceramic Society, Volume 27, Issues 13-15, pp3759-3764, 2007.

[WEI]   W. Weibull, http://en.wikipedia.org/wiki/Weibull_distribution.

[WIL 04] D. L. Wilcox, master thesis, FULLY COMPLIANT TENSURAL BISTABLE MECHANISMS (FTBM) WITH ON-CHIP THERMAL ACTUATION, Brigham Young University, 2004.

[WIN 06] A. Wingert, M. D. Lichter and S. Dubowsky, On the Design of Large Degree of Freedom Digital Mechatronic Devices based on Bi-stable Dielectric Elastomer Actuators. IEEE/ASME Transactions on Mechatronics, Vol. 11, No. 4, pp448-456, August 2006.

[YAO 08] Q. Yao, J.G. Dong, P. M. Ferreira, A novel parallel-kinematics mechanisms for integrated,multi-axis nanopositioning Part 1. Kinematics and design for fabrication, Precision Engineering 32, pp7–19, 2008.

References

Résumé

Au cours de la dernière décennie, des travaux de recherche importants ont été effectués dans le domaine de la microrobotique. Ces travaux concernent la conception, la fabrication et la commande de microrobots destinés à exécuter diverses tâches dans le micromonde (le monde des objets de taille micrométrique). Il s'agit notamment de tâches de manipulation d'objets artificiels ou biologiques à des fins de positionnement, de caractérisation ou de tri mais aussi pour le micro-assemblage industriel. Les recherches effectuées ont montré l'efficacité des matériaux actifs pour l'actionnement des microrobots. Toutefois, en dépit de leur haute résolution intrinsèque, ces matériaux présentent des inconvénients qui rendent la commande des microrobots difficile. Le comportement de ces matériaux et plus généralement des actionneurs qui les utilisent est souvent complexe, non linéaire et parfois non stationnaire. L'implantation de lois de commande nécessite donc l'emploi de capteurs et d'instruments coûteux et encombrants pour le traitement des signaux et l'exécution en temps réel. Dans le but de lever les difficultés citées précédemment et d'ouvrir des perspectives nouvelles pour la conception et la commande de microrobots, nous proposons une nouvelle approche pour la microrobotique appellée « microrobotique numérique » qui utilise un concept de modularité et une commande en boucle ouverte. Ces nouveaux microrobots sont construits à partir de « modules élémentaires » possédant deux états mécaniques stables et répétables. La position de l'extrémité du microrobot dépend de l'état des différents modules bistables qui le composent. Cette approche introduit un nouveau paradigme en microrobotique permettant la conception de cinématiques diverses adaptées au micromonde. Les principaux avantages de cette nouvelle microrobotique sont la modularité, l'absence de capteurs, la flexibilité, la possibilité de réaliser des robots microfabriqués et l'absence d'asservissement. Cette thèse propose la conception, la microfabrication et la caractérisation d'un module bistable.

Mots-clés: Microrobotique, mécanisme bistable, actionneur thermique, actionnement discret, mécanisme compliant, SOI wafer, commande en boucle ouverte.

Abstract

During the last decade, significant research activities have been performed in the field of microrobotics, which deals with the design, the fabrication and the control of microrobots. These microrobots are intended to perform various tasks in the so-called Microworld (i.e. the world of submillimetric objects), in particular micromanipulation tasks of single objects (artificial or biological) for positioning, characterizing or sorting as well as for industrial microassembly. Researches already done have shown that the use of active materials to actuate microrobots gives better performances than the use of traditional actuators. However, despite their intrinsic high resolution, these materials present some disadvantages, making the design of efficient controllers a hard task. Their behavior is often complex, nonlinear and sometimes non stationary. Closedloop control of the microrobots requires the integration of very small sensors and the use of bulky and expensive instruments for signal processing and real-time operating. Packaging and integration of the sensors and actuators are also hard problems. This is why building multidegrees of freedom microrobots able to perform complex tasks is difficult. To get over these difficulties, we propose an approach to perform the microfabrication of microrobots using a modular concept and an open loop control strategy. These microrobots, named "digital microrobots" are based on the design of microrobots from several "elementary modules", each offers a very good repeatability and stable positions. A binary signal switches the module between the two stable states. The position of the whole microrobot is controlled by a digital word representing the state of the modules. A paradigm is opened in the microrobotics field, allowing the design of various kinematics adapted to the microworld. The main advantages of this new microrobotic are modularity, absence of sensors, the flexibility, microfabricated robots and open-loop control.

Keywords: Microrobotics, bistable mechanism, thermal actuator, discrete actuation, compliant mechanism, SOI wafer, open loop-control.